Imaging with surface-related multiples using linear and non-linear modelling

Nath, A.

DOI
10.4233/uuid: b889f488-2e68-4f95-95ee-e0a6b7e3fa5a

Publication date
2023

Document Version
Final published version

Citation (APA)
Nath, A. (2023). *Imaging with surface-related multiples using linear and non-linear modelling*. [Dissertation (TU Delft), Delft University of Technology]. https://doi.org/10.4233/uuid: b889f488-2e68-4f95-95ee-e0a6b7e3fa5a

IMAGING WITH SURFACE-RELATED MULTIPLES USING LINEAR AND NON-LINEAR MODELLING

DELFT UNIVERSITY OF TECHNOLOGY

IMAGING WITH SURFACE-RELATED MULTIPLES USING LINEAR AND NON-LINEAR MODELLING

DELFT UNIVERSITY OF TECHNOLOGY

Dissertation

for the purpose of obtaining the degree of doctor

at Delft University of Technology

by the authority of the Rector Magnificus, Prof. dr. ir. T.H.J.J. van der Hagen

chair of the Board for Doctorates

to be defended publicly on 12 October 2023 at 10:00 am

by

Aparajita NATH

Master of Science in Exploration Geophysics,
Indian Institute of Technology, Kharagpur, India,
born in Korba, India.

This dissertation has been approved by the promotors.

Composition of the doctoral committee:

Rector Magnificus,	chairperson
Dr. ir. D.J. Verschuur,	Delft University of Technology, promotor
Prof. dr. ir. N. de Jong,	Delft University of Technology, promotor
Independent members:	
Prof. dr. L. J. Gelius	University of Oslo, Norway
Dr. A. K. Soni	Shell International
Dr. ir. D. S. Draganov	Delft University of Technology
Prof. dr. ir. E. C. Slob	Delft University of Technology
Prof. ir. C. P. J. W. van Kruijsdijk	Delft University of Technology

The work in this dissertation was financially supported by the DELPHI consortium.

Printed by: Proefschriftmaken.nl

ISBN 978-94-6366-745-6

An electronic version of this dissertation is available at
http://repository.tudelft.nl/.

CONTENTS

SUMMARY

Seismic reflection imaging aims to generate a representation of the subsurface of the earth using acoustic or elastic waves recorded in the form of seismic data. During the processing of the data for imaging, we pick a part of the data as signal and discard the rest as noise. Since so-called primary wavefields carry the single-scattering reflection response of the subsurface, they are assumed to be sufficient to carry out reflection imaging. This also means that significant effort is devoted towards removing not only the noise but also the multiple reflection events to avoid imaging artefacts, also known as cross-talk. Surface-related multiples are the multiples generated during the marine acquisition by at least one downward reflection at the water-air boundary, and tend to be the strongest in amplitude compared to the other multiples. Over the past several decades, many novel techniques have been developed to remove the surface-related multiples effectively. While we are getting better at primary-multiple separation, it is still a very challenging and expensive problem. In recent years, multiples have gained recognition as valuable signals, not just noise. Multiples also contain the reflection responses of the subsurface and since they travel different paths they often contain additional information about the subsurface compared to the primaries-only wavefields. Imaging with primaries and multiples without separation is the way forward as it avoids the expensive multiple removal steps along with providing (potentially) additional illumination from the multiples.

On the other hand, when imaging with multiples (or primaries and multiples together), we need more events on the source side, such as re-injected total data, possibly together with the direct wave. This complex source-side wavefield gives rise to cross-talk in the imaging process and other artefacts. One such method that aims to solve this issue is the inversion-based full wavefield migration (FWM) method. In this method, the available data is used to generate the reflectivity of the subsurface recursively, using all the complex wavefields, including the multiples. This method uses the re-injected measured wavefield to model the multiples in the data and in the same way, the source wavefield is used to model the primaries, leading to a 'linear' relationship between the modeled data and the subsurface reflectivity. Imaging with multiples using such an inversion-based method has been shown to outperform the primaries-only imaging method in several aspects, such as increased illumination, data infilling and better vertical resolution. However, like any data-driven method, its performance is substantially affected by compromised data; for example in the case of large chunks of missing data.

The main aim of this thesis is to explore the different strategies of imaging with surface-related multiples. We also aim to exploit and maximise the benefits of multiples in overcoming the large gaps in imaging due to missing data. This work adds to the knowledge obtained by the previous work on least-squares imaging using primaries and/or mul-

tiples. In this endeavour, a 'non-linear' imaging method is introduced that models the data iteratively; both primaries and all orders of surface multiples, starting from a given source wavefield and a velocity model. The modelling scheme and the imaging principle remain largely the same as the one used in full wavefield migration. Since this method models the data, including all the orders of surface-multiple scattering, from the provided source wavefield, we expect it to be less sensitive to the gaps in the data. The dependence of this method on receiver geometry and its performance on large acquisition gaps is tested via different kinds of data namely, numerically generated data and field-acquired data for 2D and 3D scenarios. Through examples, we see that the 'non-linear' method provides wider illumination compared to the other 'linear' imaging methods and is less dependent on the receiver geometry. We also realise that since the modelling is done non-linearly, it is sensitive to small errors in the assumed source wavefield and thus, requires knowledge of the source wavelet. On the other hand, 'linear' imaging methods (with primaries and/or multiples) have less of these sensitivities. Therefore, a hybrid method is introduced that combines the different primaries and multiples imaging methods to put the complementary benefits of the two methods together in exploiting the benefit of the multiples. In principle, the 'linear' and 'non-linear' imaging methods can be combined to aid each other in any order or scheme. In this thesis, we demonstrate one such combination and compare it with the performance and virtues of all the other methods via different examples.

Because the use of so-called ocean bottom nodes (OBN) to acquire marine data is gaining popularity, the application of the aforementioned methods on OBN data is also done to see how multiples can aid in improving the imaging results in such an acquisition scenario. These methods are also compared with the state-of-the-art mirror imaging method to further highlight that using more orders of multiples provide substantial benefits in imaging. The hybrid method provides a much more robust framework and thereby a reliable and better imaging result.

In this thesis, we will see that imaging with multiples, when tactfully utilised, can be extremely useful and, therefore, should become a standard in imaging practice.

SAMENVATTING

Seismische reflectiebeeldvorming heeft als doel een weergave van de ondergrond van de aarde te genereren met behulp van akoestische of elastische golven die zijn opgenomen in de vorm van seismische metingen. Tijdens het verwerken van de gegevens voor beeldvorming, kiezen we een deel van de gegevens als signaal en verwerpen we de rest als ruis. Aangezien zogenaamde primaire golfvelden de enkele verstrooiing van de reflectierespons van de ondergrond bevatten, wordt aangenomen dat ze voldoende zijn om reflectiebeeldvorming uit te voeren. Dit betekent ook dat er veel moeite wordt gedaan om niet alleen de ruis te verwijderen, maar ook de meervoudige reflecties of multiples om beeldvormingsartefacten, ook wel overspraak genoemd, te voorkomen. Oppervlaktegerelateerde multiples zijn de multiples die tijdens de mariene acquisitie gegenereerd worden door ten minste één neerwaartse reflectie op de water-luchtgrens, en hebben de neiging de sterkste amplitude te hebben in vergelijking met de andere multiples. In de afgelopen decennia zijn er veel nieuwe technieken ontwikkeld om de oppervlaktegerelateerde multipels effectief te verwijderen. Hoewel we steeds beter worden in het scheiden van primaire reflecties en multipels, is het nog steeds een zeer uitdagend en duur probleem. De laatste jaren worden multipels steeds meer gezien als waardevolle signalen en niet alleen als ruis. Multiples bevatten ook de reflectie informatie van de ondergrond en omdat ze verschillende paden afleggen, bevatten ze vaak aanvullende informatie over de ondergrond vergeleken met de golfvelden van alleen de primaries. Beeldvorming met primaries en multiples zonder scheiding is de beste manier om vooruitgang te boeken, omdat zo de dure meervoudige verwijderingsstappen worden vermeden en (mogelijk) extra belichting van de multiples wordt verkregen.

Aan de andere kant hebben we bij beeldvorming met multiples (of primaries en multiples samen) meer gebeurtenissen aan de bronzijde nodig, zoals opnieuw geïnjecteerde totale golfvelden, mogelijk samen met de directe golf. Dit complexe golfveld aan de bronzijde geeft aanleiding tot overspraak in het beeldvormingsproces en andere artefacten. Een van de methoden die dit probleem probeert op te lossen is de op inversie gebaseerde migratiemethode met volledig golfveld (FWM). Bij deze methode worden de beschikbare gegevens gebruikt om het reflectievermogen van de ondergrond recursief te genereren met behulp van alle complexe golfvelden, inclusief de multiples. Deze methode gebruikt het opnieuw geïnjecteerde gemeten golfveld om de multiples in de metingen te modelleren en op dezelfde manier wordt het brongolfveld gebruikt om de primaries te modelleren, wat leidt tot een 'lineaire' relatie tussen de gemodelleerde metingen en de reflectiviteit van de ondergrond. Beeldvorming met multiples met behulp van een dergelijke op inversie gebaseerde methode blijkt in verschillende opzichten beter te presteren dan beeldvorming met alleen primaries, zoals een betere belichting, data aanvulling en een betere verticale resolutie. Zoals bij elke datagestuurde methode worden de prestaties echter aanzienlijk beïnvloed door gecompromitteerde gegevens, bijvoor-

beeld in het geval van grote stukken ontbrekende gegevens.

Het hoofddoel van dit proefschrift is het verkennen van de verschillende strategieën voor beeldvorming met oppervlaktegerelateerde multiples. We streven er ook naar om de voordelen van multiples te benutten en te maximaliseren bij het overbruggen van de grote gaten in de beeldvorming als gevolg van ontbrekende gegevens. Dit werk voegt toe aan de kennis die is verkregen door het eerdere werk aan de kleinste kwadraten beeldvorming met behulp van primaries en / of multiples. In dit werk wordt een 'niet-lineaire' beeldvormingsmethode geïntroduceerd die de gegevens iteratief modelleert; zowel primaries als alle ordes van oppervlakte-multiples, uitgaande van een gegeven brongolfveld en een snelheidsmodel. Het modelleringsschema en het beeldvormingsprincipe blijven grotendeels hetzelfde als bij volledige golfveldmigratie. Aangezien deze methode de gegevens modelleert, inclusief alle ordes van oppervlakte-multipelverstrooiing, vanuit het geleverde brongolfveld, verwachten we dat deze minder gevoelig is voor hiaten in de gegevens. De afhankelijkheid van deze methode van de geometrie van de ontvanger en zijn prestaties bij grote hiaten in de gegevensverzameling worden getest aan de hand van verschillende soorten gegevens, namelijk numeriek gegenereerde gegevens en in het veld verzamelde gegevens voor 2D- en 3D-scenario's. Aan de hand van voorbeelden zien we dat de 'niet-lineaire' methode de beste resultaten oplevert. Aan de hand van voorbeelden zien we dat de 'niet-lineaire' methode een bredere belichting geeft in vergelijking met de andere 'lineaire' beeldvormingsmethoden en minder afhankelijk is van de geometrie van de ontvangers. We realiseren ons ook dat, omdat de modellering niet-lineair gebeurt, deze gevoelig is voor kleine fouten in het veronderstelde brongolfveld en dus kennis van de bronwavelet vereist. Aan de andere kant hebben 'lineaire' beeldvormingsmethoden (met primaries en/of multiples) minder van deze gevoeligheden. Daarom wordt een hybride methode geïntroduceerd die de verschillende primaries en multiples beeldvormingsmethoden combineert om de complementaire voordelen van de twee methoden samen te brengen en de voordelen van de multiples te benutten. In principe kunnen de 'lineaire' en 'niet-lineaire' beeldvormingsmethoden worden gecombineerd om elkaar te helpen in elke volgorde of schema. In dit proefschrift demonstreren we één zo'n combinatie en vergelijken we deze met de prestaties en voordelen van alle andere methoden aan de hand van verschillende voorbeelden.

Omdat het gebruik van zogenaamde ocean bottom nodes (OBN) voor het verwerven van mariene gegevens steeds populairder wordt, worden de bovengenoemde methoden ook toegepast op OBN-gegevens om te zien hoe multiples kunnen helpen bij het verbeteren van de beeldvormingsresultaten in een dergelijk verwervingsscenario. Deze methoden worden ook vergeleken met de state-of-the-art spiegelbronafbeeldingsmethode om verder te benadrukken dat het gebruik van meer ordes van multiples aanzienlijke voordelen oplevert in de beeldvorming. De hybride methode biedt een veel robuuster raamwerk en daardoor een betrouwbaarder en beter beeldvormingsresultaat.

In dit proefschrift zullen we zien dat beeldvorming met multiples, mits tactvol gebruikt, uiterst nuttig kan zijn en daarom een standaard zou moeten worden in de beeldvormingspraktijk.

1

INTRODUCTION

1.1. SEISMIC REFLECTION IMAGING

Using visible light is the most common way for humans to image an object. When light hits the surface of an object, it is reflected and is then registered by our eyes to be further distinguished by our brain in terms of colour, shape and size among many other characteristics. The light here is an electromagnetic wave that helps us in visualising the surface of an object. For visualising areas where light (visible spectrum of electromagnetic waves) cannot reach, scientists explored other kinds of waves that can penetrate the surface of the object and inspect its interiors. For electromagnetic waves, an example of a popular method is the X-ray imaging method (Spiegel, 1995), where the interiors of a human body or airport luggage can be examined non-invasively. Figure 1.1a shows one such example where an x-ray is used to image the fractured bone of a human hand that is otherwise not visible to the naked eye.

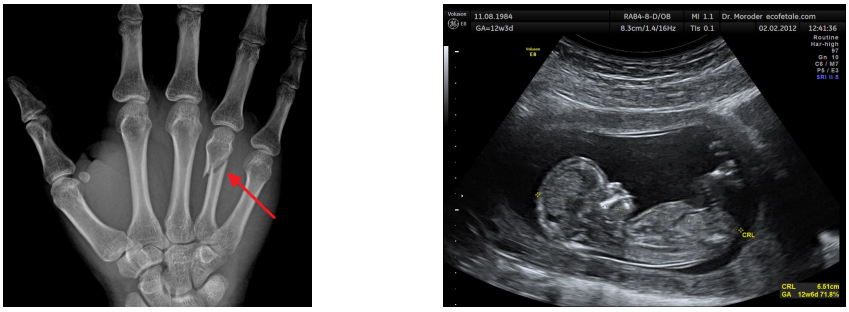

(a) ***(b)***

Figure 1.1 *a) An X-ray image of a hand. The fractured bone (fourth metacarpal) is pointed with the red arrow. Source: Louis Philippe Lessard, CC BY-SA 3.0, via Wikimedia Commons. b) Ultrasound image of a human fetus in a womb, viewed at 12 weeks of pregnancy. Source: Wolfgang Moroder, CC BY-SA 3.0, via Wikimedia Commons.*

1

Acoustic waves or sound waves are also used in several such applications to image targets otherwise unreachable or unresolvable by other forms of signals. For example, in medical imaging, ultrasound (Jensen, 2007) is used to examine a developing fetus instead of X-rays since X-rays can be harmful to fetal development. Figure 1.1b shows an ultrasound image of a human fetus acquired during pregnancy. In geophysics, mostly* seismic waves have been used to extract structural information below the Earth's surface with varying scales of applications such as earthquake seismology (Båth, 1966), oil and gas exploration (Bjorlykke, 2010), carbon dioxide storage (Carcione et al., 2006), groundwater exploration (Martin et al., 2013) and even for a much shallower application such as engineering seismic risk analysis. Besides earthquake seismology, the seismic waves are generated via active sources, which travel through the Earth's subsurface formations. Upon encountering a change in medium properties, such as density and propagation velocity, a part of the energy is either reflected, refracted, absorbed or transmitted. In exploration-related geophysical applications, these reflected (or refracted) waves are used to get an image of the target zone via a process called *seismic imaging* or *seismic migration* (Biondi, 2006).

In this thesis, we will be focusing on the aspect of seismic imaging that particularly deals with the exploration of the Earth for locating natural resources, e.g., hydrocarbon reservoirs, or for monitoring subsurface processes like carbon dioxide injection. In such seismic methods, the seismic waves are generated by controlled sources such as explosives, vibrators or air guns (Dondurur, 2018). The energy propagating as seismic waves illuminates the subsurface area, gets reflected, refracted or diffracted from the subsurface in the Earth and is in turn recorded by an array of geophones or hydrophones. Figure 1.2a shows a land seismic survey using a vibrator as the energy source and geophones as data receivers, while figure 1.2b shows a typical marine survey using airguns as the source and hydrophones as the receivers attached to a streamer.

Figure 1.3 shows examples of marine and land seismic recordings. As can be observed, it looks nothing like the Earth's subsurface. However, this data has several reflection arrivals from interfaces between different layers of the subsurface. This often is enough information to give us a detailed subsurface image, although after several processing steps. For example, the arrows in figure 1.3a point towards the different reflection events in a marine seismic recording. The event marked in yellow is the direct arrival, which has no information on the subsurface beyond the first layer and, hence, is removed from the data before imaging. The events marked with red are the primary reflection events, i.e., the events where the incident wavefield has undergone reflection once. The events marked in blue are the multiples, where the incident wavefield undergoes more than one reflection. In figure 1.3b, the areas marked within green triangles highlight background noises, more specifically correlation noise (solid triangle) and ground roll noise (dashed triangle), which need to be removed from the data before imaging is done. Some other noises that may be present in seismic data are ghost reflections, low-frequency and swell noise. In a conventional imaging flow, the data is processed to remove all the noises (to the best of the current technological ability), including the multiples, to leave only the

*Seismic experiments have also been carried out on the Moon (Kovach et al., 1971) and Mars.(Lognonné et al., 2019)

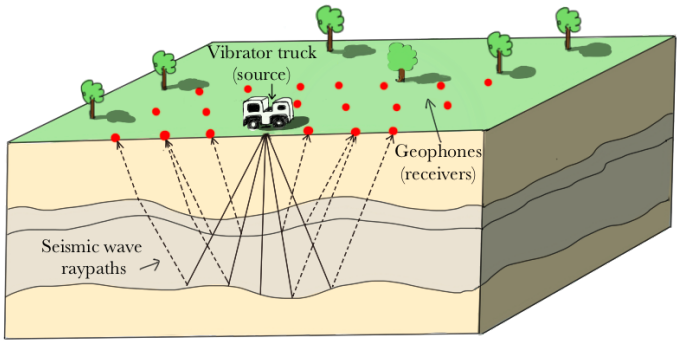

(a) *Land seismic survey*

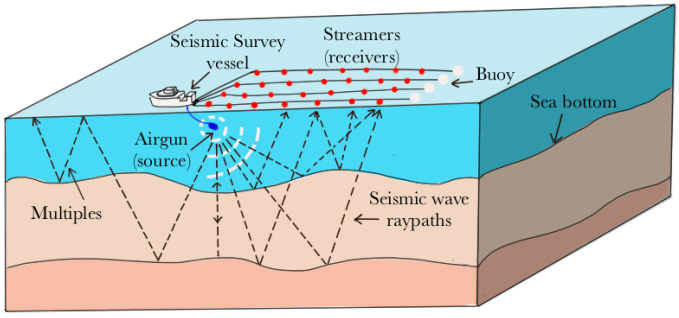

(b) *Marine seismic survey*

Figure 1.2 *Schematic diagram depicting the process of a seismic survey carried out in two different environments, land and marine.*

primary data (Yilmaz, 2001; Biondi, 2006). This primary data is then imaged to give us a primaries-only seismic image.

A basic seismic imaging process involves some processing to map the seismic data in vertical time or, using a subsurface propagation velocity model, map the seismic data in depth locations. This, however, leads to many errors caused by diffractors, dipping events and assuming an incorrect velocity. The process of *Migration* maps the dipping events to their right location and collapses the diffraction energy to the right diffractors (Yilmaz, 2001) using wave-propagation techniques along with imaging principles.

1.2. SHORT HISTORY

Ever since the active seismic data was confirmed to be correlated to reflections from the subsurface of the Earth, the Geophysics community has been constantly in pursuit of getting the best subsurface images via reflection seismology. Although the earlier methods until the 1930s made rather inaccurate assumptions such as wrong velocities, flat earth and non-existence of faults, they still generated enough interest for exploration

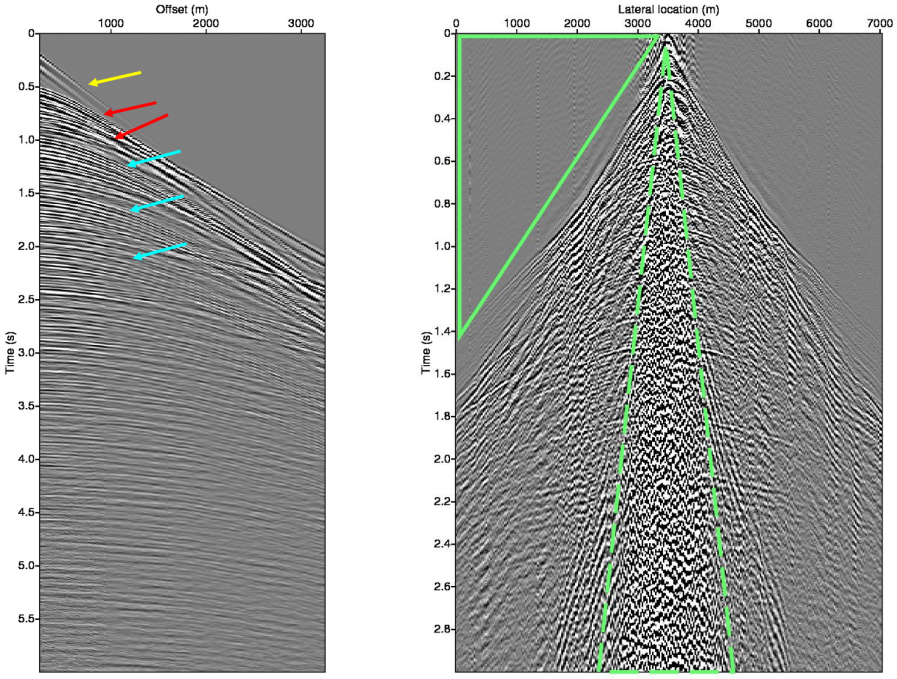

(a) *An example of marine seismic data.*

(b) *An example of land seismic data.*

Figure 1.3 *Examples of seismic data in land and marine environments represented as common shot gather (multiple receivers recording data generated by one source).*

services (Bednar, 2005).

Soon enough, seismic migration started being applied via mechanically migrating the seismic events via the principle of isochron mapping. These popular methods include zero-offset migration and slant-stack migration, which continue to be popular to this day. These methods started acknowledging the dips in the reflector but they had their limitations with noisy data, poor velocity information, and diffraction energy among others.

Hagedoorn (1954) used Huygens' principle to put forth the idea of equal travel time curves or wavefronts to find reflection surfaces. With the advent of digital computing, the common midpoint (CMP) stack (Mayne, 1962) became popular. A CMP stack takes data from a large survey containing data from non-zero offset data, applies a normal moveout correction (NMO) to the CMP gather, stacks the traces and produces an output image of zero offset 'unmigrated' traces at each midpoint location. A CMP stack result is quite stable and is still used as a baseline image to compare migration results (Gray, 2016). However, CMP stack images work under a flat-Earth assumption and, hence, provide unreliable results in areas with varying dips.

Around the 1960s, using computers for imaging became more commonplace. This made

way for the implementation of Hagedoorn's migration principle on a commercially viable scale. These were implemented by summation along a hyperbolic diffraction curve.

Claerbout (1970) introduced the one-way acoustic wave propagation instead of the full wave equation, in order to overcome the computational cost. Claerbout produced downgoing and up-going wavefields by approximately solving the differential equation in space. The method was used to extrapolate the source wavefield forward (in time) and the recorded wavefield backward (in time) for every depth. Claerbout (1971) thereby introduced imaging conditions based on the interaction between the upgoing and downgoing wavefields. The imaging condition states that *whenever an upgoing and downgoing wavefields meet, there must be a reflector*; or to put it in other words, computationally an image is formed when the downgoing and upgoing wavefields correlate with each other. Other variants involved transforming the data into frequency and wavenumber domain and extrapolating the recorded wavefield downward either in one leap (Stolt, 1978) or depth by depth by the phase shift method (Gazdag, 1978). While Claerbout (1970) described the one-way wave propagation using a finite difference approach, Berkhout (1982) described an integral approach of shot profile migration using his matrix formulation via the explicit convolution operator **W**.

Schneider (1978) used Green's third identity to produce wavefield at image locations from the recorded wavefield at the surface. This is popularly known as Kirchoff migration, which is similar to the diffraction summation mentioned above but corrected for phase and amplitude. Kirchoff migration method could be seen as a wave-equation compliant version of the Hagedoorn's principle from 1954. Gray (2016) describes the method and the development of the Kirchhoff method in further detail.

Hemon (1978) described a full-wavefield two-way equation for modelling and migration. It addressed the dip limitation of the one-way methods. In 1983, this was rediscovered as reverse-time migration(RTM) (Baysal et al., 1983; McMechan, 1983; Whitmore, 1983). RTM can also image prism waves and turning waves. However, because of high computational expense, this method only became popular around the 2000s.

Another major leap in imaging was the application of inverse theory to migration using least-squares migration (LSM). Nemeth et al. (1999) incorporated the iterative LSM in the Kirchoff migration method. LSM was further extended to include the one-way wave equation migration as described by Kühl and Sacchi (2003) or Kaplan et al. (2010). In this method, the observed data is simulated using a forward-modelling process for a given velocity model. The goal is to minimise the residual between the observed and modelled data at every iteration. The reflectivity model is updated in every iteration by applying the imaging principle on back propagated residual on the receiver side and forward propagated source wavefield on the source side until a minimum threshold is reached. Least-squares migration successfully improved the migration image by compensating for variable illumination issues or inadequate seismic acquisition. However, the performance of this method is dependent on a good velocity model and modelling parameters.

Figure 1.4 shows a comparison between imaging results from the standard open-loop primary wavefield migration (PWM) method (figure 1.4a) and a least-squares migration

method (figure 1.4a) (closed-loop PWM). The example is generated on a 5400-meter-wide and 1500-meter-deep synthetic model, similar to the model in Verschuur and Berkhout (2015). Receivers are placed throughout the surface at an interval of 20 m. Sources are kept on the surface with extremely coarse spacing, i.e., at 600 m, 1550 m, 2700 m, 3750 m and 4800 m, and the data is generated by finite-difference modelling. The latter result shows much better-imaged diffractions and improved resolution of the different subsurface layers.

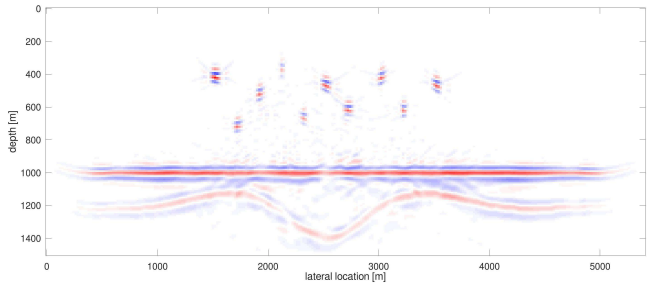

(a)

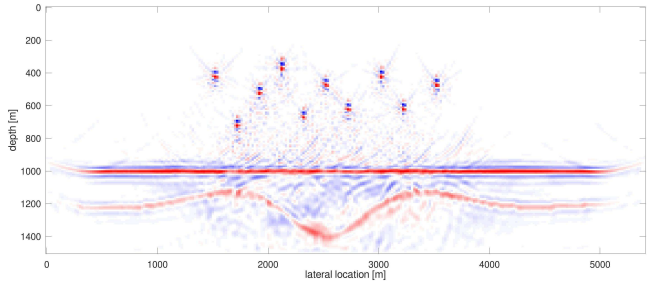

(b)

Figure 1.4 *Imaging results comparing a) standard imaging method using 'open-loop' primary wavefield migration vs b) least-squares migration (or closed-loop migration) using the same geometry.*

1.3. SEISMIC MULTIPLES

Multiples or *multiple reflections* are defined as seismic events that have undergone more than one order of reflection or scattering in the subsurface (Sheriff, 1991). Figure 1.5a shows how multiples are generated. Multiples can be classified broadly into two kinds:

- Free-surface multiple: A multiple that has undergone at least one downward reflection at the free surface.
- Internal multiple or interbed multiple: A multiple that has all of its reflections occurring beneath the surface.

Figure 1.5b depicts the different kinds of multiples. Figure 1.6 shows what multiples look like in post-stack data.

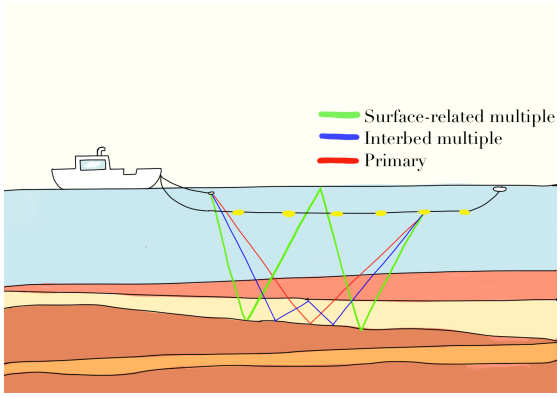

(a) *Cartoon depicting how multiples are generated*

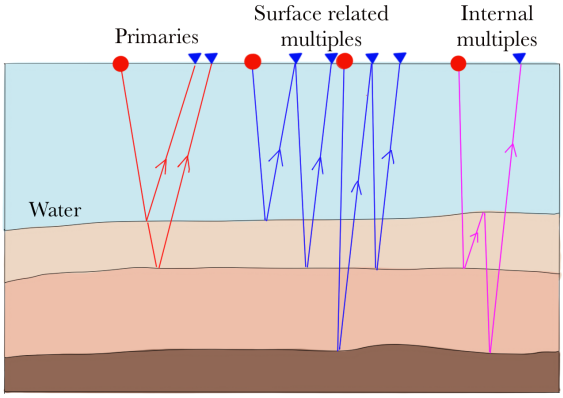

(b) *Kinds of multiples*

Figure 1.5 *Illustrations of primaries and multiples in terms of their wave paths.*

1.3.1. MULTIPLES AS NOISE

As earlier stated, Claerbout's imaging principle says, "reflectors exist at points in the Earth where the first arrival of the downgoing wave is time coincident with an upgoing wave" (Claerbout, 1971). However, imaging with multiples in the data while applying such traditional imaging principles leads to artefacts in the image when the multiple events coincide with the incident wavefield. Hence, traditionally, multiples have been deemed as noise as they lead to cross-talk in the image. Since free-surface/ surface-related multiples often tend to be much stronger than interbed multiples, they tend to obstruct the deeper image details, making them particularly problematic. Over the decades, several kinds of multiple-elimination techniques have been developed, most of them often focusing only on surface-related multiples. They can be categorised broadly as follows:

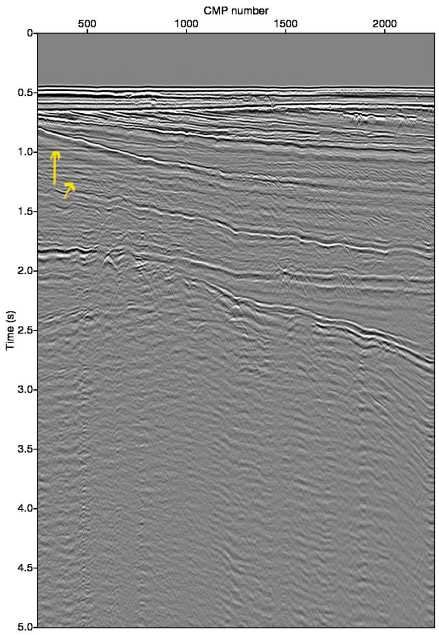

Figure 1.6 *A stack section depicting the free-surface multiples (yellow arrows).*

1. *By using the difference in geometric behaviour*; these methods rely on the difference in moveout between a primary and a multiple such as stacking, slant–stack (Treitel et al., 1982), f–k filtering (Embree et al., 1963; March & Bailey, 1983; Duncan & Beresford, 1994) and Radon filtering (Hampson, 1986; Foster & Mosher, 1992).

2. *Deconvolution-based suppression methods* that are based on periodicity or predictability of the multiples. These are predictive deconvolution (Lokshtanov, 1999) and multi-channel deconvolution (Morley & Claerbout, 1983; Lamont et al., 1999).

3. *Wavefield prediction and subtraction methods* such as model-based ones that extrapolate the measured wavefield down to the water-bottom and back up to the surface to predict the next order of multiples (Berryhill & Kim, 1986; Wiggins, 1988, 1999); or the popular data-driven method such as Surface related multiple elimination (SRME) (Verschuur et al., 1992) where the multiples are predicted by multi-dimensional convolution of the data that are subtracted adaptively from the original data (Berkhout & Verschuur, 1997; Verschuur & Berkhout, 1997).

4. *Inversion based methods* such as Estimating Primaries by Sparse Inversion (EPSI) (Van Groenestijn & Verschuur, 2009), robust-EPSI method (Lin & Herrmann, 2013) and Closed loop SRME (CL-SRME)(Lopez & Verschuur, 2014).

1.3.2. MULTIPLES AS SIGNAL

In recent years the consensus is changing about the utility of multiples. Multiples travel different paths compared to primaries and, therefore, can illuminate a wider area or shadow zones (Liu et al., 2011), this property can help in overcoming the limitations of the employed acquisition geometry (Berkhout & Verschuur, 1994; Guitton, 2002; Brown & Guitton, 2005; Muijs et al., 2007; Whitmore et al., 2010; Liu et al., 2011; Lu et al., 2013; Zhang & Schuster, 2014). Multiples also contain smaller reflection angles and therefore can aid in improved resolution of images (Berkhout & Verschuur, 2003). Berkhout (2012b) and Berkhout and Verschuur (2016) demonstrate these properties via an example of how with very few shots a subsurface is better illuminated along with better vertical resolution since multiples not only illuminate areas that are unreachable by the primaries but also contribute to the vertical resolution because of improved angular illumination. Therefore, methods need to be developed in order to utilise the benefits offered by the multiples.

Lately, a lot of focus has been put towards including multiples in the imaging methods as they potentially increase the migration aperture. Reiter et al. (1991) used primaries and multiples (receiver side ghost, after separation) from ocean bottom hydrophone data to image the subsurface by applying a Kirchhoff scheme. De Roeck et al. (2001) extended this method to surface data by model-based multiple imaging. Sheng (2001) applied cross-correlogram migration to CDP data in order to migrate multiples. Berkhout and Verschuur (1994) and Guitton (2002) migrate multiple reflection via a shot record migration scheme, Berkhout and Verschuur (2003) by transforming multiples into primary reflections, while Shan (2003) uses source-receiver depth migration to migrate multiple reflections.

As multiples are complex wavefields, the interference of upgoing and downgoing waves would still leave noise in the form of cross-talks in the image. Additionally imaging with multiples without separating the primaries would be the ideal way forward as it reduces an expensive additional step. Brown (2002) and He and Schuster (2003) tackled both these issues as they migrated multiples and primaries jointly using a least-squares method. Youn and Zhou (2001), Liu et al. (2011), and Fleury and Snieder (2011) used two-way wave equation-based reverse time migration after modifying it to image the multiple reflections. This method overcomes the angle limitations of one-way propagators and is typically used to target complex waves such as internal multiples. Whitmore et al. (2010) used dual-sensor towed streamer data to separate the up/downgoing components of a wavefield for multiple imaging. Malcolm et al. (2009) includes surface as well as internal (first-order) multiples via one-way wave propagators, while Berkhout (2012a), Davydenko (2016), and Davydenko and Verschuur (2017) further developed this concept by including all orders of multiples in Full Wavefield Migration scheme.

Tarantola (1984) brought about Full Waveform Inversion (FWI) that simultaneously aimed to invert the whole data as an inversion step to explain the subsurface properties. FWI generates a high-resolution velocity model. Brown and Guitton (2005) devised a least-squares inversion method that inverted the primaries and the multiples simultaneously (LSJIMP) to get the reflection image of the subsurface. Efforts at multiple migration using

seismic interferometry have also been made (Sheng, 2001; Yu & Schuster, 2002; Schuster et al., 2004; Jiang et al., 2005).

1.3.3. FULL WAVEFIELD MIGRATION

For the course of this work, we shall engage ourselves with the one-way propagators for imaging with the multiples and follow the Full Wavefield Migration (FWM) approach (Berkhout, 2014b). FWM uses Full wavefield modelling (FWMod) (Berkhout, 2014a) to generate its forward-modelled data. FWMod includes scattering and transmission effects and, therefore, helps with the migration of the primaries, surface and internal multiples as it generates total reflection data. In FWM, the velocity model is given and the reflectivity model is generated iteratively in a closed-loop least-squares method until the modelled data fits the measured data. The least-squares method helps eliminate the cross-talk generated via multiples in imaging. FWM re-injects the measured wavefield as the corresponding source for the surface multiples. This includes the surface multiples in an imaging mechanism; simultaneously while performing primaries-only imaging with the original source wavefield. This helps in migrating primaries as well as the surface-related multiples by establishing a linear relationship between the surface multiples and their sub-event primaries. This obviously eliminates the need for multiple removal. This method can also be used to also migrate only the surface-related multiples by using just the re-injected measured data as the source and the recorded surface-related multiples as the measured data. In that case, primaries will be treated as noise and should actually be removed from the data. Since the measured data is used both as incident and reflected field, calibration of source wavelets would no longer be necessary (Davydenko & Verschuur, 2017). Naturally, as mentioned earlier, since multiples travel different paths compared to the primaries, using multiples in imaging FWM also performs well in data with small gaps in acquisition. However, since this method relies on the reinjection of recorded data as incident wavefield, it is assumed that the complete downgoing wavefield (with some gaps) has been recorded. Thus, for the area under large gaps, current methods have been incapable of exploiting the power of multiple scattering. This calls for alternative imaging strategies that make the most out of the available data to mitigate this problem.

1.4. THESIS OBJECTIVE

In my thesis, we extend the least-squares migration method for primaries (Nemeth et al., 1999) or multiples (Brown & Guitton, 2005; Zhang & Schuster, 2014; Liu et al., 2016; Davydenko & Verschuur, 2017) to overcome incomplete data issues specifically by focusing on exploiting surface multiples in various ways.

I hereby present a 'non-linear' imaging scheme that compensates for unrecorded data by synthetically modelling all the surface-related multiples, starting from the original source wavefield. I examine the dependence of this method on receiver geometry and its ability to allow us to overcome large acquisition gaps. This method relates to the model-based multiple imaging methods proposed by Jiang et al. (2007), except with an iterative closed-loop approach.

I further combine the existing 'linear' methods along with our proposed 'non-linear' imaging scheme in a hybrid method in order to exploit the benefits of both methods. In my work, we only concern the use of surface-related multiples in imaging. However, the forward model that we describe can be extended to include internal multiples (Berkhout, 2014a; Davydenko & Verschuur, 2017).

1.5. CONTRIBUTIONS AND THESIS OVERVIEW

List of original contributions done in this thesis:

- A 'non-linear' imaging method is proposed, that models all the wavefields (primaries and multiples) iteratively starting from the original source wavefield. The performance and the limits of this method are tested on synthetic data.
- The benefit provided by the non-linear imaging method to fill the imaging gaps due to gaps from data acquisition is investigated. The capability of this method on synthetic as well as field data with large data gaps is also verified.
- A hybrid imaging method that combines the linear and the non-linear imaging methods is introduced. The effectiveness of these methods has been tested for both synthetic and field data from streamer acquisition and ocean-bottom node (OBN) acquisition.
- A novel way of implementing the non-linear imaging method on OBN data has been formulated. This method includes all the orders of multiples in imaging.

Here I summarise a chapter-wise outline of this thesis:

- **Chapter 2**: In this chapter, the theory behind using multiples in imaging via Full wavefield migration is described. The notation that would be used throughout the thesis is described here. The wavefield modelling algorithm is explained for both primaries and multiples. Full Wavefield Modelling that we use in our migration algorithms is elaborated upon. Further, migration with primaries only, multiples only, and primaries and multiples in a 'linear' inversion scheme is described. A 'non-linear' migration method is introduced, where the multiples are modelled in a non-linear fashion. The performance of the various imaging methods is compared via illustrative examples.
- **Chapter 3**: Large gaps may arise in the data due to many reasons. In this chapter, the different imaging options in the case of data with large gaps are explored. The virtue of imaging with multiples is shown in this scenario and the added capability of the non-linear imaging method is shown. A hybrid method that combines the benefits of both the linear as well as non-linear imaging methods is introduced in this chapter. The sequence of combining the imaging methods in a hybrid method depends on the imaging scenario. The performance of the different imaging methods is compared via a synthetically generated example.
- **Chapter 4**: For this chapter, we further compare the performance of the different methods described in the previous chapters in overcoming large data gaps through various 2D and 3D examples. First, we test the methods on numerically generated

2D data; this also includes an example where we explore data around an island. We then test our methods on 2D data from Saga Vøring basin. Finally, we implement our methods on a 3D synthetic streamer data, generated to mimic OBN type acquisition, i.e., few sources but dense receiver carpet. Through these examples, we see the benefit of using multiples in improving our migration output.

- **Chapter 5**: In this chapter, we explore imaging with multiples on data acquired using ocean-bottom nodes (OBN). We thereby introduce a new strategy to implement the non-linear imaging method for OBN data. We compare our various methods of using surface-related multiples in an OBN acquisition scenario with the mirror imaging method to test the benefits of using higher-order multiples. To demonstrate this, we use a 2D numerically generated OBN data as an example.
- **Chapter 6**: In this chapter, we summarise the work done in this thesis and the conclusions derived from it. We also suggest recommendations for future works that continue and develop our findings.

BIBLIOGRAPHY

Båth, M. (1966). Earthquake seismology. *Earth-Science Reviews, 1*(1), 69–86.

Baysal, E., Kosloff, D., & Sherwood, J. (1983). Reverse time migration. *Geophysics, 48*(11), 1514–1524.

Bednar, J. (2005). A brief history of seismic migration. *Geophysics, 70*(3), 3MJ–20MJ.

Berkhout, A. (1982). *Seismic migration, imaging of acoustic energy by wave field extrapolation, A: Theoretical aspects*. Elsevier (second edition).

Berkhout, A. (2012a). Combining full wavefield migration and full waveform inversion, a glance into the future of seismic imaging. *Geophysics, 77*(2), S43–S50.

Berkhout, A. (2012b). *Seismic migration: Imaging of acoustic energy by wave field extrapolation*. Elsevier.

Berkhout, A. (2014a). An outlook on the future of seismic imaging, part I : Forward and reverse modelling. *Geophysical Prospecting, 62*, 911–930.

Berkhout, A. (2014b). An outlook on the future of seismic imaging, part II : Full-wavefield migration. *Geophysical Prospecting, 62*(5), 931–949.

Berkhout, A., & Verschuur, D. (1994). Multiple technology: Part 2, migration of multiple reflections. In *SEG technical program expanded abstracts 1994* (pp. 1497–1500). Society of Exploration Geophysicists.

Berkhout, A., & Verschuur, D. (1997). Estimation of multiple scattering by iterative inversion, part i: Theoretical considerations. *Geophysics, 62*(5), 1586–1595.

Berkhout, A., & Verschuur, D. (2003). Transformation of multiples into primary reflections. In *SEG technical program expanded abstracts 2003* (pp. 1925–1928). Society of Exploration Geophysicists.

Berkhout, A., & Verschuur, D. (2016). Enriched seismic imaging by using multiple scattering. *The Leading Edge, 35*(2), 128–133.

Berryhill, J., & Kim, Y. (1986). Deep-water peg legs and multiples: Emulation and suppression. *Geophysics, 51*(12), 2177–2184.

Biondi, B. L. (2006). *3D seismic imaging*. Society of Exploration Geophysicists.

Bjorlykke, K. (2010). *Petroleum geoscience: From sedimentary environments to rock physics*. Springer Science & Business Media.

Brown, M. (2002). Least-squares joint imaging of primaries and multiples. In *SEG technical program expanded abstracts 2002* (pp. 890–893). Society of Exploration Geophysicists.

Brown, M., & Guitton, A. (2005). Least-squares joint imaging of multiples and primaries. *Geophysics, 70*(5), S79–S89.

Carcione, J. M., Picotti, S., Gei, D., & Rossi, G. (2006). Physics and seismic modeling for monitoring CO2 storage. *Pure and Applied Geophysics, 163*(1), 175–207.

Claerbout, J. (1970). Coarse grid calculations of waves in inhomogeneous media with application to delineation of complicated seismic structure. *Geophysics*, *35*(3), 407–418.

Claerbout, J. (1971). Toward a unified theory of reflector mapping. *Geophysics*, *36*(3), 467–481.

Davydenko, M. (2016). Full wavefield migration: Seismic imaging using multiple scattering effects. *(Doctoral Dissertation)*.

Davydenko, M., & Verschuur, D. (2017). Full-wavefield migration: Using surface and internal multiples in imaging. *Geophysical Prospecting*, *65*(1), 7–21.

De Roeck, Y.-H., Cognet, J.-M., Chavent, G., & Clement, F. (2001). Free surface multiple removing via iterative prestack migration. *63rd EAGE Conference & Exhibition*, Article cp-15-00304.

Dondurur, D. (2018). Chapter 2 - marine seismic data acquisition. In D. Dondurur (Ed.), *Acquisition and processing of marine seismic data* (pp. 37–169). Elsevier.

Duncan, G., & Beresford, G. (1994). Slowness adaptive fk filtering of prestack seismic data. *Geophysics*, *59*(1), 140–147.

Embree, P., Burg, J., & Backus, M. (1963). Wide-band velocity filtering—the pie-slice process. *Geophysics*, *28*(6), 948–974.

Fleury, C., & Snieder, R. (2011). Reverse-time-migration of multiply scattered seismic waves. In *SEG technical program expanded abstracts 2011* (pp. 3382–3387). Society of Exploration Geophysicists.

Foster, D. J., & Mosher, C. C. (1992). Suppression of multiple reflections using the radon transform. *Geophysics*, *57*(3), 386–395.

Gazdag, J. (1978). Wave equation migration with the phase-shift method. *Geophysics*, *43*(7), 1342–1351.

Gray, S. H. (2016). Seismic imaging. In *Encyclopedia of exploration geophysics* (S1–1). Society of Exploration Geophysicists.

Guitton, A. (2002). Shot-profile migration of multiple reflections. In *SEG technical program expanded abstracts 2002* (pp. 1296–1299). Society of Exploration Geophysicists.

Hagedoorn, J. (1954). A process of seismic reflection interpretation. *Geophysical prospecting*, *2*(2), 85–127.

Hampson, D. (1986). Inverse velocity stacking for multiple elimination. In *SEG technical program expanded abstracts 1986* (pp. 422–424). Society of Exploration Geophysicists.

He, R., & Schuster, G. (2003). Least-squares migration of both primaries and multiples. In *SEG technical program expanded abstracts 2003* (pp. 1035–1038). Society of Exploration Geophysicists.

Hemon, C. (1978). Equations d'onde et modeles. *Geophysical prospecting*, *26*(4), 790–821.

Jensen, J. (2007). Medical ultrasound imaging. *Progress in biophysics and molecular biology*, *93*(1-3), 153–165.

Jiang, Z., Sheng, J., Yu, J., Schuster, G., & Hornby, B. (2007). Migration methods for imaging different-order multiples. *Geophysical Prospecting*, *55*(1), 1–19.

Jiang, Z., Yu, J., Schuster, G., & Hornby, B. (2005). Migration of multiples. *The Leading Edge*, *24*(3), 315–318.

Kaplan, S., Routh, P., & Sacchi, M. (2010). Derivation of forward and adjoint operators for least-squares shot-profile split-step migration. *Geophysics*, *75*(6), S225–S235.

Kovach, R. L., Watkins, J. S., & Landers, T. (1971). Active seismic experiment. *Apollo 14 Preliminary Science Report*, 163–174.

Kühl, H., & Sacchi, M. (2003). Least-squares wave-equation migration for avp/ava inversion. *Geophysics*, *68*(1), 262–273.

Lamont, M., Hartley, B., & Uren, N. (1999). Multiple attenuation using the mmo and isr preconditioning transforms. *The Leading Edge*, *18*(1), 110–114.

Lin, T. T., & Herrmann, F. J. (2013). Robust estimation of primaries by sparse inversion via one-norm minimization. *Geophysics*, *78*(3), R133–R150.

Liu, Y., Chang, X., Jin, D., He, R., Sun, H., & Zheng, Y. (2011). Reverse time migration of multiples for subsalt imaging. *Geophysics*, *76*(5), WB209–WB216.

Liu, Y., Liu, X., Osen, A., Shao, Y., Hu, H., & Zheng, Y. (2016). Least-squares reverse time migration using controlled-order multiple reflections. *Geophysics*, *81*(5), S347–S357.

Lognonné, P., Banerdt, W. B., Giardini, D., Pike, W. T., Christensen, U., Laudet, P., De Raucourt, S., Zweifel, P., Calcutt, S., Bierwirth, M., et al. (2019). SEIS: Insight's seismic experiment for internal structure of mars. *Space Science Reviews*, *215*(1), 1–170.

Lokshtanov, D. (1999). Multiple suppression by data-consistent deconvolution. *The Leading Edge*, *18*(1), 115–119.

Lopez, G., & Verschuur, D. (2014). Closed-loop srme-a new direction in surface multiple removal algorithms. *76th EAGE Conference and Exhibition 2014*, *2014*(1), 1–5.

Lu, S., Whitmore, N., & Valenciano, A. (2013). Challenges and opportunities in 3d imaging of sea surface related multiples. In *SEG technical program expanded abstracts 2013* (pp. 4111–4115). Society of Exploration Geophysicists.

Malcolm, A., Ursin, B., & De Hoop, M. (2009). Seismic imaging and illumination with internal multiples. *Geophysical Journal International*, *176*(3), 847–864.

March, D., & Bailey, A. (1983). A review of the two-dimensional transform and its use in seismic processing. *First break*, *1*(1).

Martin, R., Harris, B., & Martin, R. (2013). High resolution seismic reflection for hydrogeology-where is the value? *ASEG Extended Abstracts*, *2013*(1), 1–4.

Mayne, W. H. (1962). Common reflection point horizontal data stacking techniques. *Geophysics*, *27*(6), 927–938.

McMechan, G. (1983). Migration by extrapolation of time-dependent boundary values. *Geophysical prospecting*, *31*(3), 413–420.

Morley, L., & Claerbout, J. (1983). Predictive deconvolution in shot-receiver space. *Geophysics*, *48*(5), 515–531.

Muijs, R., Robertsson, J., & Holliger, K. (2007). Prestack depth migration of primary and surface-related multiple reflections: Part II :identification and removal of residual multiples. *Geophysics*, *72*(2), S71–S76.

Nemeth, T., Wu, C., & Schuster, G. (1999). Least-squares migration of incomplete reflection data. *Geophysics*, *64*(1), 208–221.

Reiter, E. C., Toksöz, M. N., Keho, T. H., & Purdy, G. (1991). Imaging with deep-water multiples. *Geophysics*, *56*(7), 1081–1086.

Schneider, W. (1978). Integral formulation for migration in two and three dimensions. *Geophysics*, *43*(1), 49–76.

Schuster, G., Yu, J., Sheng, J., & Rickett, J. (2004). Interferometric/daylight seismic imaging. *Geophysical Journal International*, *157*(2), 838–852.

Shan, G. (2003). Source-receiver migration of multiple reflections. In *SEG technical program expanded abstracts 2003* (pp. 1008–1011). Society of Exploration Geophysicists.

Sheng, J. (2001). Migrating multiples and primaries in cdp data by crosscorrelogram migration. In *SEG technical program expanded abstracts 2001* (pp. 1297–1300). Society of Exploration Geophysicists.

Sheriff, R. (1991). Encyclopedic dictionary of exploration geophysics: Soc. *Expl. Geophys*.

Spiegel, P. K. (1995). The first clinical x-ray made in america–100 years. *AJR. American journal of roentgenology*, *164*(1), 241–243.

Stolt, R. (1978). Migration by fourier transform. *Geophysics*, *43*(1), 23–48.

Tarantola, A. (1984). Inversion of seismic reflection data in the acoustic approximation. *Geophysics*, *49*(8), 1259–1266.

Treitel, S., Gutowski, P., & Wagner, D. (1982). Plane-wave decomposition of seismograms. *Geophysics*, *47*(10), 1375–1401.

Van Groenestijn, G., & Verschuur, D. (2009). Estimating primaries by sparse inversion and application to near-offset data reconstruction. *Geophysics*, *74*(3), A23–A28.

Verschuur, D., & Berkhout, A. (1997). Estimation of multiple scattering by iterative inversion, part ii: Practical aspects and examples. *Geophysics*, *62*(5), 1596–1611.

Verschuur, D., & Berkhout, A. (2015). From removing to using multiples in closed-loop imaging. *The Leading Edge*, *34*(7), 744–759.

Verschuur, D., Berkhout, A., & Wapenaar, C. (1992). Adaptive surface-related multiple elimination. *Geophysics*, *57*(9), 1166–1177.

Whitmore, N. (1983). Iterative depth migration by backward time propagation. In *SEG technical program expanded abstracts 1983* (pp. 382–385). Society of Exploration Geophysicists.

Whitmore, N., Valenciano, A., Sollner, W., & Lu, S. (2010). Imaging of primaries and multiples using a dual-sensor towed streamer. In *SEG technical program expanded abstracts 2010* (pp. 3187–3192). Society of Exploration Geophysicists.

Wiggins, J. (1988). Attenuation of complex water-bottom multiples by wave-equation-based prediction and subtraction. *Geophysics*, *53*(12), 1527–1539.

Wiggins, J. (1999). Multiple attenuation by explicit wave extrapolation to an interpreted horizon. *The Leading Edge*, *18*(1), 46–54.

Yilmaz, Ö. (2001). *Seismic data analysis: Processing, inversion, and interpretation of seismic data*. Society of exploration geophysicists.

Youn, O., & Zhou, H. (2001). Depth imaging with multiples. *Geophysics*, *66*(1), 246–255.

Yu, J., & Schuster, G. (2002). Joint migration of primary and multiple reflections in rvsp data. In *SEG technical program expanded abstracts 2002* (pp. 2373–2376). Society of Exploration Geophysicists.

Zhang, D., & Schuster, G. (2014). Least-squares reverse time migration of multiples. *Geophysics*, *79*(1), S11–S21.

2

FULL WAVEFIELD MIGRATION: LINEAR AND NON-LINEAR IMAGING

*

The full wavefield migration (FWM) algorithm combines primaries and multiples and has shown significant improvement in the imaging results compared to the conventional migration algorithms that consider primaries only. The FWM implements a closed-loop least-squares method that helps in avoiding the crosstalk noise arising from imaging with a multi-scattering wavefield. This chapter describes the theory behind how FWM includes multiples in migration. We describe forward and inverse wavefield extrapolation that forms the backbone of our wavefield modelling algorithm - Full Wavefield Modelling (FWMod). This modelling method is used to perform the FWM. Lastly, we introduce a non-linear migration method, where the multiples are modelled in a non-linear fashion.

2.1. NOTATION

For our modelling and imaging algorithms, we use the discrete matrix notation given by Berkhout (1982). The vector $\vec{P}^{\pm}(z_m,\omega)$ for frequency ω is the monochromatic *pressure wavefield* in the frequency domain measured at depth level z_m. The superscripts + and − represent the upgoing and downgoing directions of the wavefield, respectively. For a 3D scenario, each element of this vector denotes the monochromatic pressure value at different grid locations $x_k, k = 1,2,..X_m$ and $y_l, l = 1,2,..Y_m$ of the same horizontal subsurface depth location z_m, $P^{\pm}(x_k, y_l, z_m, \omega)$. The acoustic monochromatic pressure $\vec{P}(z,\omega)$ at the depth z can therefore be described as:

$$\vec{P}(z,\omega) = [P(x_1,y_1,z,\omega)\cdots P(x_{N_x},y_1,z,\omega)|P(x_1,y_2,z,\omega)\cdots P(x_{N_x},y_2,z,\omega)| \\ P(x_1,y_{N_y},z,\omega)\cdots P(x_{N_x},y_{N_y},z,\omega)]^T. \quad (2.1)$$

*A part of this chapter has been published in Nath and Verschuur (2020)

The 2D representation of equation 2.1 will thus be:

$$\vec{P}(z,\omega) = \begin{bmatrix} P(x_1,z,\omega) \\ P(x_2,z,\omega) \\ \vdots \\ P(x_{N_x},z,\omega) \end{bmatrix}. \tag{2.2}$$

For our convenience a monochromatic wavefield $\vec{P}^{\pm}(z_m,\omega)$ will be referred to as $\vec{P}^{\pm}(z_m)$.

The *wavefield propagation operator*, matrix $\mathbf{W}^{\pm}(z_m;z_n)$ connects the wavefields between two levels z_m and z_n. It denotes a monochromatic one-way forward wavefield propagation operator that extrapolates the wavefield from depth level z_n to z_m. The superscripts $+$ and $-$ describe downward and upward propagation, respectively. $G(x_j,z_m;x_i,z_n)$ is the 2D and $G(x_j,y_q,z_m;x_i,y_p,z_n)$ is the 3D Green's function describing the impulse response at a spatial location x_j,z_m (or x_j,y_q,z_m for 3D) for a source at x_i,z_n (or x_i,y_p,z_n for 3D).

For propagation in a 2D space, an element in the i^{th} column and the j^{th} row of the propagation matrix is given via the following relation (Wapenaar, 2014):

$$[\mathbf{W}^{\pm}(z_m;z_n)]_{ji} = \pm 2\frac{1}{\rho(x_i,z_n)}\frac{\delta G(x_j,z_m;x_i,z_n)}{\delta z}; \tag{2.3}$$

where $\rho(x_i,z_n)$ signifies the volume density at location x_i,z_n. For a 3D space, and element in the i^{th} column and the j^{th} row of the propagation sub-matrix $[W^{\pm}_{q,p}(z_m;z_n)]$, is represented by (Kinneging et al., 1989):

$$[\mathbf{W}^{\pm}_{q,p}(z_m;z_n)]_{ji} = \pm 2\frac{1}{\rho(x_i,y_p,z_n)}\frac{\delta G(x_j,y_q,z_m;x_i,y_p,z_n)}{\delta z}, \tag{2.4}$$

where q and p represent the y coordinates y_q and y_p at depth $z=z_m$ and z_n, respectively and $\rho(x_i,y_p,z_n)$ denotes the volume density at location x_i,y_p,z_n. Therefore, we represent the propagation matrix $\mathbf{W}^{\pm}(z_m;z_n)$ as:

$$\mathbf{W}^{\pm}(z_m;z_n) = \begin{bmatrix} \mathbf{W}^{\pm}_{1,1}(z_m;z_n) & \mathbf{W}^{\pm}_{1,2}(z_m;z_n) & \cdots & \mathbf{W}^{\pm}_{1,Y_n}(z_m;z_n) \\ \mathbf{W}^{\pm}_{2,1}(z_m;z_n) & \mathbf{W}^{\pm}_{2,2}(z_m;z_n) & \cdots & \mathbf{W}^{\pm}_{2,Y_n}(z_m;z_n) \\ \vdots & \vdots & \ddots & \cdot \\ \mathbf{W}^{\pm}_{Y_m,1}(z_m;z_n) & \mathbf{W}^{\pm}_{Y_m,2}(z_m;z_n) & \cdots & \mathbf{W}^{\pm}_{Y_m,Y_n}(z_m;z_n) \end{bmatrix}. \tag{2.5}$$

$\mathbf{W}^{\pm}(z_m;z_n)$ can be seen as the spatial-impulse response at depth level z_m due to a spatial impulse at depth level z_n. This propagation matrix can also be written as a product of sub-matrices:

$$\mathbf{W}^{+}(z_m;z_0) = \prod_{n=0}^{m-1}\mathbf{W}^{+}(z_{n+1};z_n), \tag{2.6}$$

meaning recursive wavefield extrapolations across all intermediate depth levels. It follows from equation 2.3 and 2.4, that for a vertically invariant medium, $\mathbf{W}^{\pm}(z_m; z_n)$ in the wavenumber-frequency domain can be written as a phase shift operator (Gazdag, 1978; Wapenaar et al., 1989):

$$W^{\pm}(k_x, k_y, z_m; z_n) = e^{-jk_z|z_m - z_n|}. \tag{2.7}$$

The reflectivity operator $\mathbf{R}^{\cup}(z_m)$ is a matrix that refers to the reflectivity values at a certain boundary, situated at depth z_m (Berkhout, 1982; Davydenko & Verschuur, 2017). For a locally reacting boundary (angle-independent reflection), the matrix is a diagonal matrix with each diagonal element $R_{i,i}(z_m)$ denoting the angle-independent reflectivity at grid location x_i of depth z_m. A superscript $\cap$ or $\cup$ refers to the reflection from below and above a boundary, respectively. For angle-dependent reflections, each column of $\mathbf{R}^{\cup}(z_m)$ describes a spatial convolution operator that produces angle-dependent reflection. Angle-dependent parameterisation will be further discussed in appendix A.

2.2. FORWARD MODELLING

Accurate modelling of seismic wave propagation is an essential component of a seismic imaging or inversion algorithm. A modelling algorithm should provide a close enough explanation for the various complex phenomena that arise in the earth model for it to be helpful in an imaging method. Except for random noise, any modelling scheme that fails to represent the events in the data will lead to sub-optimal imaging results. For example, omitting converted waves in modelling may lead to a loss of information regarding certain geological structures like salt bodies in the final image. Furthermore, not modelling multiples during imaging leads to cross-talk in the imaging results. For different kinds of modelling methods, the reader is directed to Carcione et al. (2002).

FWMod is an operator-driven algorithm that uses an integral equation for describing the seismic wavefield (Berkhout, 2014a). The choice of this forward modelling is driven by the fact that it does not require detailed elastic subsurface information. Instead, propagation operators defined by a macro velocity model and scattering operators defined by the reflectivity model, describing the subsurface response are used, which is considered sufficient for the migration process.

2.2.1. WAVEFIELD MODELLING FOR PRIMARIES ONLY

In primary wavefield modelling, the propagation of downgoing wavefield forward extrapolation to depth level z_m is given by:

$$\vec{P}^{+}(z_m) = \mathbf{W}^{+}(z_m; z_0)\vec{S}^{+}(z_0) \tag{2.8}$$

and the upgoing reflected wavefield at z_m is given by:

$$\vec{P}_0^{-}(z_m) = \sum_{n>m}^{m} \mathbf{W}^{-}(z_{n-1}, z_n)\mathbf{R}^{\cup}(z_n)\vec{P}^{+}(z_n). \tag{2.9}$$

Here $\vec{S}^{+}(z_0)$ represents a downgoing source wavefield leaving the surface z_0, $\mathbf{W}^{+}$ and $\mathbf{W}^{-}$ are the downgoing and upgoing propagation operators, respectively, and $\vec{P}_0^{-}(z_m)$ is the

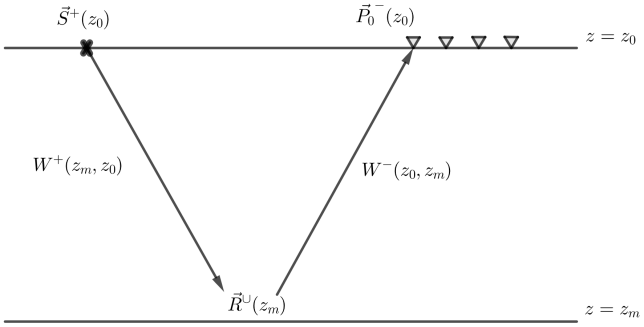

Figure 2.1 *Schematic representation of wavefield modelling for a seismic experiment showing primaries only, using the matrix notation. Image reproduced from (Kinneging et al., 1989).*

primary upgoing wavefield at depth z_m. Since we model only the first-order reflections or primary reflections, the forward model is linear with respect to the reflectivity $\mathbf{R}^{\cup}(z_n)$. Figure 2.1 shows a schematic representation of a primaries-only wavefield modelling in a seismic experiment. The Source wavefield $\vec{S}^{+}(z_0)$ propagates downwards, shown by the wavefield extrapolation matrix $\mathbf{W}^{+}(z_m; z_0)$. The wavefield is reflected upwards at different subsurface locations, denoted by the reflectivity matrix $\mathbf{R}^{\cup}(z_m)$. This is propagated back to the surface using the upward extrapolation matrix $\mathbf{W}^{-}(z_0, z_m)$, which results in the primaries only wavefield $\vec{P}_0^{-}(z_0)$ at the surface.

2.2.2. WAVEFIELD MODELLING WITH SURFACE-RELATED MULTIPLES

Given a certain propagation and scattering model, surface-related multiples can be generated in two ways: By re-injecting the measured wavefield at the surface or by modelling every order of reflection from the initial source wavefield.

SURFACE-RELATED MULTIPLES VIA RE-INJECTION OF MEASURED WAVEFIELD

In order to include surface-related multiples in the forward model via the re-injection method, some modifications are made to the incident wavefield as mentioned in equation 2.8 (Verschuur & Berkhout, 2011). We replace the primary source wavefield as mentioned in section 2.2.1 with the re-injected total measured wavefield. These act as virtual sources for higher (> 1) order of reflections. The downgoing extrapolation of the re-injected wavefields is given by:

$$\vec{M}^{+}(z_m) = \mathbf{W}^{+}(z_m; z_0)\mathbf{R}^{\cap}(z_0)\vec{P}^{-}(z_0), \tag{2.10}$$

where $\mathbf{R}^{\cap}(z_0)$ refers to the downward reflectivity operator at the surface z_0, usually taken as $\mathbf{R}^{\cap}(z_0) = -\mathbf{I}$ (Verschuur & Berkhout, 2011), which transforms the total upgoing measured wavefield $\vec{P}^{-}(z_0)$ to the (re-injected) downgoing wavefield $\mathbf{R}^{\cap}(z_0)\vec{P}^{-}(z_0)$. $\vec{M}^{+}(z_m)$ refers to the downgoing wavefield at depth z_m generated because of surface reflection. This re-injected measured wavefield is then forward extrapolated at every depth level. The upgoing reflected surface-related multiple wavefield $\vec{M}^{-}(z_m)$ at depth z_m is given

by:

$$\vec{M}^{-}(z_m) = \sum_{n=m+1}^{M} \mathbf{W}^{-}(z_m, z_n)\mathbf{R}^{\cup}(z_n)\vec{M}^{+}(z_n). \tag{2.11}$$

For preserving the linear relationship in our forward model here, we only model the surface-related multiples and not the internal multiples. However, if we use the full wavefield migration (Berkhout, 2014b), internal multiples can also be included.

Now including both the primaries and surface-related multiples in the linear forward-modelling scheme together would simply require combining the two incident wavefields mentioned in equation 2.8 and equation 2.10. We refer to this as the total downgoing wavefield $\vec{Q}^{+}(z_0)$, which is given by:

$$\vec{Q}^{+}(z_0) = \vec{S}^{+}(z_0) + \mathbf{R}^{\cap}(z_0)\vec{P}^{-}(z_0). \tag{2.12}$$

Using a similar principle as described in equation 2.11, we can simultaneously generate both primaries and multiples at each depth level as given by:

$$\vec{P}^{-}(z_m) = \sum_{n=m+1}^{M} \mathbf{W}^{-}(z_0, z_n)\mathbf{R}^{\cup}(z_n)\vec{Q}^{+}(z_n). \tag{2.13}$$

Therefore, we get a final recorded wavefield at the surface through the following:

$$\vec{P}^{-}(z_0) = \vec{P}_0^{-}(z_0) + \vec{M}^{-}(z_0); \tag{2.14}$$

$$= \sum_{n=m+1}^{M} \mathbf{W}^{-}(z_0, z_n)\mathbf{R}^{\cup}(z_n)\vec{Q}^{+}(z_n). \tag{2.15}$$

Note that, in this method, we only generate one extra round trip of each recorded wavefield. Generating multiples via re-injection leads to a linear relationship between the reflectivity and the forward model, similar to modelling primaries-only data. Since we use the recorded wavefield as the incident wavefield, the performance of this method is dependent on good receiver coverage and density.

SURFACE-RELATED MULTIPLES BY MODELLING EVERY ORDER OF MULTIPLE

Another way of modelling the data could be by starting from the primary source wavefield, generating every reflection event, primary and surface multiples, with increasing iterations. In this method, all the surface-related multiples are included incrementally in the incident wavefield using the modelled upgoing wavefield (Berkhout & Verschuur, 2014) leading to a non-linear relationship between reflectivity and the forward model. Since this method omits the reinjection of measured data to describe the multiples in the forward model, it will be less affected by missing data.

In this method, we forward model with $\vec{S}^{+}(z_0)$ as our initial incident wavefield. In subsequent iterations, we modify the downgoing wavefield $[\vec{Q}^{+}(z_0)]^{i}$ such that it generates the modelled surface multiples, based on re-injection of the *modelled* upgoing wavefield $\vec{P}_m^{-}(z_0, z_0)$ from the previous iteration. Therefore $[\vec{Q}^{+}(z_0)]^{i}$ is given by:

$$[\vec{Q}^{+}(z_0)]^{i} = \vec{S}^{+}(z_0) + \mathbf{R}^{\cap}(z_0)[\vec{P}_m^{-}(z_0, z_0)]^{i-1}, \tag{2.16}$$

where i refers to the iteration number. Similar to equation 2.13, the total upgoing wavefield for a given iteration i, at a depth z_m, can thus be derived as

$$[\vec{P}^{-}(z_m)]^{i} = \sum_{n=m+1}^{M} \mathbf{W}^{-}(z_0, z_n)\mathbf{R}^{\cup}(z_n)[\vec{Q}^{+}(z_n, z_0)]^{i}. \tag{2.17}$$

2.3. REVERSE MODELLING

For the purpose of migration, it is also essential to redatum the data that is measured at the surface to every grid location in depth within the sub-surface in order to get a migrated image in those locations after applying an imaging condition. For iterative migration, instead of redatuming the measured data, we redatum the data residual i.e., the difference between the measured data at the surface and the modelled data from the previous iteration. This can be achieved via full wavefield reverse modelling. In the case of primary wavefields, for a forward model generated by equation 2.8 and 2.9, the reverse modelling is given by:

$$\vec{P_0}^{-}(z_m) = [\mathbf{W}^{+}(z_m; z_0)]^{*}\vec{P_0}^{-}(z_0). \tag{2.18}$$

Here, the complex conjugate matrix $[\mathbf{W}^{+}(z_m; z_0)]^{*}$, is the anticausal or backward propagation operator (Wapenaar et al., 1989). For full wavefield (without the internal multiples), the reverse modelling of primaries and surface-related multiples is given by:

$$\vec{P}^{-}(z_m) = [\mathbf{W}^{+}(z_m; z_0)]^{*}\vec{P}^{-}(z_0), \tag{2.19}$$

where $\vec{P}^{-}(z_0)$ is the residual of the total measured wavefield at the surface.

An important thing to notice here is that the back propagation of the measured wavefield only accounts for the sub-event primaries, i.e. for the path related to the last bounce. For the n^{th} order of reflection, this back propagation will account for the $n-1^{th}$ order of reflection at the surface, if reinjected and downward propagated. This will work in migrating for both, the linear and the non-linear forward-modelled data as will be discussed later.

Another application of reverse modelling of data could be in estimating the source wavelet, given we are provided with an approximate reflectivity and velocity model (Davydenko & Verschuur, 2017), via back-propagating to the reflector and then further back-propagating to the source location. This process becomes important when a true-amplitude estimate of $\vec{S}^{+}(z_0)$ is not available.

2.4. MIGRATION

2.4.1. PRIMARIES-ONLY MIGRATION METHOD

When the downgoing source seismic waves encounter a reflector, an upgoing reflected wavefield is generated, which is recorded later by the receivers at the surface. Claerbout's (1971) imaging condition therefore states that, the point at which the source and receiver wavefields are in the same space and time; a reflector exists. For the 2D case, the

approximate reflection coefficient r at a horizontal and vertical location x and z is given by

$$r(x,z) = \sum_{j=1}^{N_w} \frac{P^-(x,z;\omega_j)}{P^+(x,z;\omega_j)}. \tag{2.20}$$

Here N_w is the number of frequencies we are summing over.

In order to image this reflector, we must compute the downgoing forward propagating source wavefield P^+ and backward propagating recorded wavefield P^- via a modelling method; such as the one described earlier in this chapter. Equation (2.20) after a more stable formulation (Valenciano & Biondi, 2003) can be written as:

$$r(x,z) = \sum_{j=1}^{N_w} \frac{P^-(x,z;\omega_j)(P^+(x,z;\omega_j))^*}{P^+(x,z;\omega_j)(P^+(x,z;\omega_j))^* + \epsilon}, \tag{2.21}$$

where ϵ is a stabilization parameter.

Upon considering the denominator to be a mere scaling factor, a more common practical algorithm used is the correlation imaging condition (Claerbout, 1971) given by:

$$r(x,z) \approx \sum_{j=1}^{N_w} P^-(x,z;\omega_j)P^+(x,z;\omega_j)^*. \tag{2.22}$$

For primaries-only imaging, we can substitute equation 2.8 and equation 2.9 in equation 2.22 to get:

$$r(x,z_m) \approx \sum_{j=1}^{N_w} P_0^-(x,z_m;\omega_j)P^+(x,z_m;\omega_j)^*. \tag{2.23}$$

Note that if the multiples are not removed properly from the data, the cross-correlation imaging condition could lead to cross-talk due to the wrong mapping of the multiples at a later time. Although this method provides a structural image of the earth efficiently, it is known to perform poorly in case of irregularly sampled data (Yao & Jakubowicz, 2016; Valenciano et al., 2009).

One of the solutions is to use least-squares migration (Nemeth et al., 1999), which is a data-driven iterative inversion method. The method tries to iteratively solve the following minimisation problem:

$$\underset{m}{arg\,min}\, J = \|P_{obs} - P_{mod}\|_2^2, \tag{2.24}$$

where J is the objective function, P_{obs} is the observed data and P_{mod} and m are the forward-modelled data and the earth model, respectively.

In the case of primaries-only data, for data modelled with Full Wavefield Modelling, substituting equation 2.8 and 2.9 in equation 2.24 at a certain iteration i gives:

$$\underset{\mathbf{R}}{arg\,min}\, J = \sum_{shots}\sum_{\omega} \left\| \vec{P}_0^-(z_0) - \mathbf{W}^-(z_0,z_m)\mathbf{R}_i^{\cup}(z_m)\mathbf{W}^+(z_m;z_0)\vec{S}^+(z_0) \right\|^2. \tag{2.25}$$

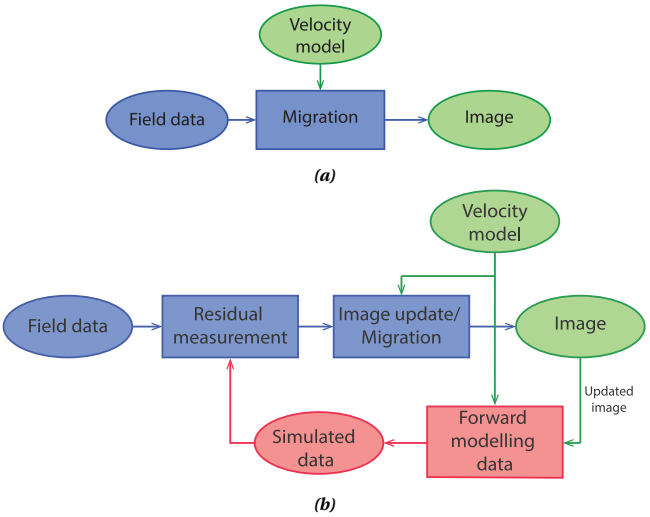

Figure 2.2 *Primary wavefield migration: a flowchart depicting a) a conventional open-loop migration method and b) an iterative least-squares migration.*

In each iteration for a given velocity model and a starting reflectivity model, we compare our forward-modelled data with the measured data to obtain the residual $(P_{obs} - P_{mod})$. The gradient of J with respect to reflectivity is obtained by migrating the residual in order to update the reflectivity for the next iteration $\mathbf{R}_{i+1}$. Figure 2.2 compares a simplified flowchart of an open-loop migration method (figure 2.2a) and the least-squares migration method (figure 2.2b). This method provides much better results with regards to improved resolution and illumination despite incomplete data (Nemeth et al., 1999).

2.4.2. MIGRATION WITH MULTIPLES

SURFACE MULTIPLES IN A 'LINEAR' INVERSION METHOD

Starting with the correlation imaging condition described in equation 2.22, for imaging with only surface-related multiples we must modify the downgoing illuminating wavefield. As already discussed in subsection 2.2.2 we could do this by substituting the original source wavefield with the re-injected measured wavefield, to get the downgoing wavefield at z_m:

$$\vec{M}^{+}(z_m) = \mathbf{W}^{+}(z_m; z_0)\mathbf{R}^{\cap}(z_0)\vec{P}^{-}(z_0) \tag{2.26}$$

and upgoing wavefield at z_m:

$$\vec{M}^{-}(z_m) = [\mathbf{W}^{+}(z_m; z_0)]^{*}\vec{M}^{-}(z_0). \tag{2.27}$$

Reflectivity can now be derived using a correlation or inversion-type imaging condition, thereby migrating the multiples (Whitmore et al., 2010; Berkhout, 2014b). This method evidently is dependent on the efficiency of the multiple separation methods. Any unremoved primary wavefield leads to cross-talk in the image.

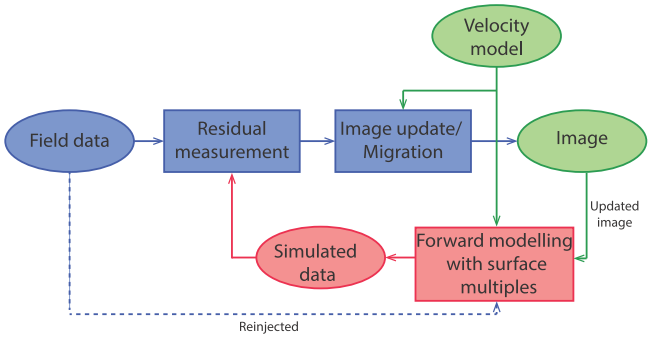

(a)

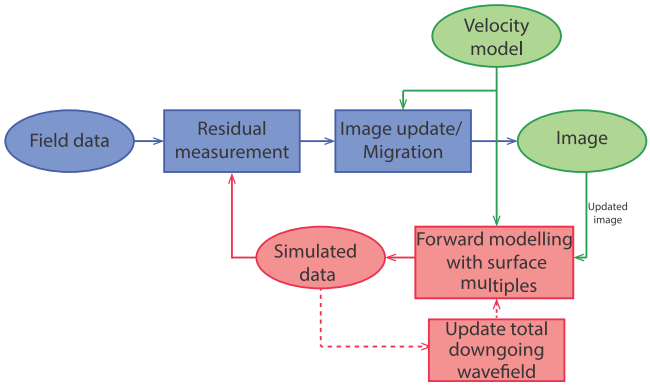

(b)

Figure 2.3 *Migration including multiples: a) Closed-loop migration including surface multiples, where the observed data is re-injected for modelling. b)Proposed method for non-linear inversion of surface multiples, where all surface multiples are built from the original source field.*

To avoid multiple separation, imaging with primaries and surface-related multiples together is another way forward. Modifying the total downgoing wavefield to include both the source wavefield and the re-injected measured wavefield gives:

$$\vec{P}^{+}(z_m) = \mathbf{W}^{+}(z_m; z_0)(\vec{S}^{+}(z_0) + \mathbf{R}^{\cap}(z_0)\vec{P}^{-}(z_0)); \tag{2.28}$$

and the upgoing wavefield at z_m is given by:

$$\vec{P}^{-}(z_m) = [\mathbf{W}^{+}(z_m; z_0)]^{*}\vec{P}^{-}(z_0). \tag{2.29}$$

Using an imaging condition on these two wavefields migrates the primaries and multiples simultaneously (Berkhout & Verschuur, 1994; Verschuur & Berkhout, 2011; Weglein, 2015; Lu et al., 2018). Since we are dealing with complex wavefields such as multiples, if we use conventional imaging methods we may still end up with unavoidable cross-talks.

Full Wavefield Migration (Berkhout, 2012)uses a least-squares minimization process with an iterative inversion method (i.e., a closed-loop approach) (Davydenko & Verschuur,

2012; Verschuur & Berkhout, 2015). The iterative minimization method takes care of the cross-talks generated with every progressing iteration. This produces an image that explains the multiples properly; given the forward model includes sub-event primaries (equation 2.12). This brings about a small change in the closed-loop method from the least-squares migration method (figure 2.2b), as can be seen in the flowchart in figure 2.3a.

In our implementation, we will mostly concern our work with data that has strong surface multiples and much weaker internal multiples. We can thereby ignore the contribution of internal multiples in imaging and only focus on the ways of benefiting from the surface-related multiples. However, they can be included in the modelling scheme in a similar non-linear fashion as surface multiples are being introduced to be more complete. For a detailed discourse on the implementation of the internal multiples and angle-dependent parameterisation, the reader is directed to Davydenko and Verschuur (2017).

Figure 2.3a depicts the flowchart of the closed-loop process. For a given iteration i, the current reflectivity operator matrix $\mathbf{R}_i^{\cup}$, is used to model seismic data using the propagation operators $\mathbf{W}$ (Berkhout, 2014a). In these methodologies, since we assume the reflection parameter to be angle-independent, $\mathbf{R}_i$ is taken to be a diagonal matrix. The cost function J_i of the iterative minimization process is given by:

$$\begin{aligned} &\underset{m}{arg\,min}\, J_i = \|P_{obs} - P_{mod}\|_2^2; \\ &\text{where,} \\ &\quad P_{obs} = P^-(z_0); \\ &\quad P_{mod} = \mathbf{W}^-(z_0, z_m)\mathbf{R}_i^{\cup}\mathbf{W}^+(z_m; z_0)(\vec{S}^+(z_0) + \mathbf{R}^{\cap}(z_0)\vec{P}^-(z_0)). \end{aligned} \tag{2.30}$$

Similar to imaging with primaries-only data, every event now (primaries and surface-related multiples) is accounted for in a single reflection event, therefore leading to a 'linear' relationship between the forward model and reflectivity. It is important to notice that only one bounce of each event in the measured wavefield is considered in the imaging process in these methods. All previous bounces are contained implicitly in the measured data that is re-injected. The residual data is then used to update the reflectivity, thereby also suppressing possible cross-talk (Berkhout, 2014b). In the case of multiples imaging, the method can overcome the limitations of coarse source sampling see e.g. Lu et al., 2014; Davydenko and Verschuur, 2017. As mentioned in section 2.2.2, since the forward model uses a recorded wavefield as an incident wavefield, it is sensitive to large data gaps.

INCORPORATING SURFACE MULTIPLES IN A 'NON-LINEAR' INVERSION METHOD

Addressing the limitations of the 'linear' inversion method in case of missing data, we introduce a 'non-linear' inversion scheme. In this method, all surface-related multiples are included incrementally in the incident wavefield using the modelled upgoing wavefield (Berkhout & Verschuur, 2014) leading to a non-linear relationship between reflectivity and the forward model as described in 2.2.2. Since this method omits the reinjection

of measured data, it is less affected by missing data. Due to the non-linear relationship, we also expect higher sensitivity to changes in the reflectivity model, as the errors in estimated reflectivities are amplified in higher-order multiples. This is evident from equation 2.17, where the total up-going wavefield is not linearly dependent on the last estimated reflectivity, but as the i^{th} power of the updated reflectivity δR, where the i is the iteration number of the closed-loop imaging method. Please note that this marginal improvement has only been observed in our inverse-crime examples shown in this chapter.

After making suitable changes for non-linear inversion in a closed-loop approach (see figure 2.3b for the flowchart), we then derive the reflectivity image using the same minimization method mentioned in equation 2.30.

Table 2.1 compares the different wavefields used for imaging in the methods described above.

Table 2.1 *Overview of imaging schemes with associated wavefields, where $[\vec{P}_m^-]^i$ refers to the modelled wavefield at iteration i.*

Imaging options			
	Option	Receiver side	Source side
Linear	Primary	$\vec{P}_0{}^-$	$\vec{S}^+$
	Surface multiples	$\vec{M}^-$	$\mathbf{R}\cap\vec{P}^-$
	Primaries and surface multiples	$\vec{P}^-$	$\vec{Q}^+ = \vec{S}^+ + \mathbf{R}\cap\vec{P}^-$
Non-linear	Primaries and surface multiples	$\vec{P}^-$	$[\vec{Q}^+]^i = \vec{S}^+ + \mathbf{R}\cap[\vec{P}_m^-]^{i-1}$

2.5. ILLUSTRATIVE EXAMPLE

Here we illustrate and compare the above-described methods, using a synthetic model given in figure 2.4. Figure 2.4a shows the reflectivity model used to generate the data; the yellow stars denoting the source locations. We use extremely coarse source spacing. The source locations at the surface are at 600 m, 900 m, 4500 m and 4800 m. This source wavelet used to generate the data is a Ricker wavelet with a dominant frequency of 20 Hz. The aim of such an extreme acquisition design is to highlight the importance of multiples in illumination when compared to primaries. For this example, we choose the receiver geometry to be dense. For this numerical example, a full wavefield synthetic data is generated using FWMod (Berkhout, 2014a) on this 2-D model, with the restriction of angle-independent reflectivity in both modelling and imaging. Using such an 'inverse crime' approach we can investigate the maximum expected performance of the proposed methodology. Figure 2.5a shows the imaging result using primary wavefield migration. As expected, we observe that only the boundaries near the source locations are well-illuminated. Figure 2.5b shows the imaging result using the linear closed-loop method using multiples only. The cross-talk generated by this method is expected because the imaging method is driven by the complex re-injected wavefield. With increas-

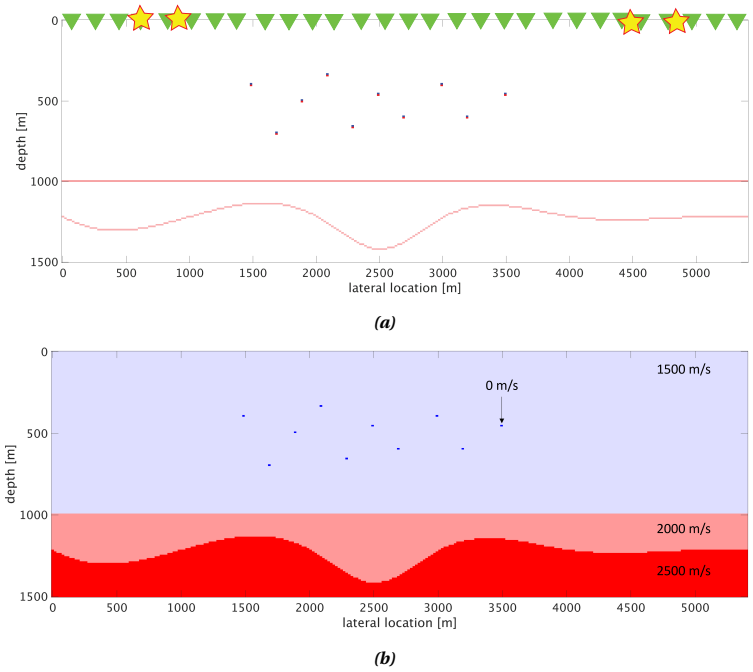

Figure 2.4 *(a) Synthetic reflectivity model with sources at 600 m, 900 m, 4500 m and 4800 m (indicated by the stars) and receivers indicated by green triangles. (b) Corresponding velocity model.*

ing iterations in the closed-loop method this, however, reduces. Figure 2.6a shows the imaging result using the linear closed-loop method using primaries and multiples. The subsurface certainly has become better illuminated due to the reinjection of measured data in migration, especially in the middle section where no sources were positioned. Figure 2.6b illustrates the alternative, non-linear method suggested in this chapter. The non-linear imaging method seems to have performed equally as well as the linear imaging method using primaries and multiples.

Although the results in figure 2.6a and 2.6b may look similar, a closer inspection shows an increase in resolution from the non-linear imaging method. This can be seen in figure 3.5, on comparison of vertical cross-sections at lateral location $x = 3000m$ from the four methods. The resolution of the image using the non-linear inversion approach is better, as the reflector peaks are higher and sharper.

2.6. DISCUSSION

Including multiples in the imaging method comes with a lot of benefits as well as unique problems. The closed-loop imaging method becomes necessary to minimise the resulting cross-talk from multiples (Davydenko & Verschuur, 2017; Lu et al., 2018).

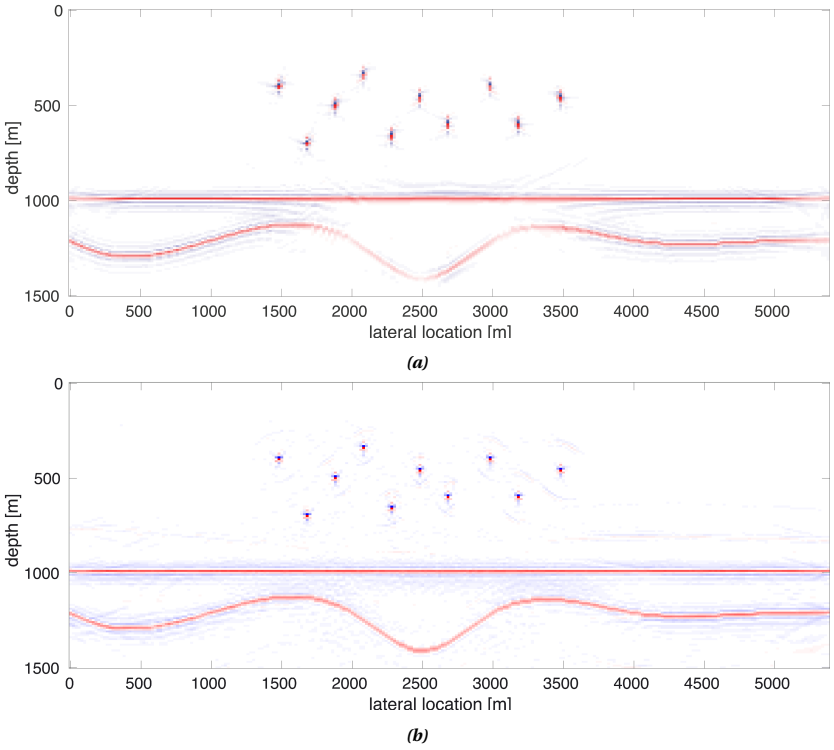

Figure 2.5 *Imaging results in a closed-loop imaging process using the 'inverse crime' modelling process: a) using primaries-only data; b) using a multiples-only 'linear' inversion method with re-injected measured data*

2.6.1. CONVERGENCE

Figure 2.8 compares the objective-function values with increasing iterations for the different imaging methods discussed in this chapter. This comparison is based on the example presented in the previous section. We show the comparison on the primaries-only imaging method, primaries and multiples in the linear imaging method, and primaries and multiples using the non-linear imaging method. This demonstrates that including multiples will require more iterations to reach convergence than the method with primaries-only data. Since the non-linear method simultaneously builds the downgoing wavefield along with migration in every iteration, it requires a few more iterations to catch up with the linear method using primaries and multiples but eventually is more efficient.

2.6.2. SENSITIVITY TO A SOURCE ERROR

The following examples show the sensitivity of the above-mentioned methods to errors in the source. A time delay of 0.04 seconds has been put on the initial source wavelet. This wavelet is a Ricker wavelet with a dominant frequency of 20 Hz. Figure 2.9a shows the imaging result using primaries-only wavefield. Figure 2.9b is a plot showing vertical cross-sections at lateral location $x = 3000\ m$ from figure 2.9a. The blue curve shows the

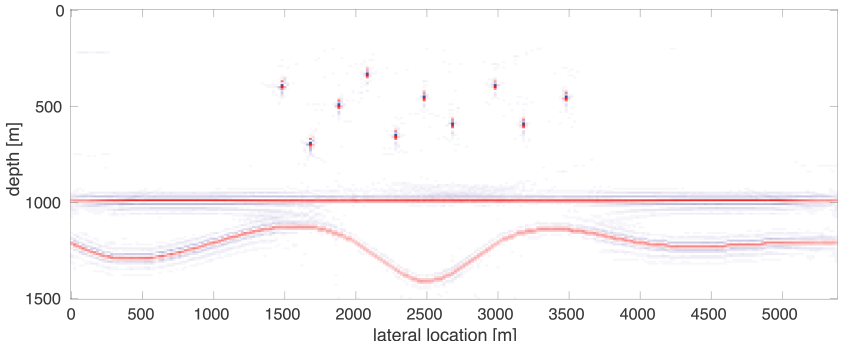

(a)

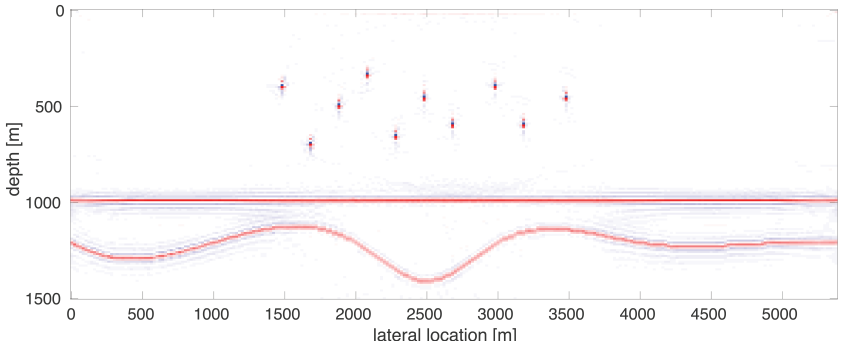

(b)

Figure 2.6 *Imaging results in a closed-loop imaging process: a) using a 'linear' inversion method with primaries and re-injected measured data; and b) using the proposed non-linear inversion method.*

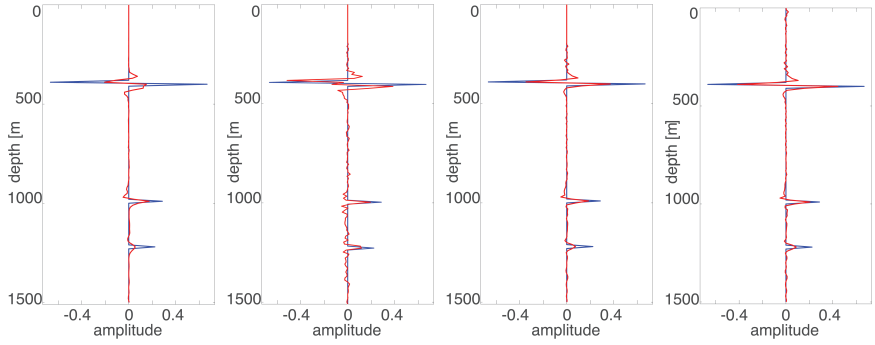

(a) *(b)* *(c)* *(d)*

Figure 2.7 *Amplitude cross-section of the reflectivity image at x=3000 m a) using primaries-only data; b) using a multiples-only linear inversion method; c) using a linear inversion method using primaries and multiples; and d) using the proposed non-linear inversion method. The blue curve depicts the actual reflectivity and the red curve shows the modeled reflectivity.*

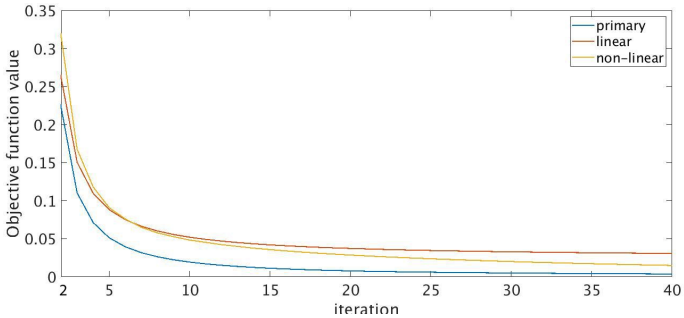

Figure 2.8 *Curves showing the objective function values vs iterations. The blue curve corresponds to the primaries-only closed-loop method, the red curve to primaries and multiples in the closed-loop linear method, and the yellow to primaries and multiples in the closed-loop non-linear method.*

real image and the red curve shows the resulting image using the wrong source wavelet. Figure 2.9c shows the imaging result using multiples-only migration method. Figure 2.9d is the corresponding vertical cross-section plot. We observe that since we eliminate the source estimation process here and image only multiples, the reflectors get mapped at the right location! We should also keep in mind that this method is dependent on a good multiple estimation (primary removal) method. Figure 2.9e and 2.9g depict imaging results using linear and non-linear imaging methods, respectively, using primaries and multiples. Figure 2.9f and 2.9h are the corresponding vertical cross-section plots. The linear imaging method in this case seems to perform slightly better than the non-linear method as the multiples are explained by the re-injected measured wavefield. This was expected, as the non-linear method explains all the multiples from the provided source wavefield. It can be clearly seen how, because of the primaries, the image is distorted; however, the contribution of multiples can be seen in locations further away from the four sources and hence they place the reflectors at the right position.

2.6.3. SENSITIVITY TO VELOCITY ERROR

Primary wavefields are stronger than their associated multiples, and, therefore, they have a strong contribution to the imaging result in methods that include both the primaries and surface multiples. In case of velocity errors in the model, linear and non-linear methods that use both primaries and surface multiples, get dominated by the primaries in the imaging result. To illustrate this effect, we use the same model from section 2.5 to generate the data, but change the source configuration (marked by red dots) in figures 2.10 and 2.12. Figure 2.10 and 2.12 show imaging results given 4% increase in the velocity model used for imaging. Figures 2.10a, 2.10b, 2.10c show the imaging result with sparse sources using the primaries-only method, using the linear primaries and multiples method and the non-linear primaries and multiples method, respectively. The dominance of primaries in the imaging result can be clearly seen albeit with a very small improvement in the methods that use multiples. The least-squares imaging method adjusts the reflector depth to best compensate for discrepancies in the travel times caused by the error in the model velocity. However, in the modelled data, the effects of the ve-

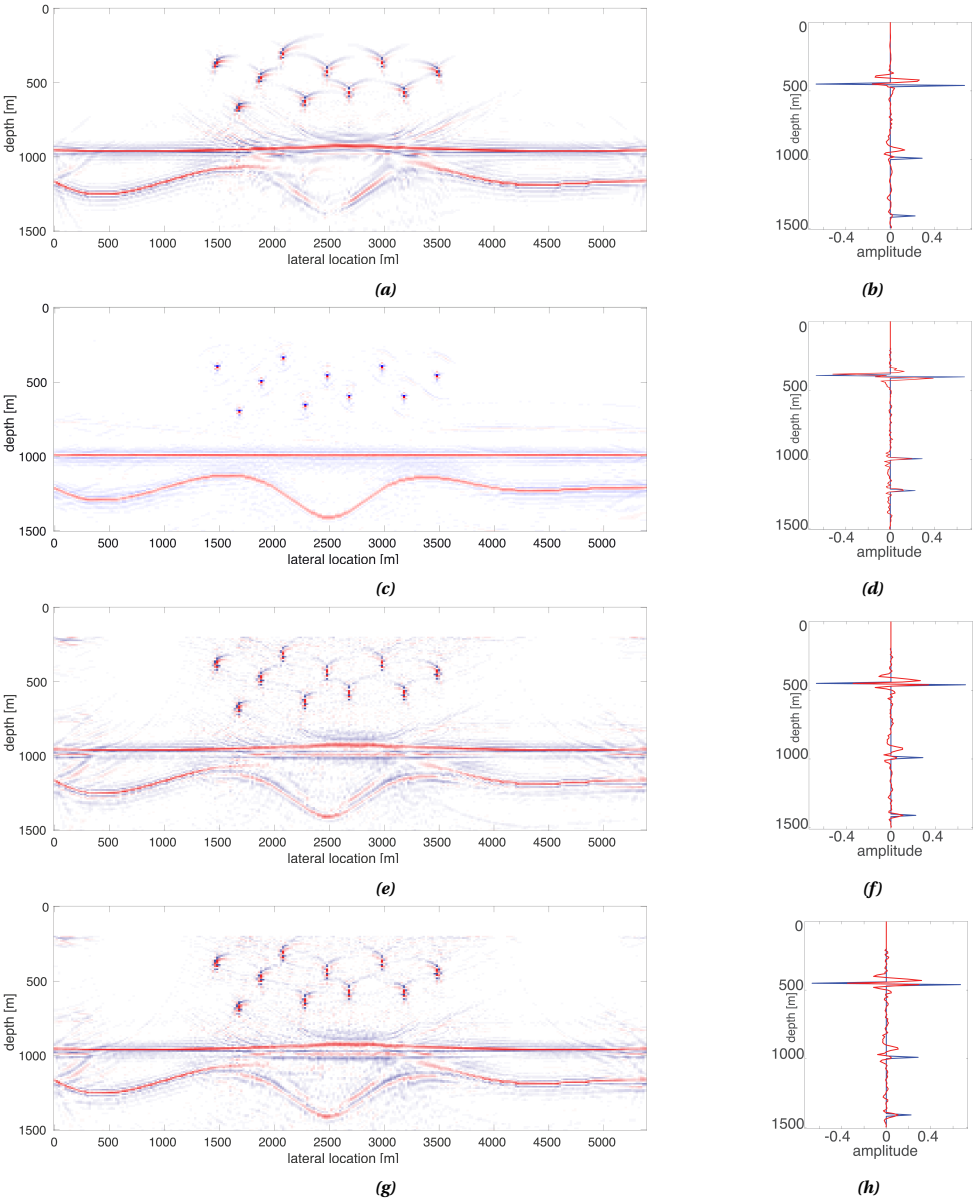

Figure 2.9 *Imaging results in a closed-loop imaging process with a wrong source wavelet: a) using primaries-only 'linear' inversion method; c) using multiples-only 'linear' inversion method; e) using 'linear' inversion method with primaries and re-injected measured data; and g) using the proposed non-linear inversion method. b), d), f) and h) show the amplitude cross-section of a), c), e) and g) at $x = 3000$ m respectively. The blue curve depicts the actual reflectivity and the red curve shows the modeled reflectivity.*

locity error are more visible as we move away from the smaller offsets due to a mismatch

in the moveout, as demonstrated in figure 2.11. These figures compare the measured data (figure 2.11a) with modelled data using the velocity model with 4% error from our example. Figure 2.11b shows the modelled data from the linear imaging method and figure 2.11b shows the modelled data from the non-linear imaging method. We see that the modelling of multiples is also affected by the velocity error in the higher offsets, with the non-linear imaging method being affected more than the linear imaging method in the modelling of the subsequent multiples.

To investigate the effect of velocity errors on primaries and multiples separately, figure 2.12a shows the imaging result with the wrong velocity model using the primaries-only method with a dense coverage of sources and receivers. Figure 2.12b shows the imaging result using the multiples-only imaging method with sparse sources. This image shows a high resemblance to figure 2.12a, despite the sparse sources. In spite of intuition, this seems to show that in practice, multiples are less sensitive to imaging with velocity errors in case of acquisition restrictions. One of the reasons may be that the multiples tend to propagate under smaller angles than primaries for a similar offset. While a larger offset is ideal for velocity estimation methods, multiples can contribute in another key way; by providing a better and more robust image. This helps in avoiding any local minima. This discrepancy between primaries and multiples can be utilised to estimate the source wavefield (Davydenko, 2016). This aspect can also be strategically exploited for better illumination and velocity estimation in methods like Joint Migration Inversion (Berkhout, 2014c; Verschuur et al., 2016) and wavefield tomography (Soubaras & Gratacos, 2018).

In the following chapter, we shall discuss the merit of the non-linear imaging method and how it may help us in increasing the illumination of the subsurface especially in obstructed acquisition areas or large data gaps.

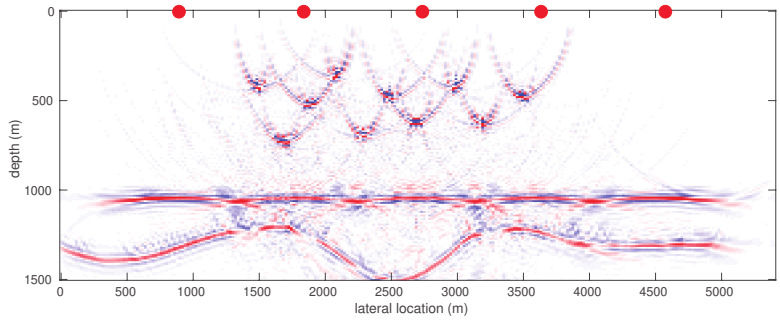

(a)

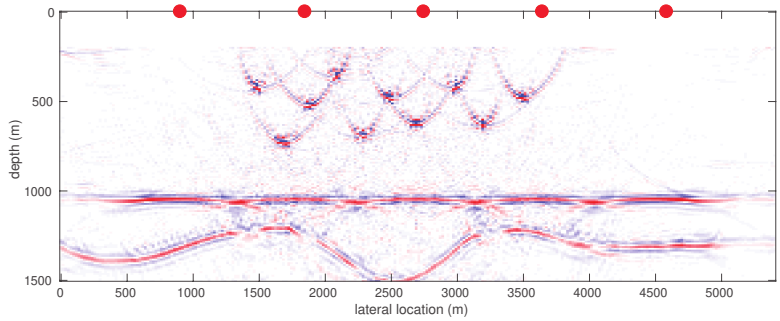

(b)

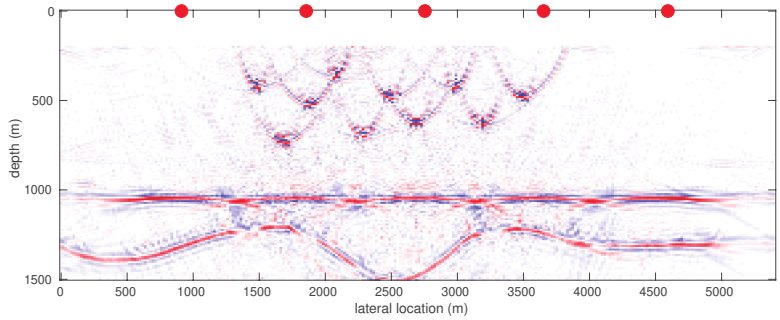

(c)

Figure 2.10 *Imaging with 4% velocity error from section 2.5 using a sparse source configuration indicated with the red dots. Imaging results using closed-loop imaging process a) using primaries only; b) using primaries and surface multiples in a 'linear' imaging method; d) using primaries and surface multiples in the proposed non-linear inversion method.*

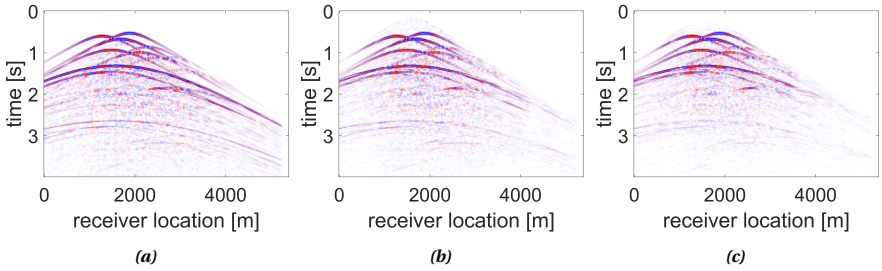

Figure 2.11 *a) Measured data. Modelled data using b) linear imaging method with 4% model velocity error, and c) non-linear imaging method with 4% model velocity error.*

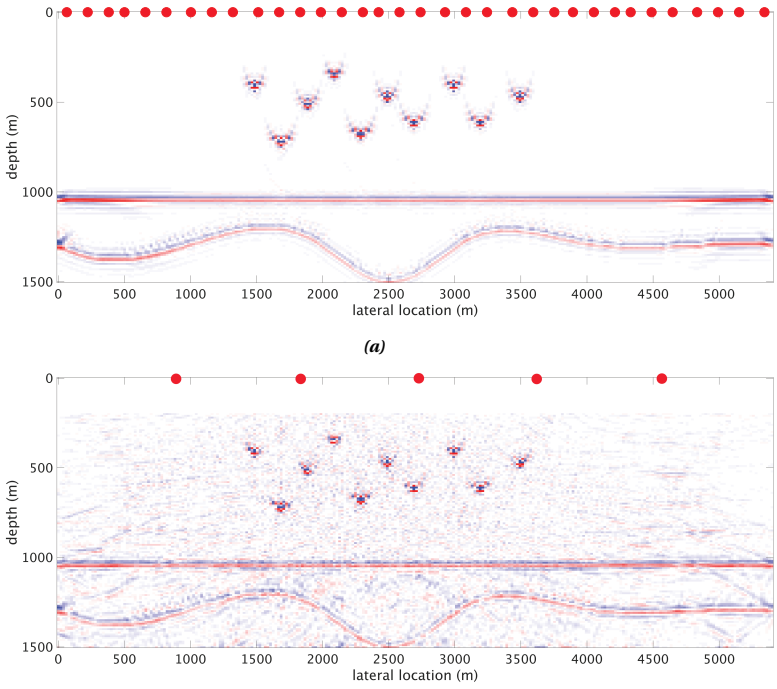

Figure 2.12 *Imaging with 4% velocity error from 2.5. Imaging results using a closed-loop imaging process a) using primaries only from a densely sampled source configuration; b) using multiples only from a sparse source configuration with a linear multiples-only imaging method.*

BIBLIOGRAPHY

Berkhout, A. (1982). *Seismic migration, imaging of acoustic energy by wave field extrapolation, A: Theoretical aspects*. Elsevier (second edition).

Berkhout, A. (2012). Combining full wavefield migration and full waveform inversion, a glance into the future of seismic imaging. *Geophysics*, *77*(2), S43–S50.

Berkhout, A. (2014a). An outlook on the future of seismic imaging, part I : Forward and reverse modelling. *Geophysical Prospecting*, *62*, 911–930.

Berkhout, A. (2014b). An outlook on the future of seismic imaging, part II : Full-wavefield migration. *Geophysical Prospecting*, *62*(5), 931–949.

Berkhout, A. (2014c). An outlook on the future of seismic imaging, part III: Joint migration inversion. *Geophysical Prospecting*, *62*, 950–971.

Berkhout, A., & Verschuur, D. (1994). Multiple technology: Part 2, migration of multiple reflections. In *SEG technical program expanded abstracts 1994* (pp. 1497–1500). Society of Exploration Geophysicists.

Berkhout, A., & Verschuur, D. (2014). Sensitivity of data acquisition in full wavefield migration. In *SEG technical program expanded abstracts 2014* (pp. 3920–3924). Society of Exploration Geophysicists.

Carcione, J., Herman, G., & Ten Kroode, A. (2002). Seismic modeling. *Geophysics*, *67*(4), 1304–1325.

Claerbout, J. (1971). Toward a unified theory of reflector mapping. *Geophysics*, *36*(3), 467–481.

Davydenko, M. (2016). Full wavefield migration: Seismic imaging using multiple scattering effects. *(Doctoral Dissertation)*.

Davydenko, M., & Verschuur, D. (2012). Demonstration of full wavefield migration in 2D subsurface models. *74th EAGE Conference and Exhibition Extended abstracts*, P275.

Davydenko, M., & Verschuur, D. (2017). Full-wavefield migration: Using surface and internal multiples in imaging. *Geophysical Prospecting*, *65*(1), 7–21.

Gazdag, J. (1978). Wave equation migration with the phase-shift method. *Geophysics*, *43*(7), 1342–1351.

Kinneging, N., Budejicky, V., Wapenaar, C., & Berkhout, A. (1989). Efficient 2d and 3d shot record redatuming. *Geophysical Prospecting*, *37*, 493–530.

Lu, S., Liu, F., Chemingui, N., Valenciano, A., & Long, A. (2018). Least-squares full-wavefield migration. *The Leading Edge*, *37*(1), 46–51.

Lu, S., Whitmore, D., Valenciano, A., & Chemingui, N. (2014). Separated-wavefield imaging using primary and multiple energy. *First Break*, *32*(11), 87–92.

Nath, A., & Verschuur, D. (2020). Imaging with surface-related multiples to overcome large acquisition gaps. *Journal of Geophysics and Engineering*, *17*(4), 742–758.

Nemeth, T., Wu, C., & Schuster, G. (1999). Least-squares migration of incomplete reflection data. *Geophysics*, *64*(1), 208–221.

Soubaras, R., & Gratacos, B. (2018). Migration velocity analysis with multiple modeling: An inversion toolbox. *80th EAGE Conference and Exhibition 2018*, Th A12 14.

Valenciano, A., & Biondi, B. (2003). 2-d deconvolution imaging condition for shot-profile migration. In *SEG technical program expanded abstracts 2003* (pp. 1059–1062). Society of Exploration Geophysicists.

Valenciano, A., Biondi, B., & Clapp, R. (2009). Imaging by target-oriented wave-equation inversion. *Geophysics*, *74*(6), WCA109–WCA120.

Verschuur, D., & Berkhout, A. (2011). Seismic migration of blended shot records with surface-related multiple scattering. *Geophysics*, *76*(1), A7–A13.

Verschuur, D., & Berkhout, A. (2015). From removing to using multiples in closed-loop imaging. *The Leading Edge*, *34*(7), 744–759.

Verschuur, D., Staal, X., & Berkhout, A. (2016). Joint migration inversion: Simultaneous determination of velocity fields and depth images using all orders of scattering. *The Leading Edge*, *35*(12), 1037–1046.

Wapenaar, C. (2014). *Elastic wave field extrapolation: Redatuming of single-and multi-component seismic data* (Vol. 2). Elsevier.

Wapenaar, C., Peels, G., Budejicky, V., & Berkhout, A. (1989). Inverse extrapolation of primary seismic waves. *Geophysics*, *54*(7), 853–863.

Weglein, A. (2015). Primaries—the only events that can be migrated and for which migration has meaning. *The Leading Edge*, *34*(7), 808–813.

Whitmore, N., Valenciano, A., Sollner, W., & Lu, S. (2010). Imaging of primaries and multiples using a dual-sensor towed streamer. In *SEG technical program expanded abstracts 2010* (pp. 3187–3192). Society of Exploration Geophysicists.

Yao, G., & Jakubowicz, H. (2016). Least-squares reverse-time migration in a matrix-based formulation. *Geophysical Prospecting*, *64*(3), 611–621.

3

EXTENDING FWM: HANDLING LARGE DATA GAPS*

To get the best result for seismic imaging using primary reflections, data with densely-spaced sources and receivers is ideally preferred. However, dense acquisition can sometimes be hindered by various obstacles, like platforms or complex topography. Such areas with large data gaps may deter exploration or monitoring, as conventional imaging strategies would either provide poor seismic images or turn out to be very expensive. Since surface-related multiples travel different paths compared to primaries, they illuminate a wider subsurface area, making them valuable in case of data with large gaps.

In this chapter, we discuss different strategies for using surface-related multiples to get around the problem of imaging in the case of a large data gap. Conventional least-squares imaging methods that incorporate surface-related multiples do so by re-injecting the measured wavefield in the forward modelling process, which makes it still sensitive to missing data. In the previous chapter, we introduced the 'non-linear' inversion approach where the surface multiples are modelled from the original source field. This makes the method less dependent on the receiver geometry, and therefore, effectively exploiting the information from surface multiples in case of limited illumination. However, such an approach is sensitive to the knowledge of the source properties.

Therefore, in this chapter, we will propose a 'hybrid' method that combines the 'non-linear' imaging method with the conventional 'linear' multiple imaging method, which further improves our imaging result. The strategy can be changed with regard to the sequence order of the linear and non-linear method, and the kind of data to be used, depending on the target as well as the initial conditions. We will illustrate the method with an example that shows the benefit of combining the two strategies.

*Part of this chapter has been published in Nath and Verschuur (2020).

3.1. IMAGING WITH GAPS

Seismic data can sometimes end up with large gaps due to several reasons such as bad topography, lack of access, infrastructure (e.g., an obstructing platform), legal or environmental considerations or failing equipment. If we use conventional seismic imaging algorithms that use primary reflection data only, migration artefacts become unavoidable (Hou & Symes, 2017). A common practice in such scenarios is re-acquiring the data specifically targeting the missed zone. For instance, to illuminate areas under a physical obstruction such as platforms, undershooting has become standard practice (Hill, 1986, OGP report, 2011). However, the large offsets between the sources and receivers take a toll on the vertical resolution of the data and more efforts and ivestments need to be put into acquiring additional high-resolution data (Games et al., 2015). Figure 3.1a illustrates via an example one such acquisition on the same model (figure 2.4a) from section 2.5 using again the same four source locations. Receivers are placed throughout the surface at an interval of 20 m except from x = 1900 m to x = 3500 m where a wide receiver gap is applied (see figure 3.1a).

Figure 3.2 shows one shot record with the gap in the data modelled using FWMod on the model in figure 3.1a and 3.1b (Inverse-crime example). Figure 3.3a shows the closed-loop image obtained from primaries-only data. Note that the middle part of the image is obtained via 'undershooting'. The effects in the image due to missing receivers are clearly visible as the reflectors and shallow diffractors around the gap are not imaged properly.

In the previous chapter, we saw how multiples help in increasing illumination as they travel different paths compared to primaries. This could prove to be helpful in such cases of limited illumination. Using surface-related multiples linearly, i.e., via re-injecting the total measured response $\mathbf{R}^{\cap}\vec{P}^{-}$ as the illuminating source wavefield (Verschuur & Berkhout, 2011) in the migration method may provide a better image compared to primaries-only migration, especially in case of smaller gaps (Davydenko & Verschuur, 2017). Figure 3.3b shows the imaging result using the primaries and multiples in a closed-loop linear inversion method, as mentioned earlier. Indeed, we do see some improvement in this image compared to figure 3.3a. However, since the linear method relies on the reinjection of recorded data as incident wavefield, it is assumed that the complete downgoing wavefield has been recorded. Therefore, the effect of the gap is still evident in figure 3.3b. Figure 3.3c illustrates the imaging result from the proposed non-linear inversion method. The deeper reflectors as well as the shallow scatterers are better imaged here. It can be seen in figure 3.4a that the data is not modelled well near the gap, causing a poor minimization of residual data at far offsets, as shown in figure 3.4c. Thus, for the area under large gaps, linear imaging methods have fallen short in exploiting the power of multiple scattering.

The 'non-linear' imaging scheme, however, compensates for unrecorded data by synthetically modelling all the surface-related multiples, starting from the original source wavefield. In this way the dependence on receiver geometry becomes less strong, allowing us to overcome large acquisition gaps. This can be viewed as the extension of

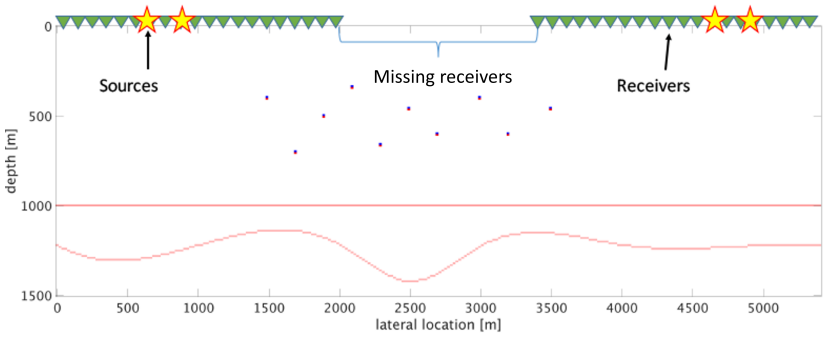

(a)

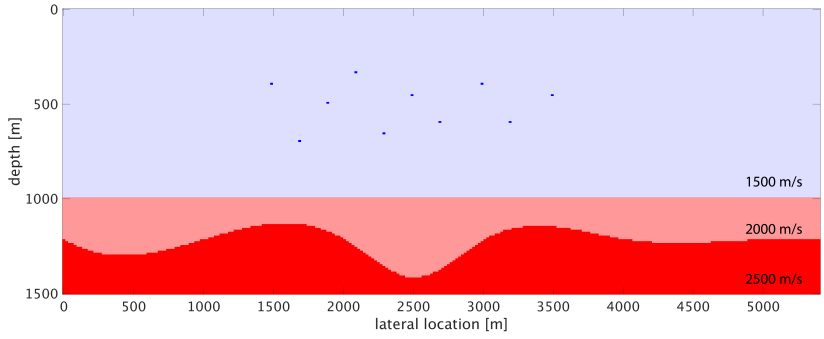

(b)

Figure 3.1 *a) Synthetic reflectivity model with sources at 600 m, 900 m, 4500 m and 4800 m (indicated by the stars) and receivers indicated by green triangles. b) Corresponding velocity model.*

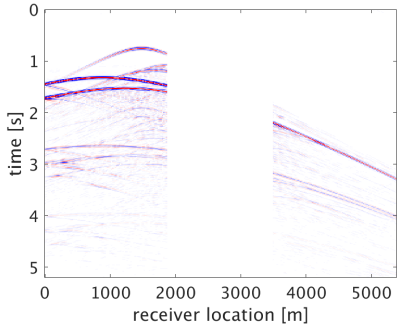

Figure 3.2 *A shot record data with a gap in the middle. The data is generated via FWMod and the gap is artificially created by putting a mask of zeroes over the traces in the gap.*

the least-squares migration method for primaries to overcome incomplete data issues (Nemeth et al., 1999) by including surface multiples in various ways. Furthermore, it relates to the model-based multiple imaging method proposed by Jiang et al. (2007), ex-

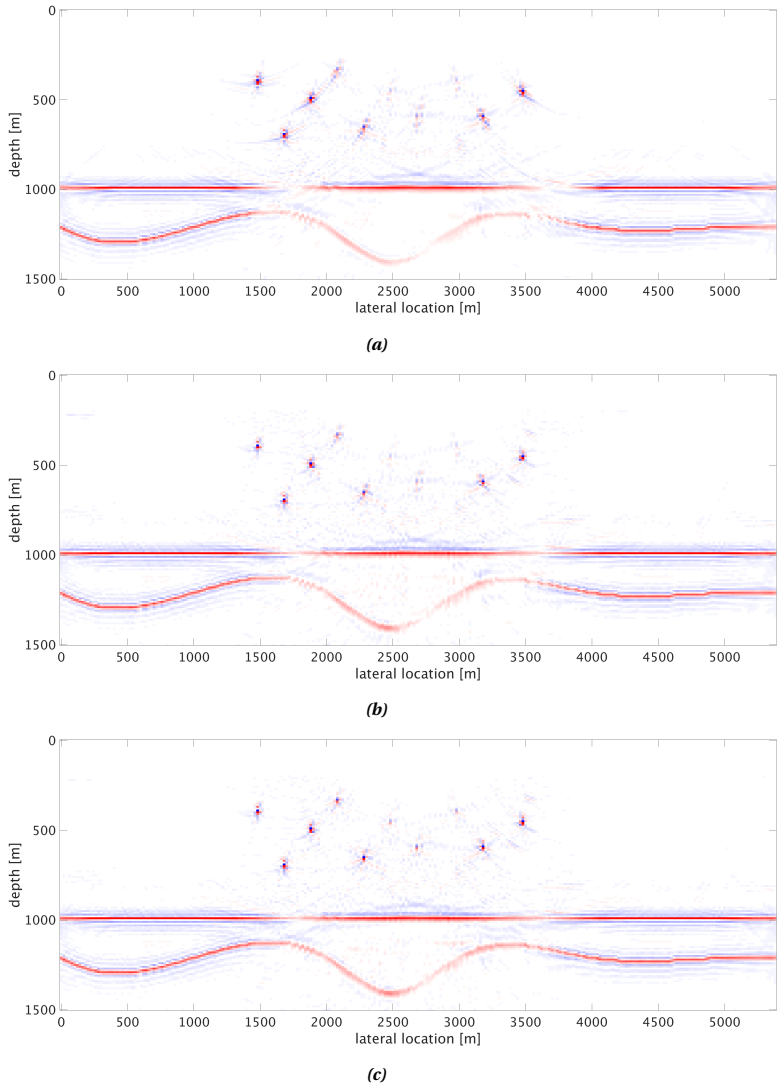

Figure 3.3 *Imaging results in a closed-loop imaging process using the 'inverse crime' modelling process: a) using primaries-only data; b) using a 'linear' inversion method with re-injection of the measured data; c) using the proposed non-linear inversion method.*

cept with a closed-loop approach. The modelled data from the 'non-linear' method has improved around the area with the missing data as well as at far offsets of the first-order multiple (figure 3.4b), therefore, we see an improvement in the data fit as well, i.e. a reduction in the residual data (see figure 3.4d). Figure 3.5 shows a comparison of vertical cross-sections of the images at lateral location x=2700 m obtained from the three methods using primaries and multiples. The image using the non-linear approach (see

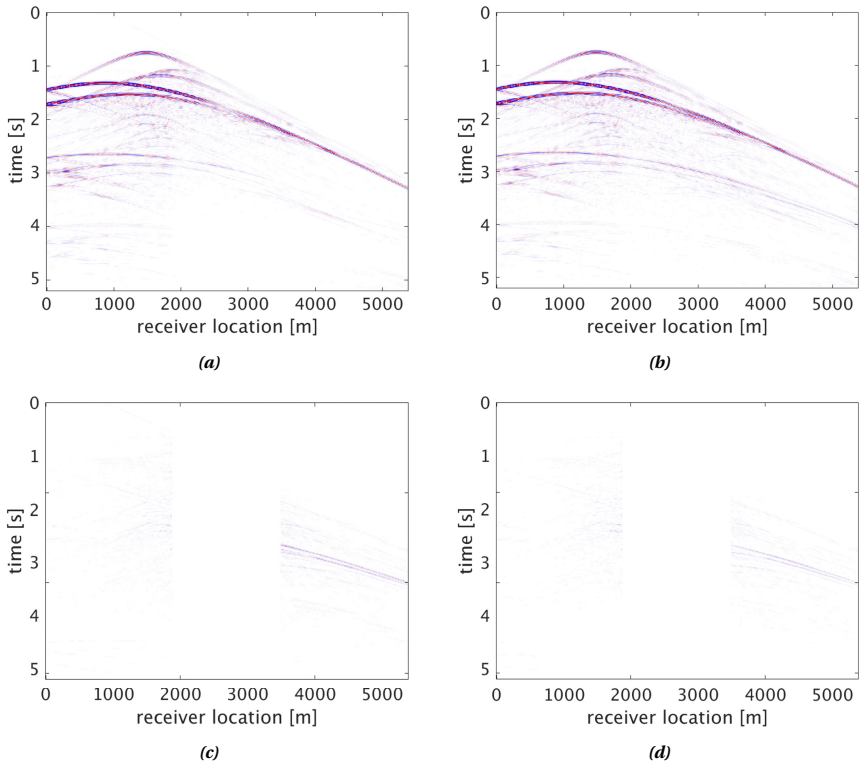

Figure 3.4 *modelled shot record data for the source at x=900 m using a) the linear inversion method, b) the non-linear inversion method. Residual data for source at x=900 m for c) the linear inversion method, d) the non-linear inversion method.*

figure 3.3c) indeed contains much better results than the other two approaches. The shallow diffractors are imaged better, and the reflector peaks are also higher and sharper, as shown in figure 3.5c.

3.2. HYBRID METHOD

While the non-linear method performs better in the case of incomplete sampling, it comes with its own shortcomings. Table 3.1 compares the benefits and drawbacks of the two multiples imaging methods mentioned above. As the relationship between the forward model and reflectivity is non-linear, this method is naturally more sensitive to errors. This means that, although potentially a higher resolution can be obtained, the inversion process can be trapped in a local minimum. Since the non-linear method requires modelling the data starting from a source wavefield, the image is quite sensitive to errors in the source wavelet. In contrast, the linear imaging method does not require knowledge of the wavelet because measured data is used as both incident and reflected field, thereby making it robust. As the 'linear' and 'non-linear' methods complement

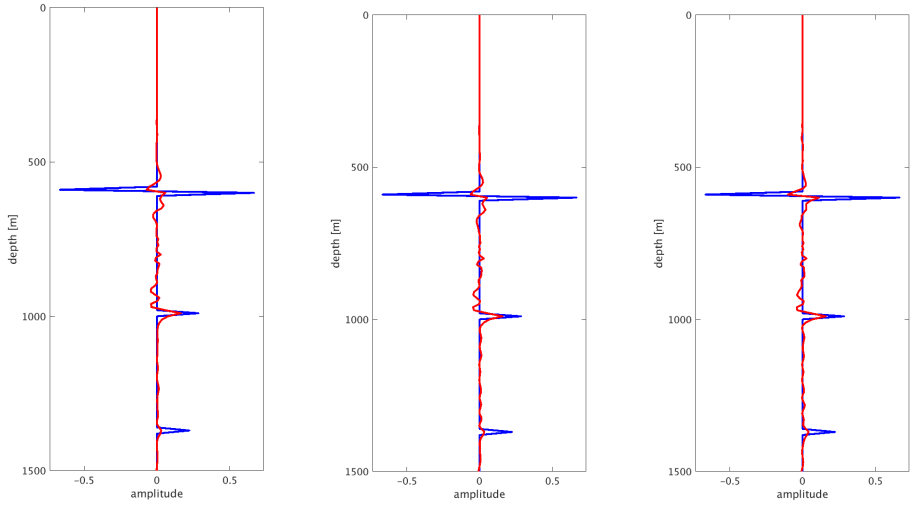

Figure 3.5 *Amplitude cross section of the reflectivity image at x=2700 m a) using primaries only inversion method; b) using a linear inversion method; c) using the proposed non-linear inversion method.*

Table 3.1 *Table comparing the benefits and the drawbacks of the linear and non-linear migration method.*

Imaging with Multiples		
	Benefits	**Drawbacks**
Linear Imaging Method	• Broad illumination due to re-injection of multiples. • No need for source wavelet in case of imaging with only multiples. • Method is robust due to re-injection of measured data.	• Dependent on receiver density. • No resolution improvement compared to the method using dense primary data.
Non-linear Imaging Method	• Broader illumination because of non-linear inclusion of multiples. • Potential for improved resolution. • Less dependence on receiver locations.	• Problem is non-linear; sensitive to small errors. • Requires knowledge of the source wavelet for data generation.

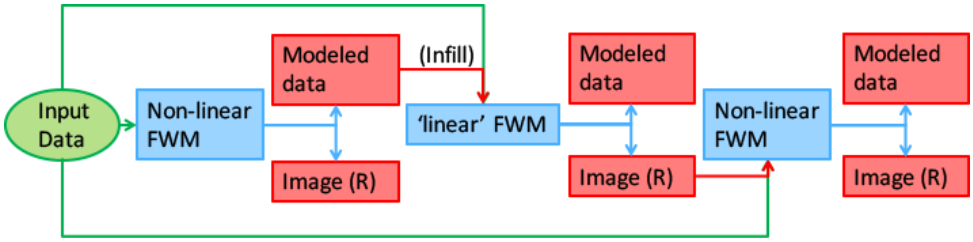

Figure 3.6 *A flowchart demonstrating the hybrid multiples imaging method.*

each other in their drawbacks and benefits, a hybrid approach that combines the two methods by successively applying them may give the best solution.

In case of missing data in the example suggested in section 3.1, a suggested strategy (figure 3.6) for data with a gap is as follows (Nath & Verschuur, 2017) :

1. As the 'non-linear' inversion method creates a better-modelled data in case of acquisition gaps (such as in our example in figure 3.4b), we first start with the non-linear inversion process on the data with gaps.

2. Then we use the modelled shot record gathers from the non-linear inversion method to fill in the gaps of the measured seismic data.

3. As the 'linear' inversion method is more robust, we use this infilled data in the 'linear' inversion method to obtain an intermediate subsurface image.

4. Finally, as the 'non-linear' inversion method better explains the missing data, we feed this reflectivity image received from the previous step as a jump start to the 'non-linear' inversion method along with the original measured data. This provides the final image.

3.2.1. EXAMPLE

To illustrate this hybrid method, we continue with the same example. Figure 3.7d shows the intermediate imaging result of the hybrid approach. The modelled shot record gather from the non-linear imaging method (figure 3.7b, same as figure 3.4b) is used to fill the gaps in the measured seismic data, as shown in figure 3.7c. This shot record data is then used in our linear imaging method, which is more robust to get a reflectivity image. Since the 'non-linear' inversion method better explains the missing data, in the final step of the hybrid approach, we feed this reflectivity image (figure 3.7d) to the 'non-linear' inversion method as a jump-start along with the original measured data to give the result shown in figure 3.7e. Despite a very large gap, the method manages to fill in the image with the help of modelled as well as measured multiples. Figure 3.8a shows the final modelled data we get from the hybrid approach. The complementary residual data from this hybrid approach, displayed in figure 3.8b, shows that the modelling process performs successfully in explaining the data around the gap but also for the larger offsets.

Figure 3.9 shows a comparison of vertical cross-sections of the images at lateral location

x=2700 m obtained from the three methods using primaries and multiples. The image using the hybrid approach (see figure 3.7e) indeed contains much better results than the other two approaches. The shallow diffractors are now imaged properly, the reflector peaks are also higher and sharper, as shown in figure 3.9c, and the residuals are reduced compared to the other methods mentioned previously.

3.3. CONCLUSION AND DISCUSSION

In this chapter, we saw the benefit of using the non-linear imaging method compared to the linear imaging method when subjected to data with large gaps. This method models the multiples non-linearly, and therefore, helps in creating unrecorded data; this further aids in imaging with data that have huge gaps. However, the non-linear imaging method is sensitive to errors in the source field and velocity model and, hence, is susceptible to poor results. To counter that, we suggest using a more robust method: the linear imaging method in combination with the non-linear imaging method. This hybrid method indeed performs better in case of limited illumination as it brings the benefits of both the linear and non-linear imaging methods together.

An essential thing to keep in mind is that the hybrid method is not restricted to the sequence explained in section 3.2. For instance, in the case of a poor initial source wavelet, starting with the non-linear method may turn out to be a problem. However, in such a case we can start with the multiples-only linear imaging method to get an initial and more accurate estimate of the subsurface image. This can be followed by an iterative source estimation method using that initial image (Davydenko & Verschuur, 2017), and then proceeded with a suitable combination of linear and non-linear imaging methods, to tackle the issue of gaps. In this way, we can get much better imaging results while taking advantage of all the methods consecutively.

In our method, we exclusively utilise the surface-related multiples to image the area under the gap. Imaging with internal multiples (Malcolm et al., 2009; Davydenko & Verschuur, 2013; A. Zuberi & Alkhalifah, 2013; M. Zuberi & Alkhalifah, 2014) could also give way to illuminating such areas using a similar principle of iterative modelling. However, internal multiples are usually weaker than surface multiples, so exploiting their extra illumination is challenging.

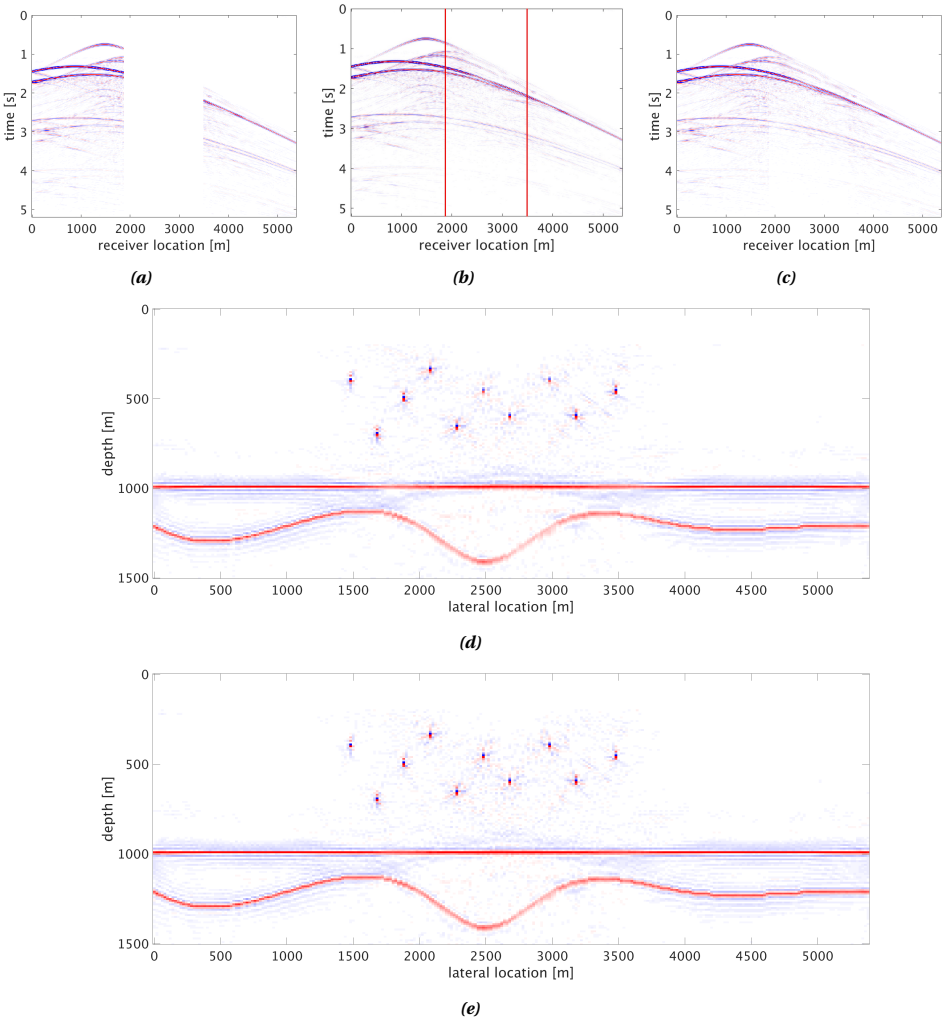

Figure 3.7 *The Hybrid scheme demonstrated via the 'inverse-crime' modelling process. a) Measured shot gather for the source at 900 m. b) Modelled shot record data for the source at x=900 m using non-linear inversion. c) Data from a) after putting an infill in the gap received from b) (shown within red lines) for an intermediate step in the hybrid scheme. Imaging results of the hybrid scheme: d) after using the data from c) for linear inversion; e) final result of the hybrid method using linear and non-linear inversion methods using d) as the initial image.*

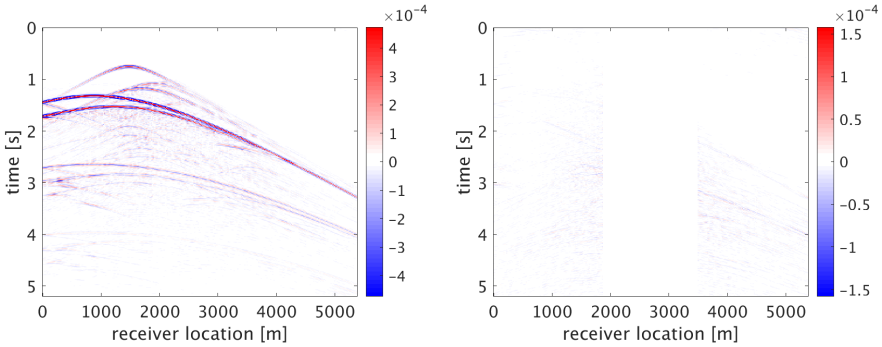

(a) *(b)*

Figure 3.8 *modelled shot record data and the residual data for the source at x=900 m using the hybrid scheme.*

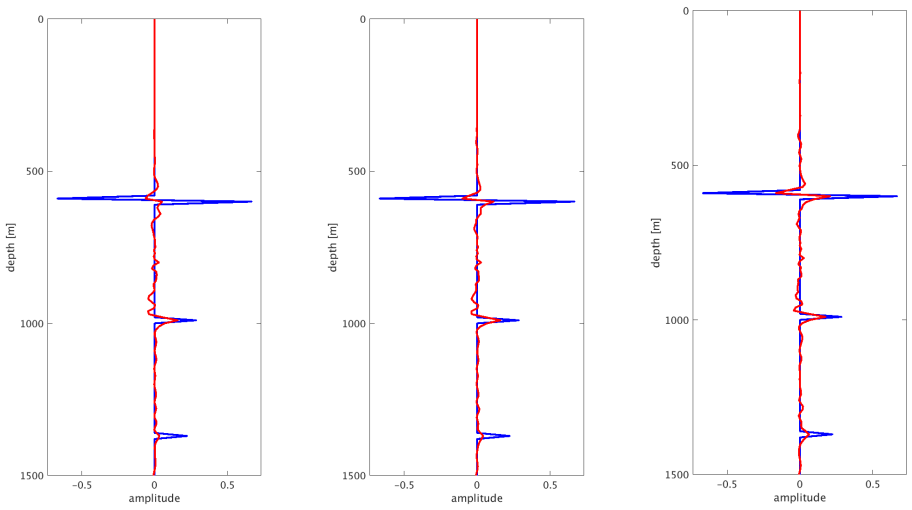

(a) *(b)* *(c)*

Figure 3.9 *Comparison of the amplitude cross-sections of the reflectivity image at x=2700 m from results in figure 3.7 a) using a linear inversion method (same as figure 3.5b); b) using the proposed non-linear inversion method (same as figure 3.5c); c) using the hybrid method. The blue curve depicts the original reflectivity while the red plot shows the modelled reflectivity.*

BIBLIOGRAPHY

Davydenko, M., & Verschuur, D. (2013). Full wavefield migration, using internal multiples for undershooting. *SEG Technical Program Expanded Abstracts 2013*, 3741–3745.

Davydenko, M., & Verschuur, D. (2017). Full-wavefield migration: Using surface and internal multiples in imaging. *Geophysical Prospecting*, *65*(1), 7–21.

Games, K., Pretty, A., Stennett, I., Wakefield, N., & Mann, D. (2015). High resolution seismic undershooting of platforms–stretching the limits. *First Break*, *33*(3), 39–45.

Hill, A. (1986). Two-ship undershooting of a production platform: The magnus high-resolution seismic project. *Oceanology*, 191–202.

Hou, J., & Symes, W. (2017). True amplitude imaging for incomplete seismic data. *SEG Technical Program Expanded Abstracts 2017*, 4534–4539.

Jiang, Z., Sheng, J., Yu, J., Schuster, G., & Hornby, B. (2007). Migration methods for imaging different-order multiples. *Geophysical Prospecting*, *55*(1), 1–19.

Malcolm, A., Ursin, B., & De Hoop, M. (2009). Seismic imaging and illumination with internal multiples. *Geophysical Journal International*, *176*(3), 847–864.

Nath, A., & Verschuur, D. (2017). Migration strategies of using surface-related multiples in case of incomplete seismic data. *79th EAGE Conference and Exhibition Extended abstracts*, Th P1 06.

Nath, A., & Verschuur, D. (2020). Imaging with surface-related multiples to overcome large acquisition gaps. *Journal of Geophysics and Engineering*, *17*(4), 742–758.

Nemeth, T., Wu, C., & Schuster, G. (1999). Least-squares migration of incomplete reflection data. *Geophysics*, *64*(1), 208–221.

OGP report. (2011). *An overview of marine seismic operations* (Vol. Report 448). OGP Publications.

Verschuur, D., & Berkhout, A. (2011). Seismic migration of blended shot records with surface-related multiple scattering. *Geophysics*, *76*(1), A7–A13.

Zuberi, A., & Alkhalifah, T. (2013). Imaging by forward propagating the data: Theory and application. *Geophysical Prospecting*, *61*, 248–267.

Zuberi, M., & Alkhalifah, T. (2014). Generalized internal multiple imaging. *Geophysics*, *79*(5), S207–S216.

4

ANALYSIS WITH EXAMPLES FROM STREAMER ACQUISITION TYPE DATA* †

In this chapter, we will further compare and illustrate the performance of the linear primaries-only migration method, the linear and non-linear primaries and multiple migration method and the hybrid method in streamer acquisition type data. We use numerically generated 2D and 3D data to test these methods in different scenarios. We will also test our methods on 2D field data. One of the main objectives is to show how multiples, in different ways, uplift the migration output. We also suggest a method of imaging with multiples around an island via an 'inverse crime' example. The non-linear imaging scheme seems to show a good improvement, especially in the near-surface imaging around gap areas.

4.1. 2D NUMERICAL EXAMPLES

In this section, we will test our method on synthetically generated 2D data. For our first example, we use data generated via acoustic finite-difference modelling. For our second example, we create an island model to generate data via FWMod. This is an attempt to understand how we can image around areas with gaps due to an island feature.

*Examples from this chapter have been published in Nath and Verschuur (2020) and Nath et al. (2019).
†Parts of this chapter have been published in Nath and Verschuur (2020).

4.1.1. FINITE-DIFFERENCE DATA

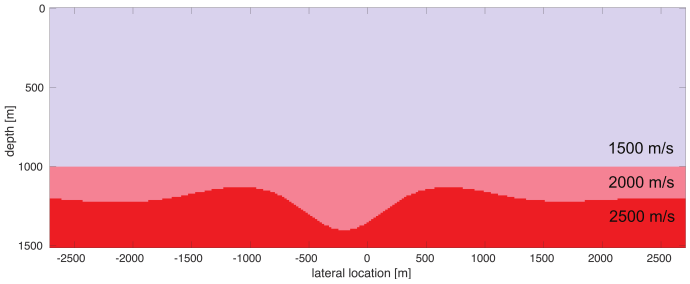

(a) *Velocity model*

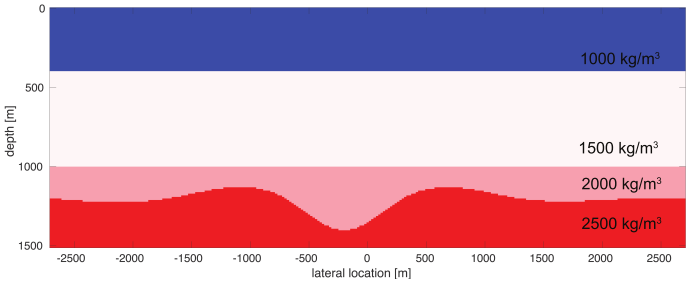

(b) *Density model*

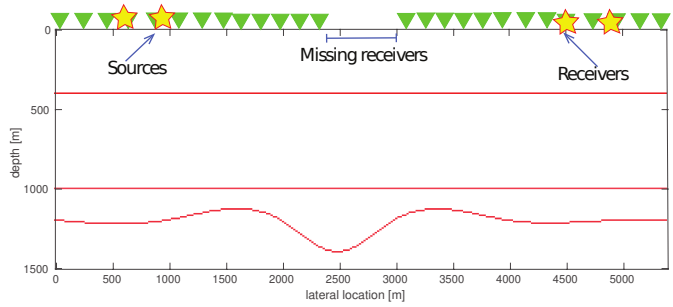

(c) *Reflectivity model*

Figure 4.1 *(a) Velocity model; (b) density model; and (c) reflectivity model with sources at 600 m, 900 m, 4500 m and 4800 m (indicated by the stars) and receivers indicated by green triangles. A gap in the receivers has been created at x=2400 m to x=3000 m.*

In this example, synthetic data are generated using acoustic finite-difference modelling on the model shown in figure 4.1. Figure 4.1a and 4.1b are the corresponding velocity and density models used to generate the data. Figure 4.1c is the resulting true reflectivity image. Figure 4.2 is one of the modelled data gathers. We use four sources at the surface, i.e. at 600 m, 900 m, 4500 m and 4800 m, indicated by stars in figure 4.1c while receivers are spread throughout the surface except from x=2400 m to x=3000 m.

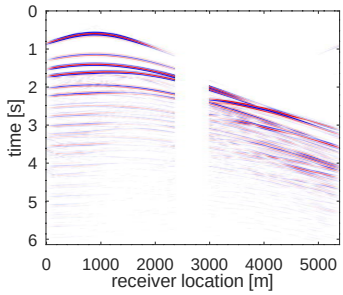

Figure 4.2 *Shot gather data for a source at 900m lateral location in the model of figure 4.1.*

Figure 4.3a shows the imaging result using the primaries-only data (after multiples were removed). The effects in the image due to missing receivers are prominently visible. There is a massive gap in the water bottom around the missing receivers. The gap barely starts to repair around the reflectors below 1000 m and is still poorly imaged. Figure 4.3b shows the imaging result using primaries and multiples via the closed-loop linear inversion method mentioned earlier. Upon comparison with figure 4.3a, the benefits of using the free-surface multiples are already visible here. The improvements in the image can be noticed not only at the shallowest reflector but also in the deeper reflectors (marked by black arrows). Correspondingly, the data (see figure 4.4a) is not modelled well around the missing receivers. Figure 4.3c illustrates the imaging result from the 'non-linear' imaging method. The shallowest reflector can be seen better imaged around the area with the receiver gap (marked with the black arrow), with quite an improvement in the modelled data (figure 4.4c). Figure 4.3d shows the final imaging result obtained via the hybrid method. A further improvement is seen upon a comparison of the image in figure 4.3d with figure 4.3b, and more so when compared to figure 4.3a. Corresponding residuals for the linear, non-linear and the hybrid method are shown in figure 4.4b, 4.4d and 4.4f. Upon comparison of the residuals, different things come to light. While the 'non-linear' imaging method fills up the gap and thereby explains the data (multiples and primaries) around the gap better, the 'linear' imaging method is much better at modelling the data especially the higher order multiples in smaller offsets. The residual data from the hybrid method when compared to the 'linear' and 'non-linear' imaging method shows an overall better fit of the modelled data. The residual data is well resolved at higher offsets when compared to the other methods. When compared to the 'non-linear' method, it is equally well explained around the gap and slightly better at resolving the higher order multiples. Note that the improvements are less prominent as in the 'inverse crime' examples shown in the previous chapter. This may suggest that a better handling of angle-dependent reflectivity is necessary as in this implementation of FWMod the reflectivity is considered angle-independent, while the input data has all the amplitude variation with offset (AVO) effects. Cross-talk can also be seen in the image since multiples are being used for imaging as well. This however reduces with more iterations, i.e. with better modelling of the data in the closed-loop least-squares inversion process.

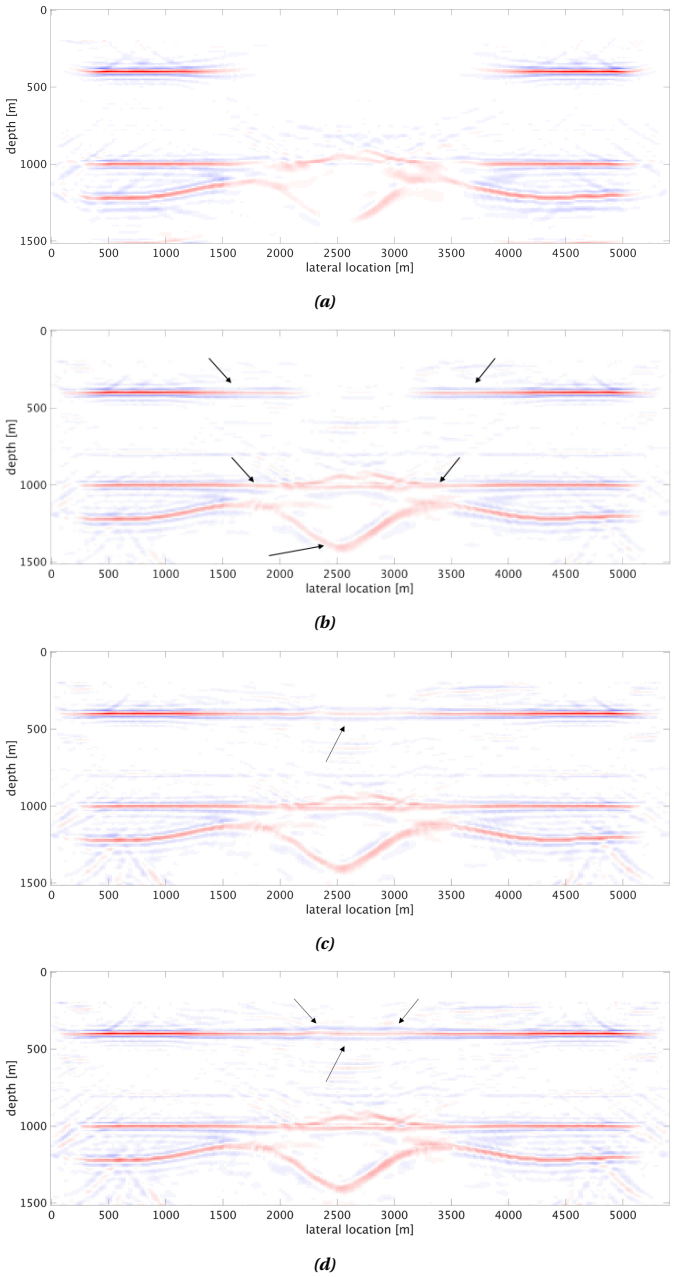

Figure 4.3 *Imaging results in a closed-loop imaging process based on finite-difference modelled input data: a) using primaries-only data; b) using primaries and multiples in a 'linear' imaging method; c) using the proposed non-linear inversion method with primaries and multiples; d) result of the hybrid method.*

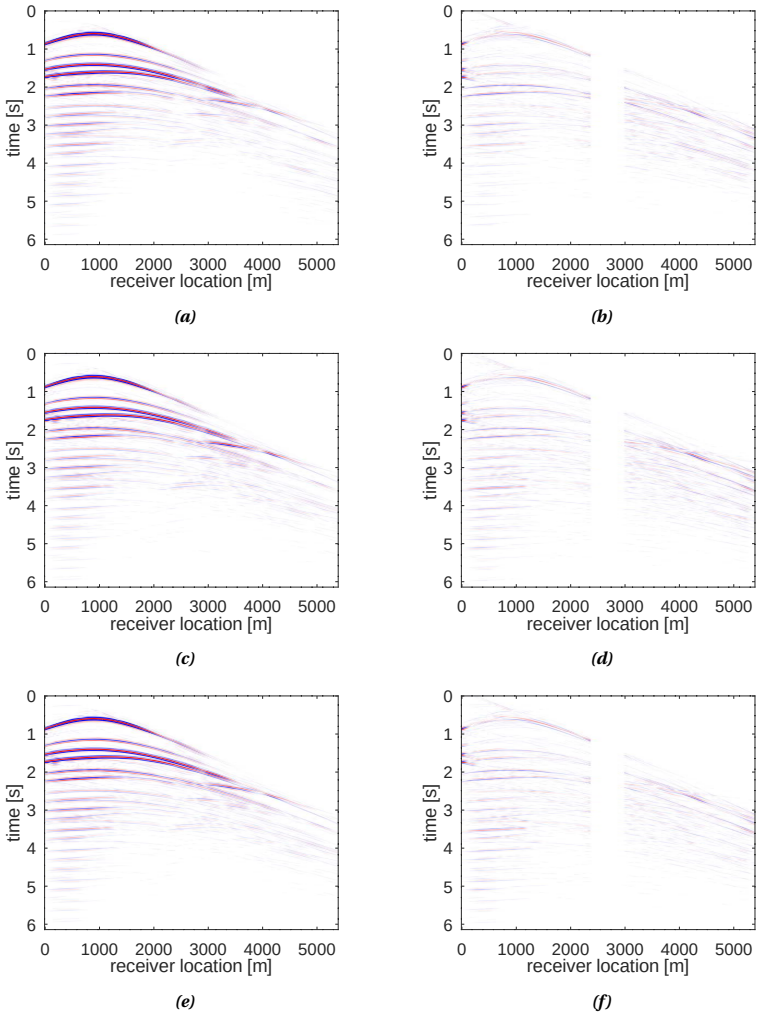

Figure 4.4 *Modelled shot record data for the source at x = 900 m using primaries and multiples in a) the 'linear' inversion method; c) the 'non-linear' inversion method; e) the hybrid scheme. Residual data for source at x = 900 m for b) the 'linear' inversion method; d) the 'non-linear' inversion method; f) the hybrid scheme.*

4.1.2. ISLAND MODEL

In this example, we will try to implement and see how the different imaging methods perform in the case of an island that is obstructing marine seismic measurements (figure 4.5a). The topmost layer until the first 10 m is constructed to accommodate the surface of the island that is above the water. The layer velocities in the model have been indicated in figure 4.5a; The model also has a few low-velocity shallow diffractors. Seventeen sources are spread out at an interval of 200 m all over the water surface except in the acquisition gap from 1600 m to 4000 m due to the island. The size of the model,

including the topmost point of the island, is 1500 m in depth by 5400 m horizontally. Receivers are placed throughout the water layer at 20 m intervals, except from x = 1800 m to x = 3200 m, where a wide receiver gap is applied. For this example, a full wavefield synthetic data is generated using Full Wavefield Modelling on this 2D model. In the modelling process, only the upward reflectivity operator is updated; however, the downward reflectivity operator comprises only of the reflectivity values at the surface - i.e. the air-water and air-island layer as shown in figure 4.5b. In our example we have taken these values to be $\mathbf{R}^{\cap}_{water}(z_0) = -1$ and $\mathbf{R}^{\cap}_{island}(z_n) = -0.8$, where $z_n \leq z_0$. Figure 4.6

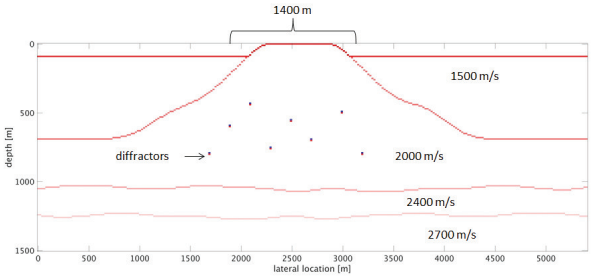

(a) *Reflectivity model*

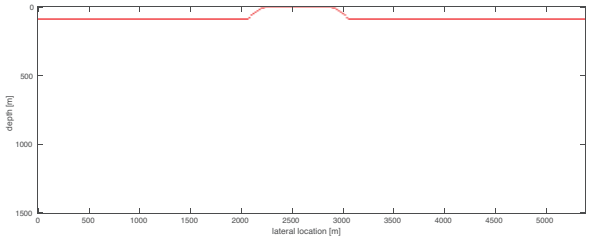

(b) *Downward reflectivity of only the surface*

Figure 4.5 *Synthetic model representing an island model, with 17 sources spread out at an interval of 200 m all over the water surface except in the gap from 1600 m to 4000 m: a) Reflectivity model b) Downward reflectivity of the surface used for modelling the multiples.*

shows the imaging results comparing three imaging methods and figure 4.7 compares the modelled data and the residuals generated for each of those imaging methods. Figure 4.7a shows a shot gather showing the measured data with the gap due to missing receivers. Figure 4.6a shows the imaging result using the closed-loop 'linear' inversion method using primaries and multiples. The effects in the image due to missing receivers are visible around the missing diffractors. It can be seen in figure 4.7b that the data is not modelled well enough near the receiver gap, this may have caused the residual data at far offsets to be minimised inadequately, as shown in figure 4.7c. Figure 4.6b illustrates the imaging result from the non-linear inversion method. Reflectors can be seen better imaged although with a very mild improvement. The modelled data (figure 4.7b) and the corresponding residual data (figure 4.7e) have also improved a little. The modelled shot record gathered from the non-linear imaging method is used to fill the gaps in the measured seismic data as shown in figure 4.7f. This shot record data is then used in our

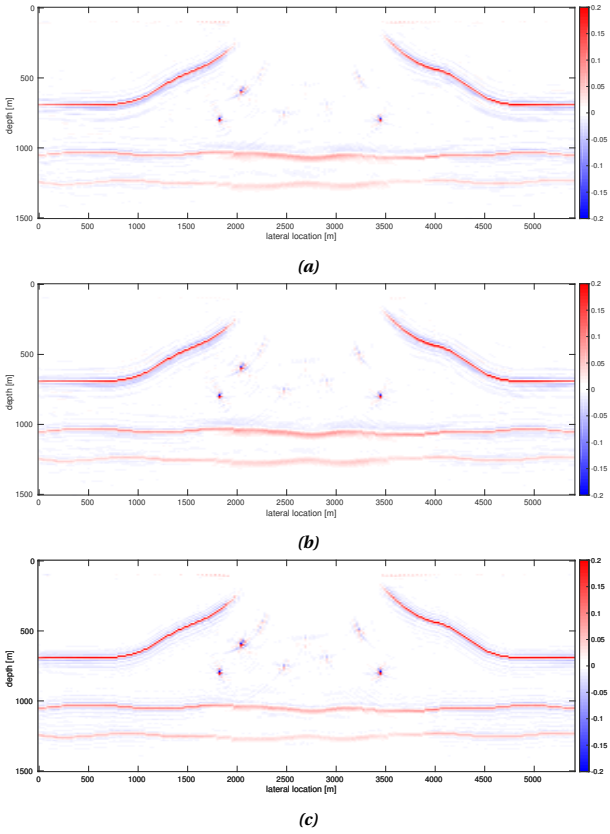

Figure 4.6 *Imaging results related to the Island model (figure 4.5) in a closed-loop imaging process for a geometry with only six sources: a) using the linear inversion method, b) using the proposed non-linear inversion method, c) final result of the hybrid method using the linear and the non-linear inversion method.*

linear imaging method, which is more robust to get a reflectivity image. The image using the hybrid approach (see figure 4.6c) shows a mild improvement in the imaging result to the non-linear method. The reflectors below the gaps are sharper and the diffractors are more visible. The modelled data seems more improved in the gap area (figure 4.7g) and the residual, as shown in figure 4.7h, has been reduced considerably compared to the other two methods mentioned.

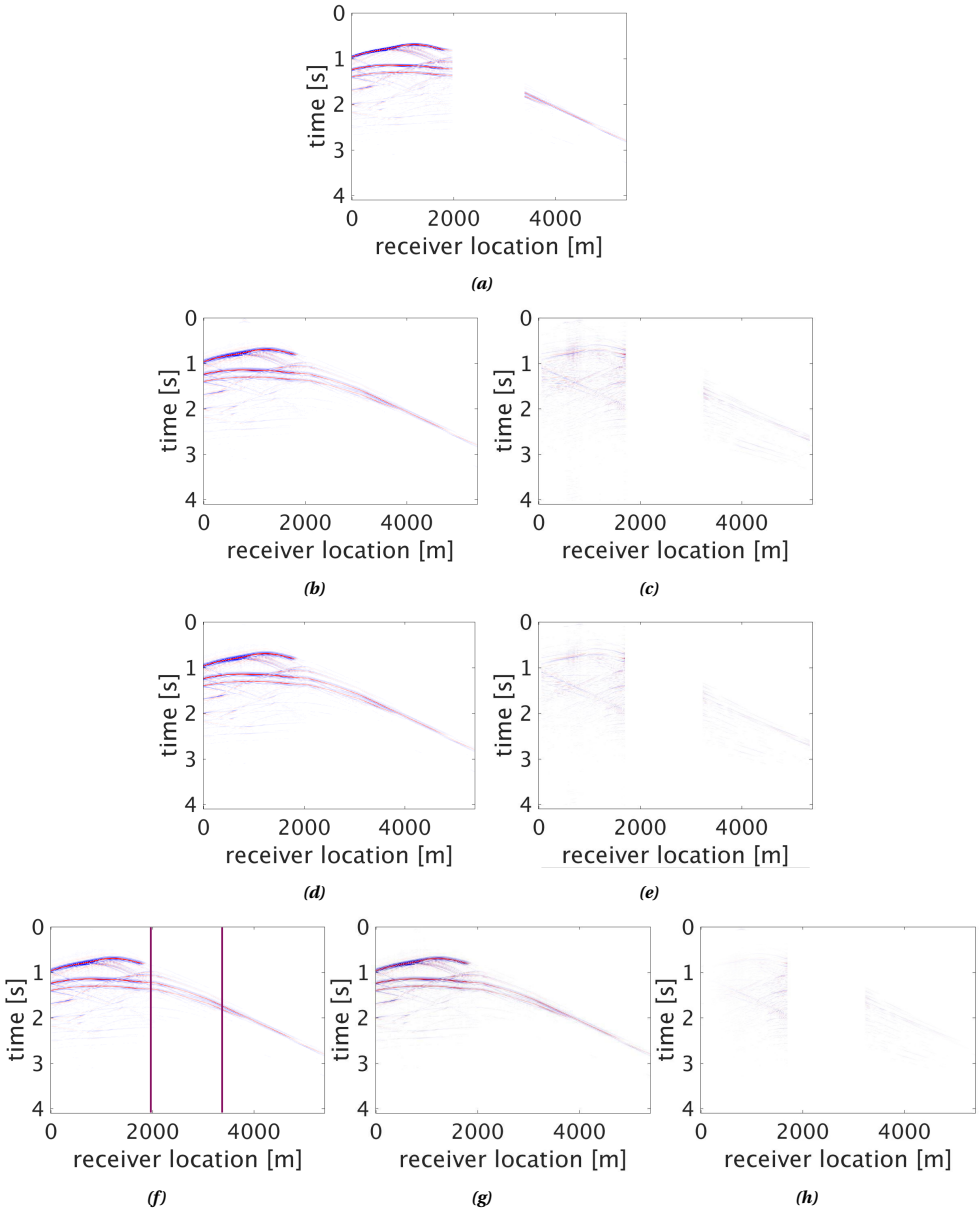

Figure 4.7 *Island model results: a) Measured data. Linear imaging scheme: b) Modelled shot record data and c) residual data. Non-linear imaging scheme: d) Modelled shot record data and e) residual data. The final result of the hybrid scheme: f) Data after putting an infill in the gap received from the non-linear inversion method (gap indicated by two vertical lines); g) Modelled shot record data and h) residual data.*

4.2. 2D FIELD DATA EXAMPLE

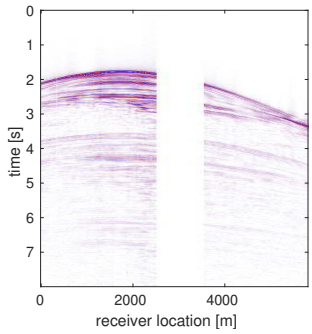

Figure 4.8 *Measured shot record data for the source at 2100 m.*

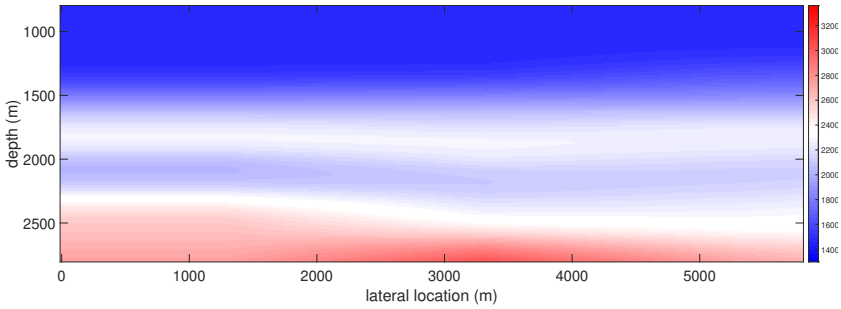

Figure 4.9 *Velocity model used for imaging.*

In this section, we compare the proposed methods on data from the Vøring basin in the Norwegian Sea. We select a subset over 5800 m of recording and use four shot records with sources at 1600 m, 2100 m, 3600 m and 4100 m. Receivers are spread along the surface at a spacing of 25 m except from $x = 2600$ m to $x = 3600$ m, yielding a 1 km receiver gap. Figure 4.8 shows one of these shot records. Note that we used the fully sampled data to construct split-spread shot records and near-offset interpolation to make initially completely sampled gathers (Kabir & Verschuur, 1995). Such pre-processing was required for the application of the Estimation of Primaries by Sparse Inversion (EPSI), see also Van Groenestijn and Verschuur (2009). Deconvolution of the data was done to remove the air-gun bubble effect and the source wavelet in our example was derived using the EPSI process. For this experiment, the four selected shots could represent an ocean-bottom node-type geometry, although sources and receivers are at the surface. For imaging, we bandlimit the data between 1-30 Hz. We use an approximate smooth velocity model generated using NMO velocities followed by an update using the JMI (Berkhout, 2014) process as shown in figure 4.9. Figure 4.12a shows the imaging result using primaries-only imaging. The effects in the image due to missing receivers can be seen below the gap area; here marked with arrows. Figure 4.12b shows the imaging result using the closed-loop 'linear' inversion method (using primaries and multiples). The contribution of multiples in filling the image gaps and improving the resolution has

been marked with arrows. Figure 4.12c illustrates the imaging result from the non-linear inversion method. It can be seen that the reflectors are better imaged around the indicated area. Figure 4.12d shows the final imaging result of the hybrid approach. The reflectors can be seen better imaged not only around the area with gap but also at the outer locations. Figures 4.13a and 4.13c are the enlarged sections of figures 4.12b and 4.12d, respectively, to highlight the improvements in imaging in the area under the gap.

In figure 4.10 we display the same shot record as figure 4.8 with the reconstructed data in the gap. Although the reconstruction for the surface multiples (starting at t=4 seconds) is somewhat weaker, we see a proper reconstruction of the primaries. Note that this information originated from the multiples. We can see some travel-time errors in a few primary events; these can perhaps be attributed to the 3D nature of the wavefield while our modelling scheme assumed the model to be 2D. Figure 4.11 compares the residuals from the linear imaging method (figure 4.11a), non-linear imaging method (figure 4.11b) and the hybrid method (figure 4.11c) using the primaries and multiples. The red arrows point towards the first-order multiples showing a better reduction of the associated residual for the hybrid method compared to the linear imaging method, indicating better modelling of the sub-event primaries in the gap for the hybrid method.

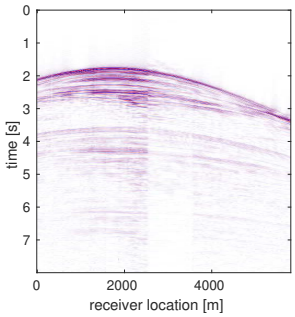

Figure 4.10 *Measured shot record data for the source at 2100 m after putting an infill in the gap obtained from the non-linear inversion process.*

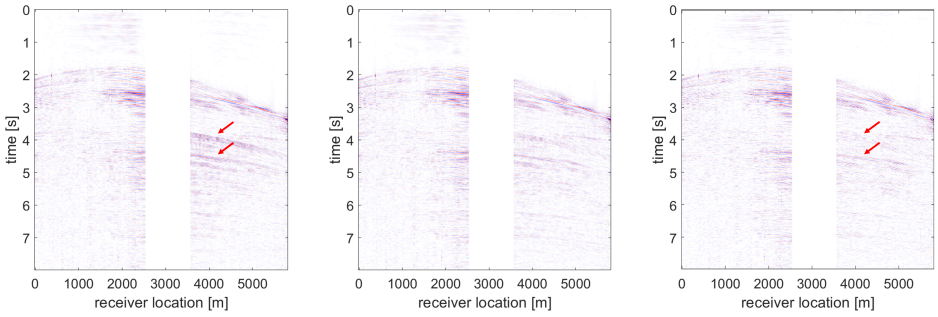

Figure 4.11 *Residual data for the gather with the source at 2100 m for a) linear imaging method, b) non-linear imaging method, and c) hybrid method. Red arrows indicate the first-order multiples in the residual data. The colour scale has been adjusted to a third compared to figure 4.10.*

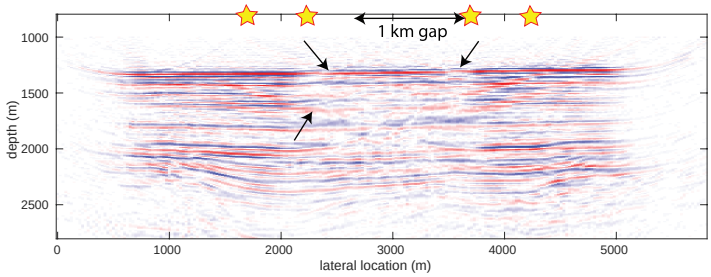

(a)

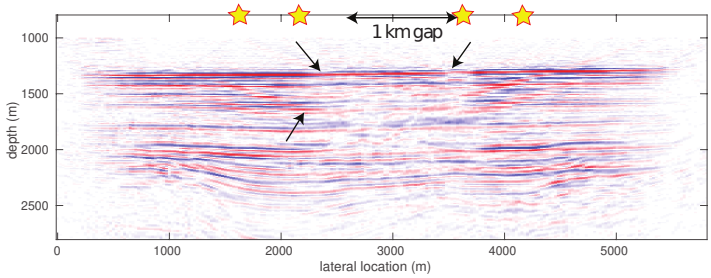

(b)

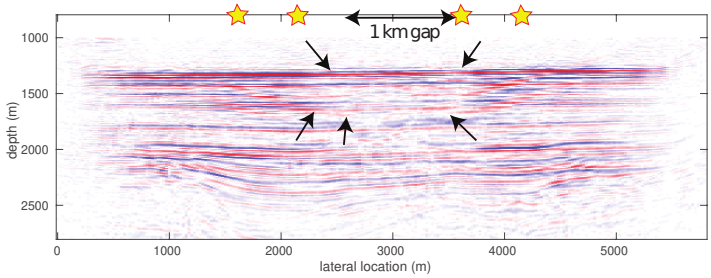

(c)

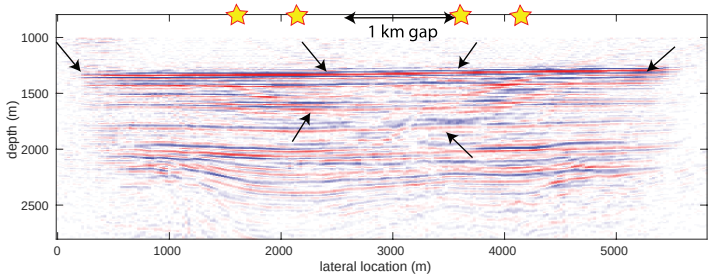

(d)

Figure 4.12 *Imaging results for the field data in a closed-loop imaging process for a geometry with only four sources: (a) using primaries only imaging, (b) using a linear inversion method, (c) using the proposed non-linear inversion method, (d) result of the hybrid method, combining the linear and non-linear inversion methods.*

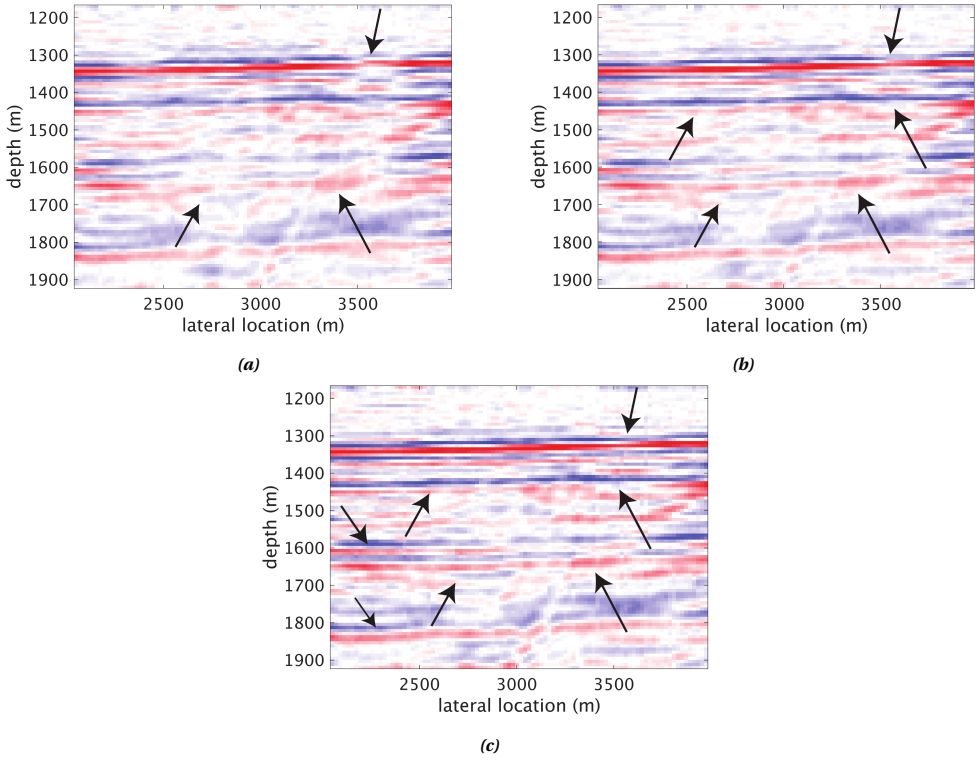

Figure 4.13 *Comparing the linear, non-linear and hybrid method in an enlarged section from* $x = 2075$ *m to* 4000 *m from (a) figure 4.12b and the corresponding section from (b) figure 4.12c and (c) figure 4.12d. The arrows indicate the regions where noticeable improvements can be observed.*

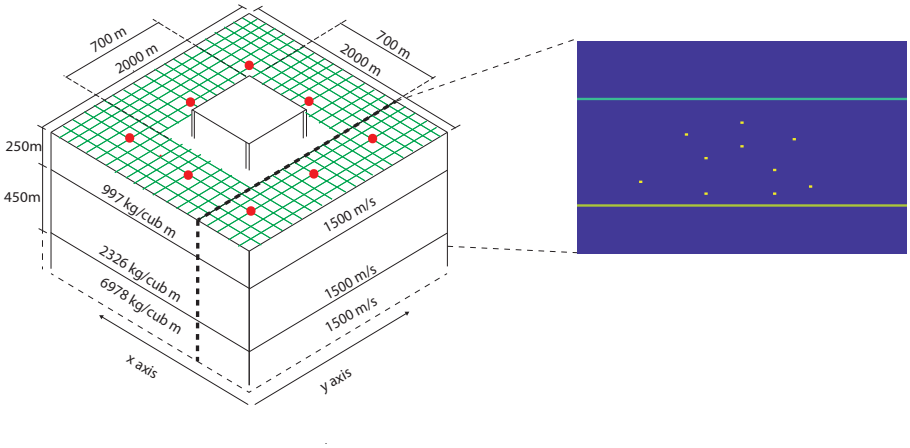

Figure 4.14 *Synthetic 3D model with sources around the platform (indicated in red). Receivers (indicated by the intersection of green lines) are spread throughout the surface except around the area of the platform. The model contains two reflectors at the depth of $z = 250$ m and 700 m respectively and several scatterers placed randomly in the second layer. The figure on the right shows a cross-section of the reflectivity model at $x = 760$ m.*

4.3. 3D NUMERICAL EXAMPLE

Here, we illustrate the 3D aspects of the imaging methods using a numerical example in a 3D model. Figure 4.14, shows the synthetic model that has been used to generate data via Full Wavefield Modelling. We are assuming the reflection parameter $\mathbf{R}$ to be angle-independent. The dimensions, densities and velocities of different layers have also been indicated in the figure. Several point scatterers have been spread all over the second layer. Figure 4.14 shows a cross-section to illustrate some of these scatterers. Eight sources are placed 300 m apart on the surface around the platform area as indicated by red dots in the figure. We put receivers in a dense grid of 20 m spacing covering the whole surface of 2 $km \times 2$ km except at the centre, where we create a gap in the centre due to the platform of dimension 700 $m \times 700$ m, as shown in figure 4.14. Although all the sources and receivers are at the surface, the configuration has been designed to emulate the OBN-type survey in terms of source and receiver sampling.

Figure 4.15a and 4.16a show the imaging result using the closed-loop imaging method with primaries-only data (without any multiples) for two different cross-sections. Figure 4.15a shows the horizontal cross-section at the first reflector, i.e. $z = 250$ m while figure 4.16a shows the vertical cross-section at $x = 760$ m of the image cube. The effects in the image due to missing receivers as well as sparse sources are clearly visible. We do not see any multiple-related cross-talk in the image since they were removed during the pre-processing step. Although the imaging method tries to explain the data in the gap, the reflector is quite diffused. Figure 4.15b and 4.16b show the imaging result using the primaries as well as multiples in a closed-loop 'linear' inversion method. We already see a great improvement in the coverage due to the multiples, the diffractors are more visible as well. However, the effects in the image due to missing receivers can still be seen here, albeit less strongly. We also see the cross-talk due to the multiples now, more

pronounced in the area below the gap. This is to be expected in imaging with multiples. Figure 4.15c and 4.16c illustrate the imaging result from the aforementioned 'non-linear' inversion method. We do see an uplift around the area with the gap, especially around the reflector at the depth of $z = 250\ m$. The 'uplift' can be seen better in figure 4.15c. Please note how the scatterers in the shallow layer of the figure 4.16c are imaged better than the one in figure 4.16b. We also see a reduction in the multiple-related cross-talk. Figure 4.15d and 4.16d show the final imaging result obtained via the hybrid method where some gap-related footprint and the cross-talk is further reduced. A considerable improvement is seen upon a comparison of the primaries-only imaging result in figure 4.15a and the final imaging result using the hybrid method in figure 4.15d.

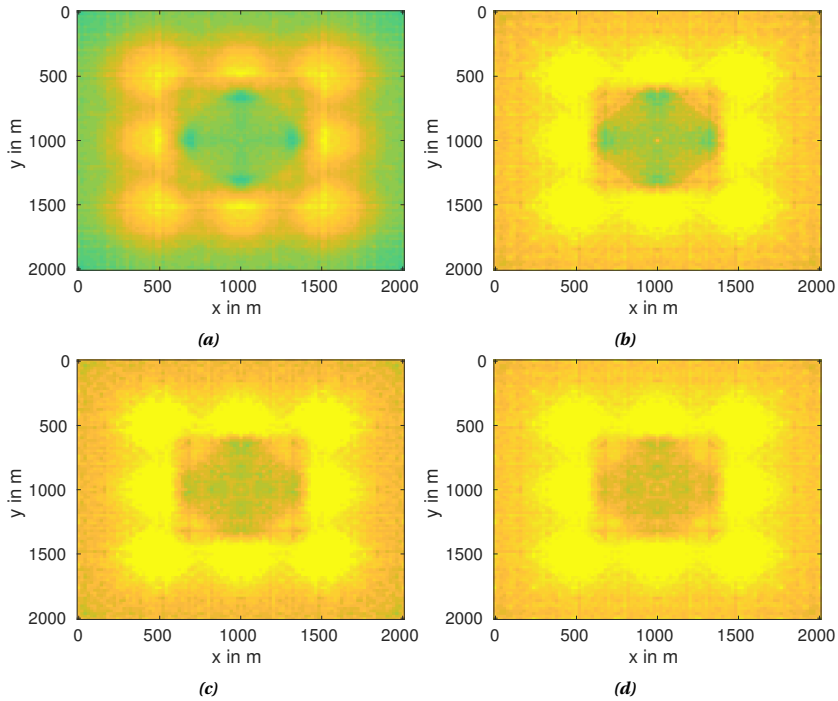

Figure 4.15 *3D example results related to fig. 4.14. Horizontal cross-section of the modelled images at the first reflector, i.e. $z = 250\ m$ in a closed-loop imaging process for geometry with sparse sources and a missing receiver gap obtained from a) primaries imaging; b) the linear imaging method that includes surface multiples; c) the non-linear imaging method and d) final result of the hybrid method.*

4.4. CONCLUSIONS AND DISCUSSION

We applied the different strategies for imaging with multiples in case of large acquisition gaps in towed streamer-type data. We tested these methods on synthetic data generated using two-dimensional as well as three-dimensional models. We also tested these methods on a 2D field data acquired in Saga Vøring basin. We also implemented our algorithm on a 3D OBN-type acquisition scenario. We try to test these methods for a case where the acquisition is obstructed due to an island. Although this preliminary study was tested on an 'inverse-crime' data, it gave us an insight into how these imaging

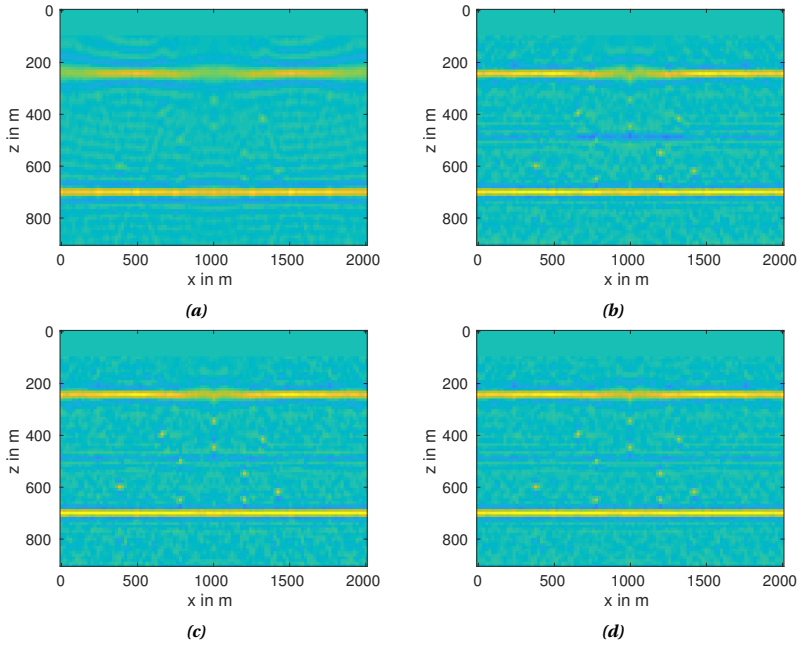

Figure 4.16 *3D example results related to fig. 4.14. Vertical cross-section of the same image cube at $x = 760$ m (fig. 4.14) in a closed-loop imaging process for a geometry with sparse sources and a missing receiver gap obtained from: a) primaries-only imaging method. The multiples were removed from the measured data and hence no cross-talk is visible in the image. b) The same cross-section of the image obtained from the linear imaging method that includes surface multiples; c) the non-linear imaging method and d) the final result of the hybrid method.*

strategies may be helpful for these scenarios. In reality, such an acquisition would be full of many more complicated components in the wavefield and would require a much more elaborate treatment. Generally speaking, we observe that the non-linear imaging method is less dependent on receiver density compared to imaging methods that include surface-related multiples via re-injecting the measured data and it does a good job at infilling the gap in data despite large missing receiver gaps. Finally, we see that a hybrid approach using both the linear and non-linear methods generally improves the result further.

The use of the non-linear and hybrid methods still requires an accurate estimation of the source wavefield. For our field data example, this wavefield could be estimated from the surface multiples via the EPSI method (Van Groenestijn & Verschuur, 2009). Also, it can be extracted from calibrating the primaries-only image with the linear imaging from the multiples, as described by Davydenko et al. (2015). More research is required for a stable and robust source wavefield estimation in this context.

In our examples, we have considered reflectivity to be a scalar quantity. Since we will be using the non-linear imaging method in case of gaps, introducing angle-dependent reflectivity (extending the parameters) may lead to overfitting. Hence, extending the reflectivity parameter to account for AVO effects may require certain constraints in the

reflectivity matrix **R**. We explore this topic further in appendix A.

BIBLIOGRAPHY

Berkhout, A. (2014). An outlook on the future of seismic imaging, part III: Joint migration inversion. *Geophysical Prospecting*, *62*, 950–971.

Davydenko, M., Verschuur, D., & van Groenestijn, G. (2015). Full wavefield migration applied to field data. *77th EAGE Conference and Exhibition 2015*, *2015*(1), 1–5.

Kabir, M., & Verschuur, D. (1995). Restoration of missing offsets by parabolic radon transform. *Geophysical Prospecting*, *43*, 347–368.

Nath, A., Verschuur, D., & Davydenko, M. (2019). Using surface multiples to image 3d seismic data with large acquisition gaps. *81st EAGE Conference and Exhibition 2019*, *2019*(1), 1–5.

Nath, A., & Verschuur, D. (2020). Imaging with surface-related multiples to overcome large acquisition gaps. *Journal of Geophysics and Engineering*, *17*(4), 742–758.

Van Groenestijn, G., & Verschuur, D. (2009). Estimating primaries by sparse inversion and application to near-offset data reconstruction. *Geophysics*, *74*(3), A23–A28.

5

OCEAN-BOTTOM NODE DATA

With the increasing popularity of seabed acquisition, be it ocean-bottom nodes (OBN) or ocean-bottom cables (OBC), it becomes necessary to explore the different strategies of imaging with multiples rather than removing them. We discuss a few such methods of using surface-related multiples to get around the problem of imaging with a large acquisition gap in an OBN acquisition scenario and compare it to the popular mirror imaging method. We get an insight into how imaging with higher-order multiples and the nonlinear imaging is beneficial in the infilling of data gaps in such an acquisition. We test our imaging methods using multiples and primaries on synthetically generated 2D numerical OBN data. Despite the large acquisition gaps, the results indicate mitigation of effects on the image previously caused by incomplete data.

5.1. INTRODUCTION

Data acquired via ocean-bottom nodes (OBN) have several benefits compared to the data acquired from steamer acquisition, such as high signal-to-noise ratio, wide azimuth range and easier access to difficult-to-reach areas (Dash et al., 2009). However, one drawback is that due to the high cost of the nodes they are usually placed at large intervals. Such sparse receiver positioning makes dense source sampling necessary (so-called 'carpet shooting'). After applying source-receiver reciprocity, we consider OBN as sparse sources located at the ocean bottom, shooting into dense receiver arrays at the surface. Conventional imaging methods on OBN data that use primaries-only data, often suffer from poor illumination. A popular imaging method for data acquired using OBN data is the mirror imaging method (Grion et al., 2007). In this method, after applying the source-receiver reciprocity and P-Z separation, a mirror source is defined. This translates to utilising the first-order receiver-side multiples. Although this improves the illumination, it still relies on a dense source sampling while ignoring the other orders of reverberations that could act as potential pseudo-source (in the reciprocal domain). Several authors have approached imaging with surface multiples in data acquired with

ocean bottom nodes (Godfrey et al., 1998; Ronen et al., 2005; Lecerf et al., 2015). Sambell (2015) and Davydenko and Verschuur (2016) have implemented FWM in the imaging of multiples in an OBN scenario. We will describe the methodology of implementing the mirror imaging method, linear imaging and the non-linear imaging method. We will also compare the imaging performance of these methods in case of a gap in the data.

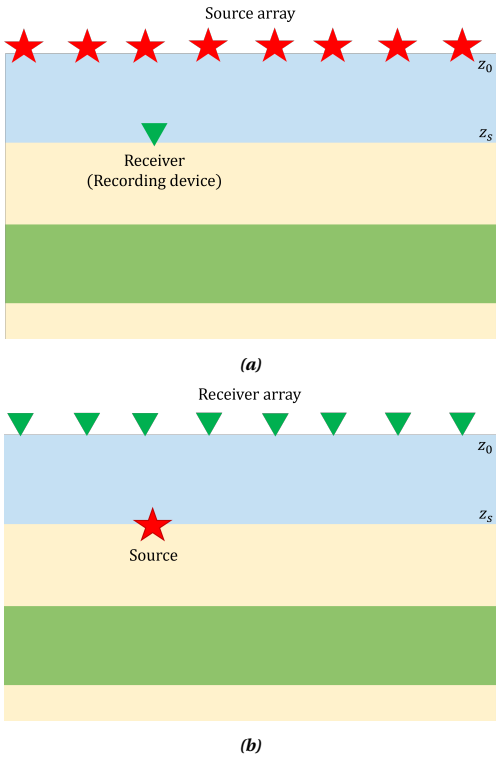

Figure 5.1 *Schematic diagram illustrating (a) source and receiver array in an OBN acquisition scenario and (b) assumed source and receiver array after applying reciprocity.*

5.2. THEORY AND METHODOLOGY

In a typical OBN survey, the receiver nodes are placed sparsely on the ocean bottom. The seismic reciprocity principle states that the time taken for a signal to travel between two points is the same regardless of which of the two points is the source or the receiver. Keeping this in mind, a common receiver gather data recorded from a setup shown in figure 5.1a will have the same seismogram as a common source gather recorded from the setup shown in figure 5.1b. Therefore, in an OBN setup, we can conveniently impose the assumption of reciprocity and exchange the sources with receivers and the nodes with sources. In data acquired by OBN (after applying reciprocity), such as shown in figure 5.2a, we can identify the following events:

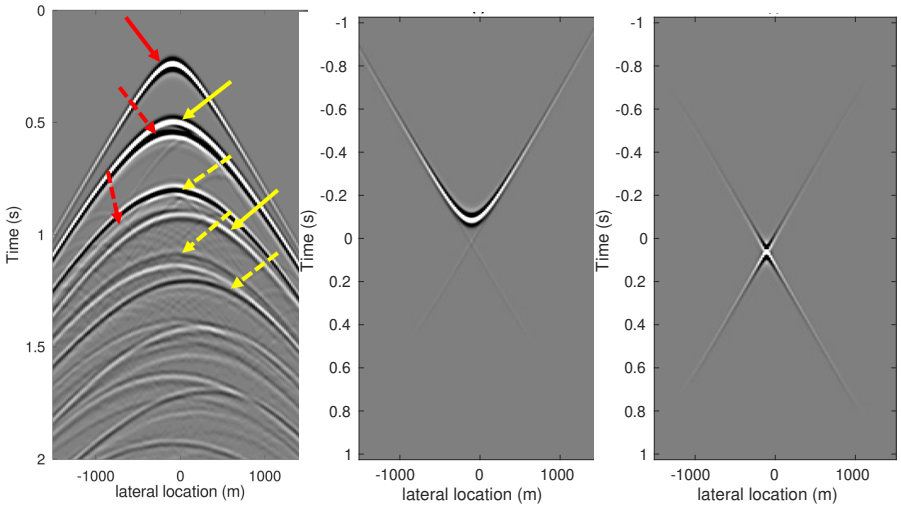

Figure 5.2 *Synthetic data generated using finite-difference modelling showing a) total measured data acquired by an ocean bottom node. The data has been generated using the model shown in figure 5.4. The solid red arrow is pointing at the direct arrival events while the dashed red arrows are pointing at the multiples associated with direct arrivals. The solid yellow arrows are pointing at a few primary events and the dashed yellow arrows are pointing at the different orders of multiples associated with these primary events. b) Source wave $\vec{S}^{+}(z_0)$ obtained by extrapolating the real source wavefield at the ocean bottom back in time to emulate an effective source wavefield at the surface. c) Same source wavefield $\vec{S}^{+}(z_s)$ upon reaching its actual source depth from the surface $z_s = 230\ m$.*

1. Primaries: these have undergone at most one order of reflection from the subsurface. This is indicated by solid yellow arrows in figure 5.2a.

2. Surface-related multiples generated by primaries: these are the wavefields generated by the primaries undergoing one or more orders of downward reflection at the water surface. These are marked by dashed yellow arrows in figure 5.2a.

3. Direct arrival: this event has never undergone any reflection at the subsurface. This has been marked by a solid red arrow in figure 5.2a.

4. Surface-related multiples generated by the direct arrival: these are the wavefields that are generated by one or more orders of downward reflection of the direct arrival at the water surface. These are indicated by dashed red arrows in figure 5.2a.

Since we will focus on imaging with multiples, we will be imaging with the total measured data, i.e. without removing any multiples from the measured data. The direct arrival does not undergo any reflection in the subsurface and, therefore, it is not helpful in reflection imaging. Hence, we can remove it from our measured data for all the imaging schemes. However, it will be used as a source field in some imaging modes.

IMAGING STRATEGIES

For imaging with the primaries-only wavefield, we could either include the source wavefield $\vec{S}^+(z_s)$ as our illuminating wavefield $\vec{Q}^+(z_s)$ at the source depth z_s or we can backward extrapolate $\vec{S}^+(z_s)$ in time to emulate an 'effective' source wavefield $\vec{S}^+(z_0)$ at the surface (figure 5.2b) such that, when added to $\vec{Q}^+(z_0)$, it focuses at the real source depth z_s (5.2c). Figures 5.3a and 5.3b illustrate these two approaches to imaging with the primaries wavefield. While both methods are interchangeable, our motivation behind defining an 'effective' source wavefield at the surface is the convenience of application in primaries and multiples imaging methods (section 2.4.2).

For multiples-only imaging, we have two options. We can either image just the first order of multiples that arise from direct waves as in mirror source imaging or we can image all the multiples by re-injecting the total measured wavefield as our illuminating wavefield. The first method has become an industry standard that uses a novel approach of wavefield separation using the P-Z summation and suppressing multiples of order two and higher. If the OBN is at a depth z_s from the sea surface, a 'mirror source' with opposite polarity is put at the depth $-z_s$, which is then used as the illuminating wavefield for imaging. Figure 5.3c shows via a schematic representation, the mirror imaging method. Under favourable circumstances and the right application, this leads to a good multiple separation and hence a reliable subsurface image. As for the second method, in a linear-imaging approach, we can use the re-injected total measured data at the surface $\mathbf{R}^{\cap}(z_0)\vec{P}^-(z_0)$ as our illuminating wavefield (figure 5.3d). This method models and images all the different orders of multiples, including the ones generated by the direct arrival and, therefore, we do not need to do any multiple separation as a pre-processing step.

Finally, *for imaging with primaries and multiples* we discuss two strategies for linear and non-linear imaging methods. The receiver side data that will be back-propagated in this case is the total measured data without the direct arrival $\vec{P}^-(z_0) - \vec{D}^-(z_0)$. For the linear imaging method with primaries and multiples, our illuminating wavefield at the surface $\vec{Q}^+(z_0)$ is a combination of the 'effective' source wavefield at the surface $\vec{S}^+(z_0)$ that is used to image the primaries-only wavefield and the re-injected total measured wavefield $\mathbf{R}^{\cap}(z_0)\vec{P}^-(z_0)$ is used to image the multiples, including the multiples from the direct arrival. The strategy so far is similar to the strategy described in section 2.4.2. For the non-linear imaging method, we will have to consider a change in our strategy. Unlike in section 2.4.2, we cannot use the same source as used for primaries-only imaging and build the multiples over several iterations. This is because the source used for primaries-only imaging cannot image the direct arrival and would fail to model the multiples associated with it in further iterations. Therefore, the illuminating wavefield at the surface $\vec{Q}^+(z_0)$ for non-linear imaging is a combination of the 'effective' source wavefield at the surface $\vec{S}^+(z_0)$, the re-injected direct arrival wavefield $\mathbf{R}^{\cap}(z_0)\vec{D}^-(z_0)$ and the re-injected modeled wavefield at the surface from the previous iteration $\mathbf{R}^{\cap}(z_0)\vec{P}_m^-(z_0)^i$, where $\vec{P}_m^-(z_0)^i$ refers to the modeled wavefield at the surface after the i^{th} iteration. Figures 5.3e and 5.3f show the difference between these two methods via schematic diagrams. Table 5.1 lists the source wavefield and the receiver side data used for imaging in all of the above-described methods.

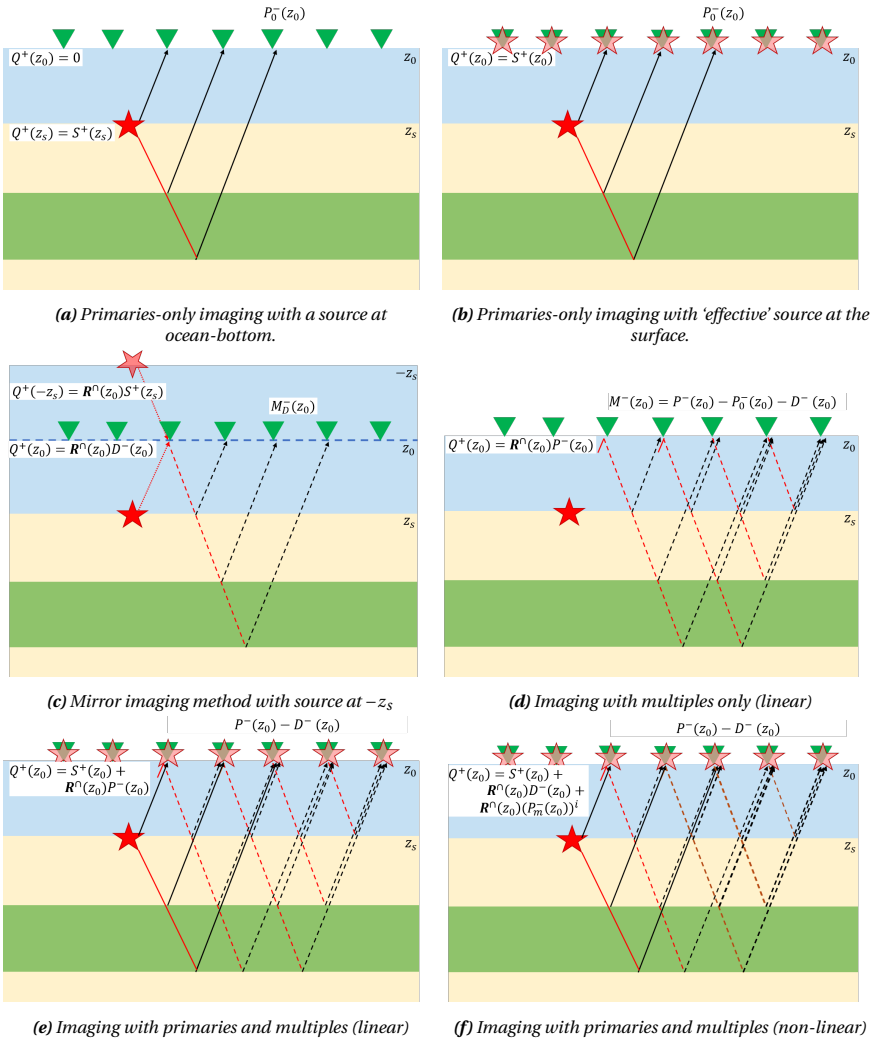

(a) *Primaries-only imaging with a source at ocean-bottom.*

(b) *Primaries-only imaging with 'effective' source at the surface.*

(c) *Mirror imaging method with source at $-z_s$*

(d) *Imaging with multiples only (linear)*

(e) *Imaging with primaries and multiples (linear)*

(f) *Imaging with primaries and multiples (non-linear)*

Figure 5.3 *Schematic diagram illustrating the source and receiver fields for the different imaging options for OBN data using ray diagrams, assuming reciprocity was applied. The green triangles show the receivers, the red star indicates the source and the translucent red stars at the surface show the 'effective' source wavefield. Red arrows indicate the source side forward propagated wavefield. Black arrows indicate the receiver side back propagated wavefield. The brown arrows indicate iteratively generated modelled wavefield that we re-inject as source side forward propagated wavefield. The solid and dashed lines refer to primaries and multiples respectively.*

5.2.1. ESTIMATING THE DIRECT WAVEFIELD

As proposed, for imaging with primary wavefields it is important to know the direct wavefield. We must note that we are including the source-ghost as a part of the direct arrival $\vec{D}^-(z_0) + \mathbf{R}^\cap(z_0)\vec{D}^-(z_0)$, but if the source is exactly at the 'theoretical' surface, direct arrival would refer to only $\vec{D}^-(z_0)$. If the measured data is not deghosted, the former as-

Table 5.1 *Table comparing the source wavefield and the receiver side data acquired using OBN for different methods (at the surface).*
$\vec{S}^{+}(z_0)$ *: back propagated source wavefield at the surface* z_0*;*
$\vec{P_0}^{-}(z_0)$ *: primaries-only up-going wavefield at the surface* z_0*;*
$\vec{D}^{-}(z_0)$ *: direct arrival (direct arrival in down going wavefield);*
$\vec{M_0}^{-}(z_0)$ *: first-order multiple from down-going wavefield;*
$\vec{P}^{-}(z_0)$ *: total measured data.*
$\vec{P}_m^{-}(z_0)^{i}$ *: modeled data at the surface after* i *iterations.*

Method	Source side data	Receiver side data
Primaries-only	$\vec{S}^{+}(z_0)$	$\vec{P_0}^{-}(z_0)$
Mirror-source	$\vec{S}^{+}(-z_s)$ or $\mathbf{R}^{\cap}(z_0)\vec{D}^{-}(z_0)$	$\vec{M_0}^{-}(z_0)$
Linear	$\vec{S}^{+}(z_0)+\mathbf{R}^{\cap}(z_0)\vec{P}^{-}(z_0)$	$\vec{P}^{-}(z_0)-\vec{D}^{-}(z_0)$
Non-linear	$\vec{S}^{+}(z_0) + \mathbf{R}^{\cap}(z_0)\vec{D}^{-}(z_0) + \mathbf{R}^{\cap}(z_0)\vec{P}_m^{-}(z_0)^{i}$	$\vec{P}^{-}(z_0)-\vec{D}^{-}(z_0)$
Multiples-only	$\vec{P}^{-}(z_0)$	$\vec{P}^{-}(z_0)-\vec{P_0}^{-}(z_0)-\vec{D}^{-}(z_0)$

sumption doesn't affect our imaging result since we use a data-driven imaging approach. We suggest the following methods of separating the direct arrivals for OBN data (before applying reciprocity):

1. *Muting*: This can be implemented in two scenarios.
   (a) After applying P-Z summation, we get the total down-going wavefield (Wang et al., 2009). If the direct arrival is well separated from the other reflection data, a mute around direct arrival gives the desired wavefield.
   (b) If the direct arrival (and receiver ghost) is well separated from the reflected events, muting around the direct waves, and scaling it by $\frac{1}{1+\mathbf{R}}$ (for hydrophone data) or $\frac{1}{1-\mathbf{R}}$ (for geophone data) gives us the direct wave estimate.
2. *Model fitting*: We model the direct wave along with the source ghost, provided we have the source and node locations. Model fitting would match the amplitude of the modelled wavefield (direct wavefield + source ghost) to the measured data. We thereby get the direct arrival by scaling the resulting modelled data by $\frac{1}{1\pm\mathbf{R}}$.

5.3. 2D NUMERICAL EXAMPLE

Here, we test the different methods using a numerical example for OBN data in a 2D model. Figure 5.4, shows the synthetic model that has been used to generate the data via finite-difference modelling. For this example, we are considering a constant velocity throughout the model to get an angle-independent reflection parameter **R**. The 2D model is 1500 m deep and 3000 m wide in dimension. Six nodes are placed on the ocean bottom at equal intervals of 280 m (denoted by the red star in figure 5.4) while leaving a large gap between the third and the fourth node to simulate the receiver gap due to a platform. We put a dense source coverage on the surface except at the centre, where we create a gap of 600 m, as shown in figure 5.4.

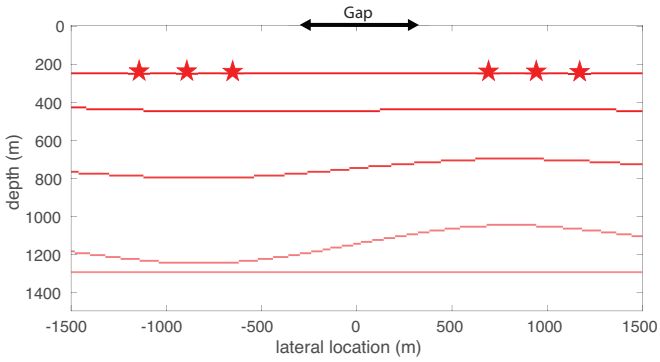

Figure 5.4 *Synthetic model illustrating an OBN acquisition. Six nodes have been placed on the ocean bottom. A dense source sampling has been done at the surface except in the gap which is 600 m wide.*

The ghost effects on the receiver side are included as a part of the source signature. Since we put our source at the surface, the direct wave (downgoing, towards the node before reciprocity) would not be accounted for, hence, we need to remove it from our measured wavefield. The upgoing part of the direct wave after reflection at the ocean bottom will be accounted for by our source. We can keep the downgoing and upgoing part of the direct wave in our re-injected wavefield as they will account for the subsequent 'mirror multiples'. Figure(5.5a) shows the total downgoing wavefield at the surface $\vec{Q}^{+}(z_0)$ for the 'linear' method.

For the non-linear method, we forward model with $\vec{S}^{+}(z_0)$ as our initial incident wavefield. Figure(5.5b) shows $\vec{Q}^{+}(z_0)$ for the 'non-linear' method. However, as mentioned earlier we also need to account for a part of the direct wave that creates the mirror multiples through our illuminating wavefield. Hence, we re-inject this part of the direct wave with $\vec{S}^{+}(z_0)$ to give us the illuminating wavefield for the first iteration $[\vec{Q}^{+}(z_0)]^1$, where the superscript refers to the iteration number. Figure(5.5(c)) represents the 'upgoing' wavefield after removing a part of the direct wavefield. After making suitable changes for non-linear inversion in a closed-loop approach, we derive the reflectivity image.

Figure 5.6a shows the imaging result using the closed-loop mirror imaging method. The cross-talk from the multiples (indicated with arrows) can be clearly seen here. The lower section of the image has not been imaged properly either. The effects in the image due to the large acquisition gap are also very apparent. Figure 5.6b shows the imaging result using the primaries as well as multiples in a closed-loop 'linear' inversion method. We already see a great improvement in the lower section of the image as the cross-talk has reduced, indicating that multiples have positively contributed to imaging. However, the effects in the image due to missing receivers can still be seen here, albeit less strongly. Some of the cross-talk from multiples still remains (indicated with arrows) due to the missing data. Figure 5.6c illustrates the imaging result from the aforementioned 'non-linear' inversion method. Although the improvement in the lower depths is not obvious, the cross-talk from multiples that was previously leaking below due to the gap in figure 5.6b has reduced to a certain extent (difference marked by arrows). This seems to imply

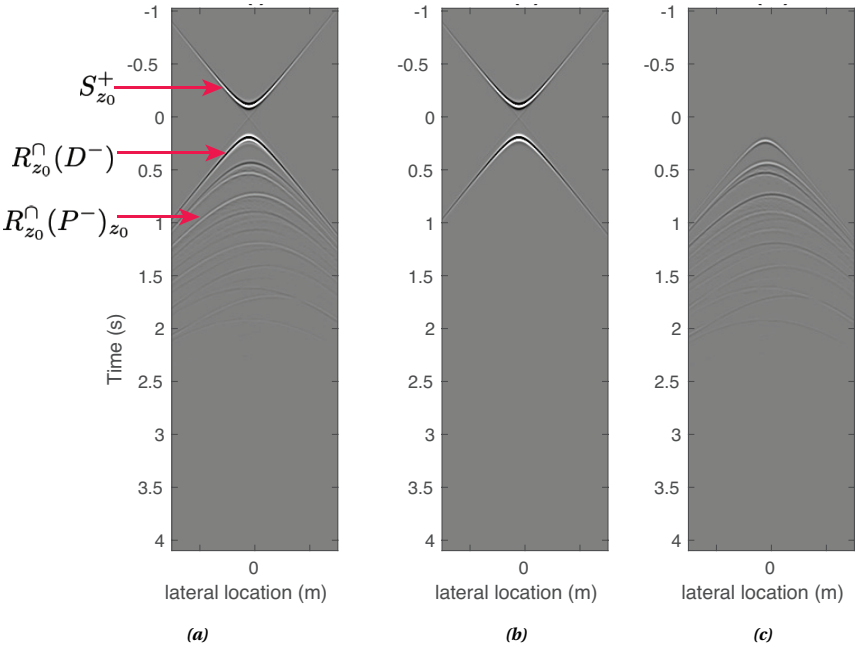

Figure 5.5 *Total downgoing wavefield at the surface $\vec{Q}^+(z_0)$ for (a) the linear method and (b) the non-linear method. (c) The 'upgoing' wavefield after removing a part of the direct wavefield.*

that the data in the gap was better modelled by this method and, hence, it could image multiples better. Figure 5.6d shows the final imaging result obtained via the hybrid method. Quite some improvement is visible upon the comparison of the resulting image in figure 5.6d and figure 5.6a.

5.4. DISCUSSION

We came up with a new strategy to image with data acquired using ocean bottom nodes. Using this method we propose to include all the order of multiples for imaging along with the primaries. In order to implement our previously described methods of using primaries and multiples imaging methods for an OBN scenario, we propose to back-propagate the measured direct arrival to the surface, assuming that source-receiver reciprocity has been applied. This is done to imitate the streamer acquisition, making our implementation of linear and non-linear imaging more obvious. It must be added that while this is our chosen method of implementing our strategies, it is not the only way to do so. We tested our strategy on a 2D scenario using numerically generated data, and the imaging results performed similarly to the results obtained on streamer data. The data was generated using finite-difference modelling, and a gap in the data was added later. We also compare the linear, and non-linear imaging methods to the mirror imaging method to especially emphasise the benefit of including more orders of multiples, not just in infilling the gaps but also in reducing the cross-talk.

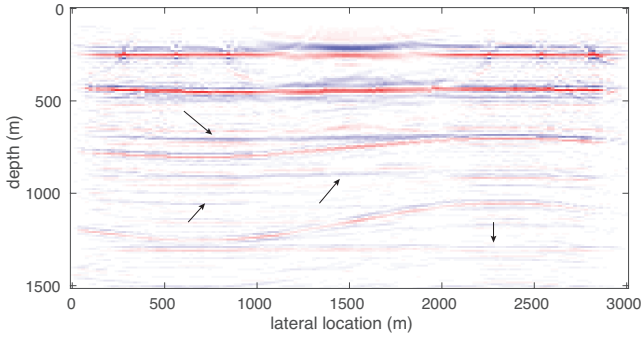

(a)

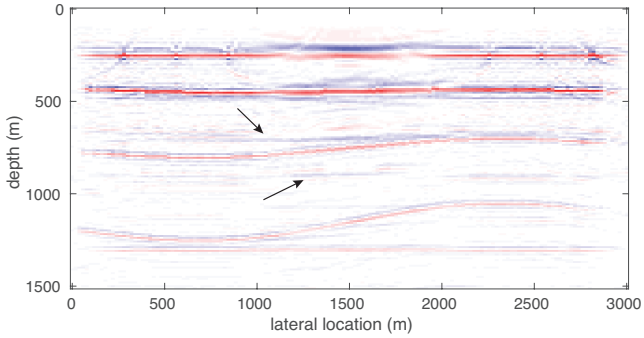

(b)

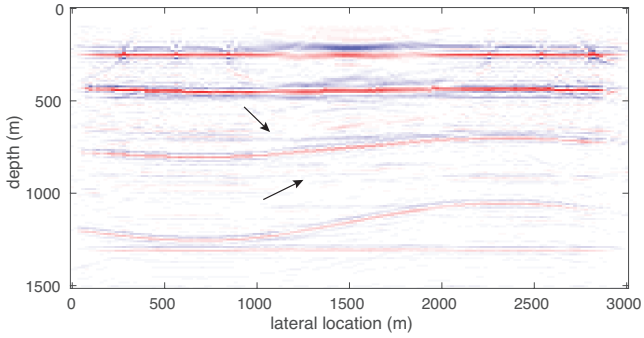

(c)

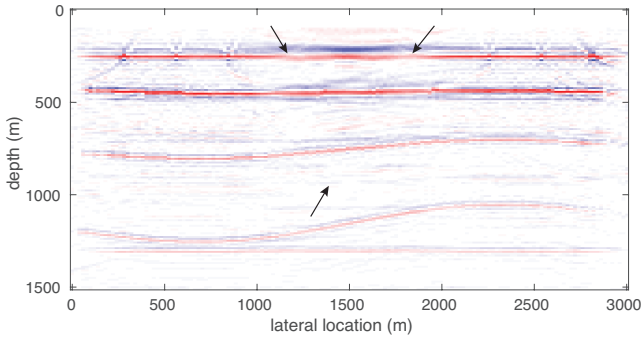

(d)

Figure 5.6 *Imaging results in a closed-loop imaging process for a geometry with only six sources: a) using mirror migration method, b)using a linear inversion method, c) using the proposed non-linear inversion method, and d) final result of the hybrid method, combining the linear and the non-linear inversion methods.*

In data acquired using OBN, removing the multiples has been a challenging exercise, especially in complex geologies. Although a lot of work is being done in the development of different deconvolution strategies that remove these multiples, we propose that including multiples in imaging with OBN data could be a very beneficial decision.

BIBLIOGRAPHY

Dash, R., Spence, G., Hyndman, R., Grion, S., Wang, Y., & Ronen, S. (2009). Wide-area imaging from obs multiples. *Geophysics*, *74*(6), Q41–Q47.

Davydenko, M., & Verschuur, D. (2016). Optimal imaging of obn data using all multiples. *2016 SEG International Exposition and Annual Meeting*.

Godfrey, R., Kristiansen, P., Armstrong, B., Cooper, M., & Thorogood, E. (1998). Imaging the foinaven ghost. In *SEG technical program expanded abstracts 1998* (pp. 1333–1335). Society of Exploration Geophysicists.

Grion, S., Exley, R., Manin, M., Miao, X., Pica, A., Wang, Y., Granger, P., & Ronen, S. (2007). Mirror imaging of obs data. *first break*, *25*(11), 37–42.

Lecerf, D., Hodges, E., Lu, S., Valenciano, A., Chemingui, N., Johann, P., & Thedy, E. (2015). Imaging primaries and high-order multiples for permanent reservoir monitoring: Application to jubarte field. *The Leading Edge*, *34*(7), 824–828.

Ronen, S., Comeaux, L., & Miao, X. (2005). Imaging downgoing waves from ocean bottom stations. In *SEG technical program expanded abstracts 2005* (pp. 963–966). Society of Exploration Geophysicists.

Sambell, K. (2015). Full wavefield migration of multi-component ocean bottom node data.

Wang, Y., Grion, S., & Bale, R. (2009). What comes up must have gone down: The principle and application of up-down deconvolution for multiple attenuation of ocean bottom data. *CSEG Recorder*, *34*(10), 10–16.

6

CONCLUSION AND RECOMMENDATIONS

6.1. CONCLUSION

In an ideal scenario, if our seismic data is densely sampled without any irregularities, we can easily get a high-quality migration image using any competent migration methods. However, irregular data is unavoidable in reality, and we end up with sub-optimal imaging results, leading to a constant search for better imaging methods. The iterative least-squares migration method with primaries-only data improves our imaging results despite these data irregularities. While removing seismic multiples from data is still a common practice, we show that incorporating multiples in imaging can improve the results of least-squares imaging, particularly for irregular data. This is because multiples add a unique value to migration images by following different travel paths than primary wavefields. Additionally, integrating multiples in imaging can avoid the often expensive step of removing them. One of the major concerns of using multiples in imaging has been the fear of unwanted cross-talk in the image. However, we show that reformulating our imaging strategies can easily incorporate multiples as a signal and mitigate those cross-talk issues. In this pursuit, this thesis explores the various imaging strategies with surface multiples.

One of our main contributions to this thesis is introducing the so-called 'non-linear' imaging method. This method extends the iterative least-squares migration method that uses data with primary wavefields and multiples. Full-wavefield migration (FWM) is an example of prior work on one such least-squares migration method. FWM uses the reinjected wavefield and the source wavefield as the total illuminating wavefield leading to a 'linear' relationship between the reflectivity and the modeled data, similar to the primaries-only imaging methods. FWM has been known to reduce cross-talk in imaging with multiples, improve imaging resolution, and overall increase the subsurface illumination due to the multiples. However, since this method uses the recorded wavefield to

re-inject as the source for multiples, it is also sensitive to significant data gaps. In the 'non-linear' imaging method, we model all the wavefields, primaries, and multiples iteratively from a given source wavefield and a 'correct' velocity model. Therefore we need data with all the primaries and surface-related multiples for this imaging method. The motivation behind developing the 'non-linear' imaging method was to perform imaging with multiples while mitigating the sensitivity to significant data gaps. Since we model the data from a given source wavefield, our result is less affected by the missing data and potentially has more impact in improving the image resolution.

Another contribution made in this thesis is the hybrid method, which follows from the 'non-linear' imaging method. Using supporting examples, we show that the 'non-linear' imaging outperforms the 'linear imaging' method in areas with large data gaps. Due to the increase in the illumination of the affected areas due to the 'non-linear' imaging method compared to the linear imaging method, we expect an improvement in the infilling of areas with data gaps and better image resolution. However, we also show via examples that since this method is non-linear, it is more sensitive to errors. Additionally, we need a reliable estimation of the source wavelet to perform this imaging method. Since the linear imaging methods that use multiples have their benefits that are complimentary to using only non-linear imaging methods, we propose a hybrid method that combines these two imaging methods in an order that depends on which method is the most efficient or would help us get out of local minima for the situation. This is desirable as we highlight that extracting the benefits from multiples is possible through different means that can bring additive benefits in the final imaging result.

Using various examples, we demonstrate the benefits of using surface-related multiples in imaging via the non-linear and hybrid methods. The method has been tested and compared with the other imaging methods on 2D and 3D numerically generated data and on field data. We explore different imaging options in case of data that has a large gap and we show how the multiples help in filling the gap. In all these examples, we could successfully show the benefits of using the non-linear imaging method over a linear imaging method. In Chapter 5, we explored imaging with multiples for the case of data acquired using ocean-bottom node acquisition. We suggest a new strategy to implement our non-linear and hybrid imaging methods in the ocean-bottom node data. We compare our imaging methods with the mirror imaging method and show how more orders of multiples only further add to the illumination and resolution of the image.

In summary, in this thesis, we show the benefits of imaging with surface-related multiples. We propose including the non-linear imaging method and a hybrid method to get better imaging results, especially in areas with limited illumination. The non-linear imaging method can potentially improve image resolution and increase illumination while being less sensitive to large missing data compared to linear imaging methods. The hybrid method combines the benefits of both linear and non-linear imaging methods, making it flexible and hence a powerful tool for imaging with multiples. We demonstrate the effectiveness of these methods through various examples using synthetic and field data in several types of acquisition scenarios. With the increasing demand for cost-effective methods, our proposed imaging strategies that use all the available signals in the form of primaries and multiples can be a valuable tool in the future.

6.2. FUTURE RECOMMENDATIONS

In this section, I will discuss some potential avenues for future research.

6.2.1. STUDYING AVO EFFECTS

In this thesis, we mainly focus on angle-independent reflectivity estimation. This assumption needs to be revised as this can only be possible where no velocity variations between layers exist. Including angle-dependent reflectivity parametrisation as described by De Bruin et al. (1990) is the most natural way to proceed in our migration scheme However, as discussed in appendix A, this could be disastrous for our non-linear imaging method as over-parametrisation could easily steer us away from the truth towards local minima. While some work has already been done by Davydenko and Verschuur (2017) in the case of linear imaging with multiples, future efforts could be made to define or limit the parametrisation ideal for our situation of non-linear imaging.

With the increasing capabilities of machine-learning (ML) applications, we can seek help in optimising parametrisation or regularisation to meet our AVO needs. This is a non-trivial problem, but a lot of effort has already been put into this area, and it could be beneficial for our case of 'non-linear' imaging. Another way of dealing with the amplitude-versus-offset effect in the data could be by reducing these effects in the input data before migration, as a pre-processing step via an ML model. This will affect our ability to perform reservoir characterisation with certainty, but it could still be helpful for our purpose.

6.2.2. ROLE OF IMAGING WITH MULTIPLES IN OBN SURVEYS

As the world undergoes the energy transition, the demand for high-resolution and cost-effective seismic imaging in areas such as wind farm construction and carbon dioxide injection is bound to increase. To meet this demand, seismic imaging can be feasible using seismic multiples acquired using a few ocean-bottom nodes. Using seismic multiples as signals reduces the overall survey cost. Imaging with them is helpful for illumination and angle coverage, especially in the shallow subsurface region (Lu et al., 2014). In this thesis, we have shown via examples how we can get good illumination with very few nodes as long as we use more orders of multiples. Research focusing on developing high-resolution, low-cost, and flexible ocean-bottom node (OBN) seismic surveys that keep seismic multiples as a signal in mind will be a beneficial topic for future research.

6.2.3. MACHINE LEARNING

Machine learning (ML) is a numerical tool with many potentials in the seismic industry (Yu & Ma, 2021). In the case of suppressing the multiples in seismic data, machine learning methods have shown promising results (Siahkoohi et al., 2019; Li et al., 2021). In the same context, we can see ML-based methods as a faster tool when compared to the traditional physics-based methods for separating seismic multiples and primaries in large data-set, which in turn can be used to facilitate imaging with multiples. This comes with the caveat that the speed and performance of the ML-based method are dependent on the quality and quantity of the training data.

For data with large gaps, extensive work is already being done in seismic processing for interpolating near offset data using machine learning (Qu et al., 2021; Wang et al., 2022). Although machine learning-based methods may not replace the current state-of-the-art physics-based algorithms, we can develop ML-based strategies to become a more cost-effective method while continuing to improve its processing quality or better; we use ML-based methods in tandem with the physics-based methods or regularisation to steer the solution towards a realistic solution (Raissi et al., 2019; Zhu et al., 2019). We suggest extending this to assist non-linear imaging in filling large data gaps by further sharpening the infilled data.

In this thesis, we describe a hybrid method that explores the benefits of using different kinds of imaging methods using multiples. We use a simplistic approach of sequentially applying the different methods, choosing the sequence based on the problem at hand and which method is most suited to solve it. In the future, we can explore the possibility of a single cost function that does a weighted combination of the cost functions used in the individual methods. Manually selecting the parameters in traditional methods is not only time-consuming but is also task-specific. ML tools can automatically learn the best parameter tuning for a specific task, which could further our gains in imaging with multiples.

6.2.4. TIME LAPSE

We show that the non-linear imaging method is more sensitive to velocity errors than the linear imaging method. This property of non-linear imaging may be important for monitoring time-lapse changes. A research project that explores this might give us exciting insights into how multiples aid in time-lapse monitoring.

BIBLIOGRAPHY

Davydenko, M., & Verschuur, D. (2017). Full-wavefield migration: Using surface and internal multiples in imaging. *Geophysical Prospecting*, *65*(1), 7–21.

De Bruin, C., Wapenaar, C., & Berkhout, A. (1990). Angle-dependent reflectivity by means of prestack migration. *Geophysics*, *55*(9), 1223–1234.

Li, Z., Sun, N., Gao, H., Qin, N., & Li, Z. (2021). Adaptive subtraction based on u-net for removing seismic multiples. *IEEE Transactions on Geoscience and Remote Sensing*, *59*(11), 9796–9812.

Lu, S., Whitmore, D., Valenciano, A., & Chemingui, N. (2014). Separated-wavefield imaging using primary and multiple energy. *First Break*, *32*(11), 87–92.

Qu, S., Verschuur, E., Zhang, D., & Chen, Y. (2021). Training deep networks with only synthetic data: Deep-learning-based near-offset reconstruction for (closed-loop) surface-related multiple estimation on shallow-water field datadl-based near-offset reconstruction. *Geophysics*, *86*(3), A39–A43.

Raissi, M., Perdikaris, P., & Karniadakis, G. E. (2019). Physics-informed neural networks: A deep learning framework for solving forward and inverse problems involving nonlinear partial differential equations. *Journal of Computational physics*, *378*, 686–707.

Siahkoohi, A., Verschuur, D. J., & Herrmann, F. J. (2019). Surface-related multiple elimination with deep learning. *SEG International Exposition and Annual Meeting*.

Wang, B., Han, D., & Li, J. (2022). Missing shots and near-offset reconstruction of marine seismic data with towered streamers via self-supervised deep learning. *IEEE Transactions on Geoscience and Remote Sensing*, *60*, 1–9.

Yu, S., & Ma, J. (2021). Deep learning for geophysics: Current and future trends. *Reviews of Geophysics*, *59*(3), e2021RG000742.

Zhu, Y., Zabaras, N., Koutsourelakis, P.-S., & Perdikaris, P. (2019). Physics-constrained deep learning for high-dimensional surrogate modeling and uncertainty quantification without labeled data. *Journal of Computational Physics*, *394*, 56–81.

A

ANGLE-DEPENDENT PARAMETRISATION FOR NON-LINEAR IMAGING

A.1. INTRODUCTION

Some of the artefacts due to strong AVO variations leak into the migrated image as the angle-independent parametrisation in our current method manages to effectively minimise the data misfit with the final image. Assuming the reflectivity operator **R** to be a diagonal matrix as described in section 2.1, only explains the average reflection in the subsurface grid points. To explain the data more accurately in order to get rid of the artefacts in our migrated image, we must include angle-dependent parametrisation in our modeling scheme. Davydenko and Verschuur (2017) explored this topic for modelling as well as imaging. However, including an angle-dependent parametrisation in the 'non-linear' imaging scheme might lead to over-parametrisation of the model, which will minimise the objective function despite wrong reflectivity values. Practically, this means that the method will not be able to reconstruct data along large gaps, but will translate the gap information in terms of a (non-physical) AVO effect. Moreover, using an angle-dependent parametrisation would be more expensive. We therefore explore the possibility of going around this problem by suggesting a small change in the 'non-linear' imaging scheme.

A.2. METHOD

Rather than updating the angle-independent reflectivity matrix simultaneously for all shot gathers, we allow each shot gather to update its own diagonal reflectivity matrix, which expands the parameter space. However, to limit this expansion we also apply a constraint in the model space. The objective function J^j for each shot j can be described

as follows:

$$J^j = J_1^j + J_2^j, \tag{A.1}$$

where the first term in the equation is the data misfit norm function:

$$J_1^j = \sum_{\omega} \left\| \vec{P}^-_{j,obs}(z_0) - \vec{P}^-_{j,mod}(z_0) \right\|^2, \tag{A.2}$$

and the second term J_2^j, is a constraint function that penalises the difference between the updated reflectivity image $\mathbf{R}^j$ from the j^{th} shot gather and the weighted average of reflectivity from every shot gather $\bar{\mathbf{R}}$:

$$J_2^j = \lambda \sum_{\omega} \left\| \mathbf{R}^j - \bar{\mathbf{R}} \right\|^2, \tag{A.3}$$

where λ determines the overall weight of this term with respect to J_1^j. $\bar{\mathbf{R}}$ is given by:

$$\begin{aligned} \bar{\mathbf{R}} &= \sum_{j=1}^{n_{shots}} \mathbf{A}^j \mathbf{R}^j; \\ \bar{R}(x_i, z_n) &= \sum_{j=1}^{n_{shots}} \frac{P_j^+(x_i, z_n)^2 R^j(x_i, z_n)}{\sum_{j=1}^{n_{shots}} P_j^+(x_i, z_n)^2 + \epsilon}. \end{aligned} \tag{A.4}$$

$\mathbf{A}^j$ here is the weight function that can be interpreted as the strength of illumination of a certain point in the model for every shot gather with respect to the total illumination. Application of this weight to the reflectivity image calculation for a shot ensures that the average weighted image is mostly determined from sources that have a good illumination in a certain image point. Therefore, in J_2^j, the difference $\mathbf{R}^j - \bar{\mathbf{R}}$ highlights the undesirable and anomalous features of $\mathbf{R}^j$ and penalises them while still allowing the local $\mathbf{R}^j$ to deviate from $\bar{\mathbf{R}}$ in case of strong AVO effects.

A.3. SYNTHETIC DATA EXAMPLE

To demonstrate and compare our method, we use the data generated via acoustic finite-difference data on the model shown in 2.4a. Figure A.4a shows the imaging result using the 'non-linear' imaging result. To highlight this situation we can look at the residual data (shown in figure A.1a), which shows how the angle-independent parametrisation fails to minimise residuals effectively at higher offsets. Figure A.2 shows images received from per shot gather update. This process lets the optimisation method minimise the residual data more effectively (see figure A.1b) with the caveat of letting image artefacts stay at larger offsets in order to reduce data misfit. We seek to avoid this by putting an additional constraint with the weighted average image of each shot gather in our cost function. Figure A.3 shows the weight functions $\mathbf{A}^j$ for each shot gather at iteration j. Figure A.4b shows the weighted average image $\bar{\mathbf{R}}$ obtained via eq.A.4, that is used as a constraint in the objective function. The final result is shown in figure A.4c. The artefacts due to strong AVO variations do seem to have been reduced when compared with the

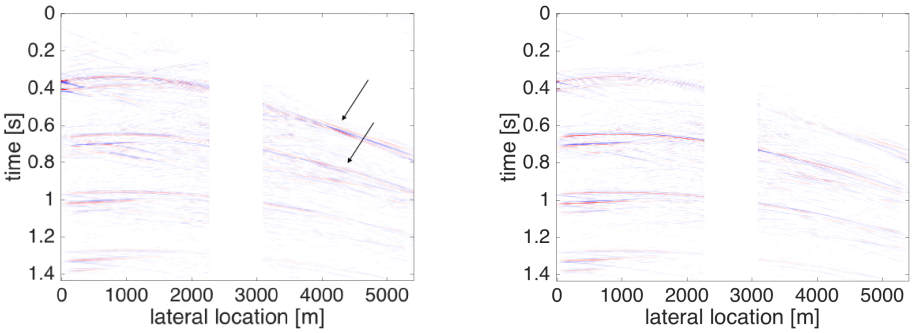

Figure A.1 *a) Residual data received from 'non-linear' inversion; for the source at 900m. The arrows point towards residual data at higher offsets that are not minimised. b) Residual data in case of per shot image update. (The image was strongly clipped for better analysis.)*

imaging result of 'non-linear' inversion method (see A.4a). Although the artefacts have been reduced, the method loses its strength in interpolation ability. Please note that this is a first step towards solving this problem. More work is required to improve the results.

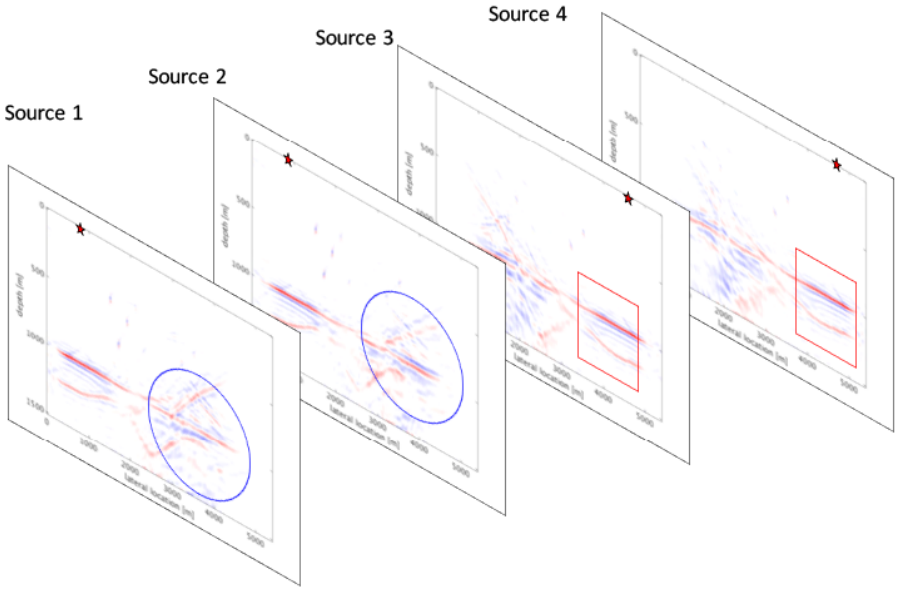

Figure A.2 *Images with corresponding source numbers, received after each shot gather updates its own angle-independent reflectivity image. The regions marked in blue circles signify artefacts in the image due to AVO affects. The region in red boxes show desirable output for the corresponding artefacts that are better imaged by other shots.*

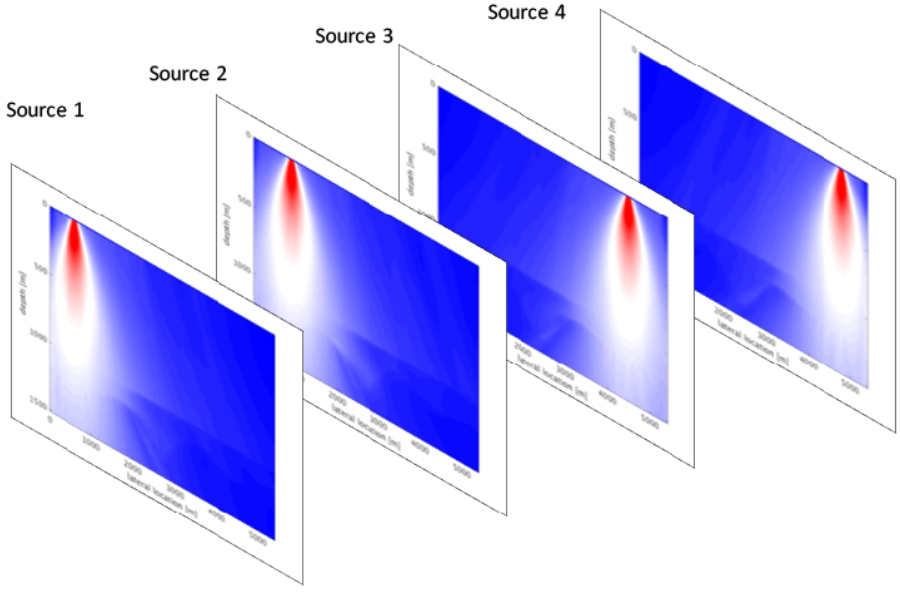

Figure A.3 *Pershot weight function* $\mathbf{A}^j$ *for each shot gather at a certain iteration* j *along with their corresponding source numbers.*

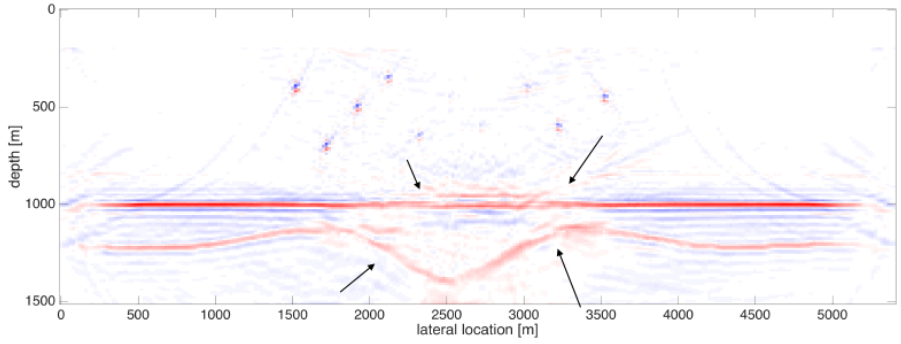

(a)

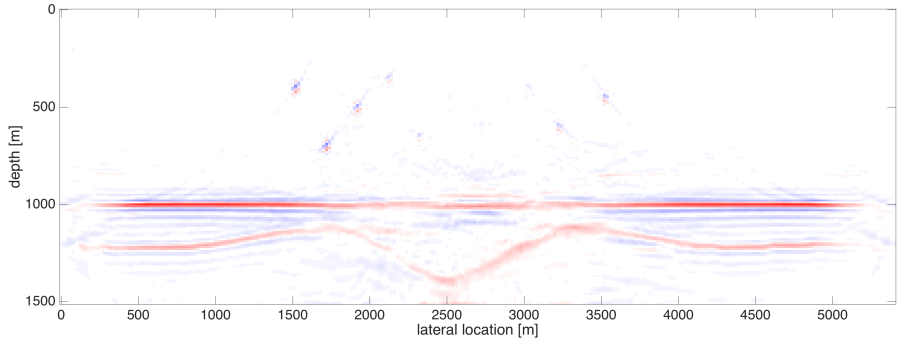

(b)

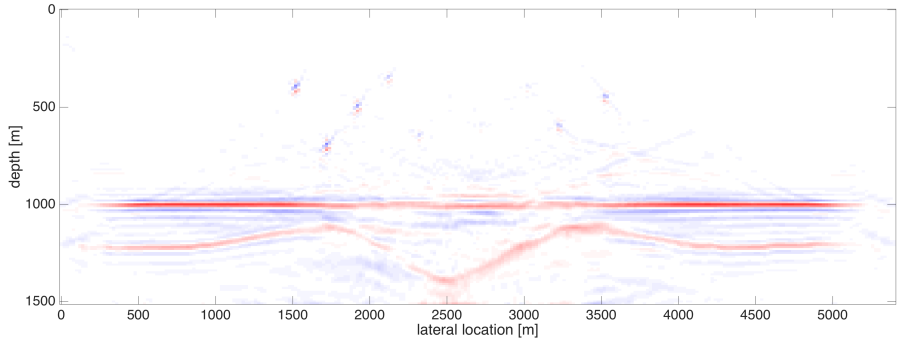

(c)

Figure A.4 *a) Arrows highlighting artefacts in the imaging result from 'non-linear' inversion method. b) Weighted image average* $\bar{\mathbf{R}}^j$ *at a certain iteration* j*. c) Final image obtained via the weighted average constraint method.*

ACKNOWLEDGEMENTS

Finishing PhD is not an easy task, much less when one is several kilometres away from home. I discovered the ultimate life hack: turning the people you meet in this foreign land into your adopted family. Turns out, no matter where we are from, we all share the same quirks, and there's an abundance of goodwill to go around. I have the extraordinary privilege of thanking a constellation of kind souls who've made my doctoral journey a little less stressful and filled with joy.

First of all, I would like to thank my supervisor Eric Verschuur. Not only have I learnt the ins and outs of Geophysics research from you, but I also got a masterclass in the fine art of being optimistic, gentle and zen-like leader from you. During the PhD, if we were having a bad day/week/month with research, a quick pilgrimage to Eric's office was like hitting the reset button on our stress levels. Finishing my PhD thesis through the pandemic while working a full-time job was quite challenging, but your unwavering support made it easier. Moreover, I consider myself incredibly fortunate since not many PhD candidates can claim to have attended their supervisor's rock concert. Eric, thank you for providing an exceptional and memorable PhD experience.

I extend my thanks to the committee members for generously dedicating their time to review my thesis. Prof. Nico de Jong, Dr. Alok Soni and Dr. Deyan Draganov, your insightful and constructive feedback has been instrumental in shaping this work. Furthermore, I extend my heartfelt gratitude to the Delphi consortium for granting me the invaluable opportunity to collaborate with esteemed researchers from across the globe. I would like to express my sincere appreciation to Margaret Van Fessem, Angela van der Sande, Annelies van Beek, Gerry, Henry den Bok, and Ronald Ligteringen for their help with my everyday administrative and technical challenges during my PhD. You made my chaos into organised chaos.

I would now like to thank my brothers and sisters in arms. My fellow Delphi colleagues, the PhD students in the extended Geoscience group of CITG, and the PhD students in the Medical imaging group, Shan, Ulaş, Apostolus, Gabriel, Dong, Tiexing, Leo, Mikhail, Abdul Rahman, Ali, Amarjeet, Shogo, Halah, Jan-Willem, Ayush, Matteo, Sidharth, Sixue, Billy, Myrna, Siamak, Junhai and Bouchaib. You are some of the smartest people I have worked with. All the conference evenings and Sponsors meetings became a lot more fun, thanks to you guys! I would especially like to thank Mikhail for unraveling the mysteries of FWM, and Shan for being my emotional support ninja.

Thanks to my friends I met in the Netherlands outside work, Milan, Petros, Francesca, Valentina, Radesh, Eldoh, the amazing people at VOX, Joy, Tariq, Shruti, Leroy, Signe, Divya (Bohra), Mandar, my time during these years was full of laughter, growth and love thanks to you guys. Ashwathi, my soul sister, thanks a lot for those late night chats, long

distance art sessions and bisi bele bath. My flatmate Divya (Varkey), your home-cooked food and chats are dearly missed. Salil, our "chai pe charcha" sessions are a highlight of my time in Delft. My Ghent family, Manuel, Bart, Mallika, Torsten, Alice, Ana, and Miriam- you made us feel at home in Europe. Thanks to Tiexing and Jing for being a source of support and delicious food during the time in UK. Thanks to my friends from IIT, Aakriti, Sugandha, Arushi, Astha and Sudharshan for your encouragement, support and entertainment during these years. I would also like to extend my thanks to my colleagues at Shearwater. I am constantly growing as a Geophysicist thanks to you.

I want to thank my parents back home. It is not easy to express my gratitude I feel for them in words. They set an incredible example for me on how to continuously evolve and embrace lifelong learning. Although it has been hard to stay away from them, their unwavering love and affection have served as a constant source of motivation every single day. I'd like to thank my brother Ankit, with whom I share my earliest memories and joy of discovering science. Additionally, I am grateful to him and my boudi for bringing my niece, Advaita, into our lives, a boundless source of pure joy. My family, Mita and Pinki mashi, Jethu, Meshos and my cousins for the much-needed entertainment, encouragement and support through these years. I would also like to thank my new and extended family that I have inherited from my husband. Especially Jyoti and Anup, you are a great inspiration and support. I feel grateful to call you my family. Finally my husband, Anurag. We have now spent a third of our lives together, a decade full of joy! You have supported me through my most challenging times and I couldn't have asked for a more supportive partner. Thank you for being you.

CURRICULUM VITÆ

Aparajita Nath

05-10-1991 Born in Korba, India.

EDUCATION

2015–2020 Ph.D candidate in Applied Physics
Delft University of Technology, Delft, The Netherlands
Thesis: Imaging with surface-related multiples using linear and non-linear modeling
Supervisor: Dr. Ir. D. J. Verschuur

2009–2014 M.Sc. and B.Sc. in Exploration Geophysics
Indian Institute of Technology, Kharagpur, India

PROFESSIONAL EXPERIENCE

2020–present Project Research Geophysicist
Shearwater Geoservices, Gatwick, The United Kingdom

2015–2019 Teaching Assistant
Delft University of Technology, Delft, The Netherlands

2014–2015 Project Research Assistant
Indian Institute of Technology Bombay, India

LIST OF PUBLICATIONS

10. **A. Nath**, A. JafarGandomi, S. Grion, *Enhanced Source Separation for Phase-Sequenced Simultaneous Source Marine Vibrator Data*, 83rd EAGE Annual Conference & Exhibition, Jun 2022, Volume 2022, p.1 - 5.

9. **A. Nath**, D. J. Verschuur, *Imaging with surface-related multiples to overcome large acquisition gaps*, Journal of Geophysics and Engineering, Volume 17, Issue 4, August 2020, Pages 742–758.

8. **A. Nath**, D. J. Verschuur, *Imaging with surface multiples on OBN data with large acquisition gaps*, SEG Technical Program Expanded Abstracts 2019. p.4624-4628.

7. **A. Nath**, D. J. Verschuur, M. Davydenko, *Using Surface Multiples to Image 3D Seismic Data With Large Acquisition Gaps*, 81st EAGE Conference and Exhibition 2019, Jun 2019, Volume 2019, p.1 - 5.

6. **A. Nath**, D. J. Verschuur, *Least-squares migration using surface-related multiples on data with large acquisition gaps*, First EAGE/SBGf Workshop on Least-Squares Migration, Nov 2018, Volume 2018, p.1 - 5.

5. **A. Nath**, D. J. Verschuur, *Using surface multiples to image across large acquisition gaps*, 80th EAGE Conference & Exhibition 2018 Workshop Programme, Jun 2018, cp-556-00056.

4. **A. Nath**, D. J. Verschuur, *Migration strategies of using surface-related multiples in case of incomplete seismic data*, 79th EAGE Conference and Exhibition 2017, Jun 2017, Volume 2017, p.1 - 5.

3. **A. Nath**, D. J. Verschuur, *Using surface-related multiples in imaging for data with large acquisition gaps*, SEG Technical Program Expanded Abstracts 2017. p.4768-4772..

2. **A. Nath**, D. J. Verschuur, *Imaging strategies using surface-related multiples for incomplete seismic data*, SEG Technical Program Expanded Abstracts 2016. p.4582-4586..

1. B. Shekar, **A. Nath**, *Gradient computation for simultaneous microseismic event location and velocity inversion by eikonal tomography*, SEG Technical Program Expanded Abstracts 2015. p.2604-2609..